Charles University in Prague

First Faculty of Medicine

Study program: Neuroscience

Irena Buksakowska, MD

Structural Patterns of Cognitive Deficits in MR Imaging

Strukturální podklady kognitivního deficitu v zobrazování magnetickou rezonancí

Doctoral Thesis

Thesis Supervisor: Doc. MUDr. Daniel Hořínek, Ph.D.
Thesis Consultant: Prof. MUDr. Jakub Hort, Ph.D.

Prague, 2019

Enclosure

I declare that I prepared the thesis independently and I mentioned all references and literature sources. I also state that the thesis has not been used for obtaining another or similar academic degrees.

I agree with the permanent depository of the thesis in the database Theses.cz for checking the similarity of theses.

Prohlášení

Prohlašuji, že jsem závěrečnou práci zpracovala samostatně a že jsem řádně uvedla a citovala všechny použité prameny a literaturu. Současně prohlašuji, že práce nebyla využita k získání jiného nebo stejného titulu.

Souhlasím s trvalým uložením elektronické verze mé práce v databázi systému meziuniverzitního projektu Theses.cz za účelem soustavné kontroly podobnosti kvalifikačních prací.

In Prague/V Praze

…….

Irena Buksakowska

Identification record:

BUKSAKOWSKA, Irena. *Structural patterns of cognitive deficits in MR imaging [Strukturální podklady kognitivního deficitu v zobrazování magnetickou rezonancí]*. Prague, 2019. 150 pages. Dissertation thesis. Charles University in Prague, First Faculty of Medicine, Department of Radiology, Second Faculty of Medicine, Charles University and Motol University Hospital. Thesis Supervisor Hořínek, Daniel.

Identifikační záznam:

BUKSAKOWSKA, Irena. *Structural patterns of cognitive deficits in MR imaging [Strukturální podklady kognitivního deficitu v zobrazování magnetickou rezonancí]*. Praha, 2019. 150 stran Dizertační práce. Univerzita Karlova v Praze, 1. lékařská fakulta, Klinika zobrazovacích metod, 2. lékařská fakulta Univerzity Karlovy a Fakultní nemocnice v Motole. Vedoucí práce Hořínek, Daniel.

Abstract

Structural and diffusion imaging patterns that can be evaluated using MRI in patients with cognitive deficits are the central theme of the proposed work. First, the clinical and neuroimaging background of dementias has been reviewed in a broader context, with a special focus on Alzheimer's disease (AD) and differential diagnoses. The second part of this thesis contains four consecutive experimental studies. The primary objective of the first two studies was to obtain structural and microstructural information on the neurodegenerative processes characteristic for AD on global and regional levels. For this purpose, several complementary approaches were used and the focus was shifted from grey to white matter (GM/WM). The following two studies focused on the differential context of WM microstructural alterations in normal pressure hydrocephalus (NPH) and distinctive patterns of WM disintegrity in temporal lobe epilepsy (TLE).

The most important conclusion of our studies is that structural and diffusion imaging proved to be useful in identifying regionally specific and disproportionate loss of brain volume and microstructure in several pathological processes underlying cognitive deterioration. The use of distinctive morphometric methods yielded complementary information on AD-related atrophy patterns, and further use of a combination of diffusion metrics appeared to facilitate interpretation of complex underlying pathological changes in AD, NPH and TLE. Whereas these MRI approaches can be useful diagnostic and differential support, further longitudinal studies should validate the prognostic value of distinctive measures in disease progression (AD) and in the identification of patients that would benefit from a surgical approach (NPH, TLE).

Keywords: magnetic rezonance imaging, morphometry, diffusion tensor imaging, Alzheimer's disease, normal pressure hydrocephalus, temporal lobe epilepsy

Abstrakt

Předkládaná dizertační práce se ve své hlavní části zabývá možnostmi detekce strukturálních a difuzních změn v MR zobrazení u pacientů s kognitivním deficitem. V širším kontextu je nejprve zmíněn podklad klinických změn a nálezů při neurozobrazení u pacientů s demencí, a to se zvláštním zaměřením na Alzheimerovu chorobu (ACh) a její diferenciální diagnostiku. Druhá část práce obsahuje čtyři experimentální studie v rámci našeho výzkumu. Hlavním cílem prvních dvou studií bylo získání strukturální a mikrostrukturální informace o neurodegenerativních procesech charakteristických pro ACh – na globální i regionální úrovni. Pro tento účel bylo použito několik komplementárních přístupů se zaměřením především na evaluaci šedé, a následně i bílé hmoty mozku. V následujících částech jsme se zaměřili na popis kontextu mikrostrukturálních změn bílé hmoty u normotenzního hydrocefalu (NPH) a charakteristických vzorců dezintegrace bílé hmoty u epilepsií temporálního laloku (TLE).

Nejdůležitějším závěrem, který lze vyvodit z našich studií je, že strukturální a difuzní zobrazování se ukázalo jako užitečné při identifikaci regionálně specifické a disproporcionální ztráty objemu mozku a mikrostruktury u některých patologických procesů, které jsou základem kognitivního zhoršení. Použití několika různých morfometrických metod vedlo k získání doplňujících informací o atrofických vzorcích souvisejících s ACh. Využití kombinace difuzních parametrů následně vedlo k usnadnění interpretace komplexních patologických změn u ACh, NPH a TLE. Zatímco obvyklé MR přístupy lze považovat za užitečnou diagnostickou a diferenciálně diagnostickou metodu u těchto onemocnění, je potřeba dalších prospektivně zaměřených studií pro potvrzení prognostické hodnoty jednotlivých MR technik v rámci detekce progrese těchto onemocnění (ACh) a rovněž pro identifikaci pacientů, u kterých je výhodou chirurgický zákrok (NPH, TLE).

Klíčová slova: zobrazování magnetickou rezonancí, morfometrie, zobrazování difuzního tenzoru, Alzheimerova choroba, hydrocefalus normálního tlaku, epilepsie temporálního laloku

Acknowledgements

Above all, I would like to express my gratitude to my supervisor, Dr. Daniel Hořínek, for being the most charismatic and devoted mentor I could wish for. I would like to thank him for the years of inspirational guidance and gracious help in many aspects of my studies and life. Without his brainstorming and visionary manner, and without his deep sense of understanding for the creative, innovative and interdisciplinary nature of our medical responsibility, this international scientific journey of mine would not be half the challenge, fun or adventure it has been. Thank you.

I would also like to thank my other supervisor, Prof. Jakub Hort, who has greatly supported me during my studies with guidance and scientific opportunities, and who has been an inspiration from the very beginning of this journey. To both my supervisors I owe special thanks for providing unique chances to participate in several international projects during the course of my study.

I would herein like to express particular gratitude to Dr. Nikoletta Szabó, Dr. Tamás Kincses, Prof. László Vécsei and other colleagues from the Neuroimaging Research Group in Szeged, Hungary, for the long-term cooperation and very special partnership. I appreciate their great support and guidance in performing and validating important portions of the projects related to this thesis, and I owe them many thanks for the solid methodological framework they have shared with me. All my visits and internships in Szeged have been invaluable learning, inspirational and problem-solving opportunities. Here I would especially like to thank Nikoletta for her great scientific and personal support, shared wisdom, experience and enthusiasm, and last but not least, her friendship.

I am also grateful for the rare opportunity to complete a one-year research fellowship at the Department of Radiology Informatics at the Mayo Clinic, Rochester, Minnesota, USA. My stay there in 2013 was possible due to a partnership programme between the Mayo Clinic and FNUSA-ICRC, which I was affiliated with. My great thanks belong to Prof. Bradley Erickson and all my colleagues from the Radiology Department, especially Dr. Roman Peter, and his wife Julia. Apart from the motivating environment and invaluable medical and academic experience, my stay there was a unique chance to meet many people who have greatly inspired me and who have had impact on me, including beyond the scope of science. Karolina and Michał Kucewicz – thank you.

My sincere gratitude goes to Dr. Martin Kynčl and Prof. Miloslav Roček from my affiliated Department of Radiology at the Hospital University Motol, Prague, for their professional and personal support, for having faith in me at every stage of my clinical-diagnostic work and always motivating me in my interdisciplinary research.

My special thanks belong to my dear friends Marta Izydorczyk-de Coster and Urszula Bieniek for their endless encouragement and help whenever it was needed.

Finally, my greatest gratitude belongs to my parents for their unconditional love, support and time shared with me and my sons Jan, Marek and Teodor – to whom I dedicate this work.

Table of Contents

List of Abbreviations

AA	Alzheimer's Association
AD	Alzheimer's disease
ADNI	Alzheimer's Disease Neuroimaging Initiative
ADRDA	Alzheimer's Disease and Related Disorders Association
ASSET	Array Spatial Sensitivity Encoding Technique
BET	Brain Extraction Tool
BRAVO	BRAin Volume imaging
CA	computational anatomy
CBD	corticobasal degeneration
CNS	central nervous system
CSF	cerebrospinal fluid
DBM	deformation-based morphometry
DKI	diffusion kurtosis imaging
DLB	dementia with Lewy bodies
DOF	degrees of freedom
DT	diffusion tensor
DTI	diffusion tensor imaging
EFNS	European Federation of Neurological Societies
FA	fractional anisotropy
FAST	FMRIB's Automated Segmentation Tool
FDT	FMRIB's Diffusion Toolbox
FIRST	FMRIB's Integrated Registration Segmentation Toolkit
FLIRT	FMRIB's Linear Image Registration Tool
FMRIB	Functional Magnetic Resonance Imaging of the Brain
FNIRT	FMRIB's Non-linear Image Registration Tool
FOD	fibre orientation distribution
FOV	field of view
FSL	FMRIB Software Library
FSPGR	Fast Spoiled Gradient Echo
FTLD	fronto-temporal lobar degeneration
FWHM	Full Width between Half Maximum values of a function

GCA	global cortical atrophy
GLM	general linear model
GM	grey matter
ICA	Independent Component Analysis
ILF	inferior longitudinal fasciculus
LA	longitudinal anisotropy
LDDMM	large deformation diffeomorphic metric mapping
LICA	Linked Independent Component Analysis
MD	mean diffusivity
MMSE	Mini Mental State Examination
MNI152	Montreal Neurological Institute template – a standard space average of 152 brains
MRI	magnetic resonance imaging
MTL	mediotemporal lobe
NEX	number of excitations
NFT	neurofibrillary tangle
NIA	National Institute on Aging
NINCDS	National Institute of Neurological and Communicative Disorders and Stroke
NPH	normal pressure hydrocephalus
ODF	Orientational Distribution Function
PCA	posterior cortical atrophy
PD	Parkinson disease
PET	Positron Emission Tomography
QBI	Q-ball imaging
RD	radial (perpendicular) diffusivity
ROI	region of interest
SBM	surface-based morphometry
SIENA(X)	Structural Image Evaluation, using Normalisation of Atrophy
SLF	superior longitudinal fasciculus
SPECT	Single-Photon Emission Computed Tomography
SPM	Statistical Parametric Mapping
SPSS	Statistical Package for Social Sciences
SVD	small vessel disease

TBM	tensor-based morphometry
TBSS	Tract-based Spatial Statistics
TE	echo time
TFCE	Threshold-Free Cluster Enhancing
TLE	temporal lobe epilepsy
TR	repetition time
T1	longitudinal relaxation time
VaD	vascular dementia
VBM	voxel-based morphometry
VCI	vascular cognitive impairment
WM	white matter
WMH	white matter hyperintensity
VP	ventriculoperitoneal

1 Introduction

Magnetic resonance imaging (MRI) has become an invaluable tool in diagnostic medicine and biomedical research and its contribution to our understanding of brain structure and function is unprecedented. Advanced MRI postprocessing methods are increasingly used in research and clinical settings to complement visual scan evaluation. Whereas gross structural abnormalities can be assessed visually, the quest for quantitative MRI biomarkers has prompted a shift towards development of techniques able to evaluate alterations occurring at the microstructural level.

In recent decades, the role of imaging techniques in providing information on topographical patterns of changes related to neurodegenerative processes has been established, and biomarkers of neuronal injury obtained with MRI have contributed to understanding of the pathogenesis of Alzheimer's disease (AD) and other dementias. Structural and diffusion imaging has become an integral part of diagnostic assessment in patients with cognitive decline, and is particularly useful in distinguishing between different underlying pathologic conditions and predicting disease progression. Regional distribution of changes may be visualised on a macroscopic scale with structural and diffusion MRI, reflecting associated deficits in cognitive domains, paralleled by regionally specific and disproportionate loss of brain volume and microstructure.

The thesis contains theoretical and experimental parts. In **Chapter 3**, theoretical clinical and neuroimaging background of dementias is reviewed in a broader context, with a special focus on AD and differential diagnoses. **Chapter 4** is divided into four subchapters, representing consecutive experimental studies, each further divided into Methods, Results, Discussion and Summary. The primary aim of the studies covered in **subchapters 4.1** and **4.2** was to obtain and discuss global and regional structural information on the neurodegenerative processes characteristic for AD. For this purpose, several complimentary approaches were used, and focus was shifted from grey to white matter. In **subchapter 4.3**, we focused on the differential context of microstructural alterations in normal pressure hydrocephalus, and distinctive patterns of white matter disintegrity were additionally evaluated in the framework of temporal lobe epilepsy – as described in **subchapter 4.4**. Summary and overall conclusions are listed in **Chapter 5**.

2 Aims

The aim of the proposed thesis is to demonstrate the utility of several structural and diffusion MRI approaches in various groups of patients with clinical manifestation of cognitive impairment. Its primary objective was to evaluate the patterns of grey matter loss and white matter disintegration in AD in comparison to normal aging (subchapters **4.1** and **4.2**) and normal pressure hydrocephalus (subchapter **4.3**). Subsequently, the same methodology has been applied to evaluate microstructural white matter changes in temporal lobe epilepsy (subchapter **4.4**). In order to better characterise structural patterns associated with selected conditions, we used several postprocessing methods, assuming that the whole-brain approach may be the most robust.

The specific aims were as follows:

1) **Identifying structural MR patterns of global, cortical and subcortical changes in AD.**
    - Patterns of global atrophy and specific regional changes on cortical and subcortical levels in AD can be analysed and visualised with the use of structural MRI. We assumed that information on AD-related atrophy patterns obtained with the use of several morphometric methods may be complementary. We further hypothesised that there is an association between these patterns. In particular, we assumed that focal regional patterns of both cortical and subcortical atrophy may present higher discriminative value than single measures of global and subcortical volumes.
    - To test the hypothesis of associated patterns of global and regionally specific volume loss in AD, we performed multilevel evaluation of brain atrophy, including cross-sectional analyses of volumetric changes in total brain, cortical and subcortical grey matter, as well as of the focal atrophy of subcortical structures. With the multilevel approach we expected to better characterise structural patterns associated with underlying AD pathology.
    - We also assumed that structures that are strongly anatomically and functionally linked may show a similar rate of size alterations. We suspected that this might be valid specifically for pathology-driven structures, but not necessarily for healthy controls.

2) **Identifying the spatial pattern of the MR diffusion motif characteristic for AD.**

- A number of studies have revealed altered diffusion parameters in AD that are related to different aspects of white matter (WM) microstructure. We assumed that these parameters should be evaluated jointly. We hypothesised that obtaining the spatial pattern of compound diffusion alterations may lead to an identification of the disease-specific marker.
- For this purpose, we used linked independent component analysis (ICA) to fuse and decompose data containing various diffusion parameters in a WM skeleton representing the core of fibre bundles. The main aim of the analysis (modified to a single modality group) was to identify the combined group-level features of diffusion parameters in AD that properly reflect their underlying variability.

3) Identifying MR diffusion patterns of white matter integrity in AD and NPH.

- Structural imaging patterns in AD, normal pressure hydrocephalus (NPH) and normal aging may be challenging to interpret in the context of widespread atrophy. We hypothesised that AD and NPH have different spatial patterns of WM microstructural changes, which can be differentiated using multiple diffusion metrics that may improve differential and diagnostic process and give more insight into the underlying processes accompanying both conditions.
- We further assumed that patient group diffusion metrics may correlate with certain CSF volumes that are characteristically altered in NPH.

4) Identifying MR diffusion patterns of white matter integrity in TLE.

- We hypothesized that right and left temporal lobe epilepsy (TLE) have distinctive spatial patterns of WM changes that can be differentiated and interpreted with the use of multiple diffusion parameters. To test this hypothesis, we compared global WM microstructure in the core of fibre bundles in both right and left TLE with the use of TBSS analysis.

3 Theoretical part

3.1 Clinical background

3.1.1 Alzheimer's disease (AD)

Alzheimer's disease (AD) is the most common type of dementia in the elderly and one of the most common neurodegenerative disorders, characterized by gradual cognitive decline. Worldwide, it has been estimated that the prevalence of AD was set to rise to 35.6 million people globally by 2010 (Dartigues 2009) and at least 50 million people were believed to be living with AD or other dementias in 2018 (Patterson 2018), with the imposition of an enormous social and financial burden. It has been estimated that one in ten people age 65 and older has AD, and the percentage increases with age, reaching 32% for age 85 and older (Hebert et al. 2013).

Although a growing number of studies suggest that the prevalence of AD and other dementias in higher-income countries may have tended to decline in the past 25 years at the individual levels, due to increasing standards of education and improved control of cardiovascular risk factors, the global number of people living with AD and other dementias is expected to grow rapidly due to the growth of the aging population (He et al. 2015) (Alzheimer's Association. 2019 Alzheimers's Disease Facts and Figures. 2019). Whereas the 65-and-older population is expected to nearly double over the next three decades, the global population of the "oldest old" – people aged 80 and older – is projected to more than triple by 2050 (He et al. 2015). Similarly, recent reports forecast that current estimates for AD prevalence may almost double every 20 years, reaching 75 millions in 2030 and 131.5 millions in 2050 (Patterson 2018) and the social and economic burden will continue to grow, especially in low-and middle-income countries, where there is currently no evidence of declining tendency for risk of AD and other dementias (He et al. 2015).

3.1.1.1 Clinical presentation

Current diagnostic National Institute on Aging (NIA) and the Alzheimer's Association (AA) guidelines (2011) recognize that AD begins many years before the onset of symptoms, being defined by structural changes in the brain, not by symptoms (Alzheimer's Association. 2019

Alzheimers's Disease Facts and Figures. 2019). Accordingly, in the revised NIA-AA criteria, a conceptual distinction is made between AD pathophysiological processes and the various clinically observable symptoms designating different qualitative and quantitative clinical expressions of disease (Jack et al. 2011). The original NINCDS-ADRDA definitions and guidelines (1984) have been revised accordingly to broader terms of the entire spectrum of the disease (Jack et al. 2011), including earliest signs of AD pathological findings in the absence of clinical features, through early presentation of symptoms with at least partially preserved functionality (mild cognitive impairment – MCI) to severe stages of AD-related dementia which refers to the stage along this continuum where symptoms begin to impair daily activities.

Precise demarcation between normal cognition and MCI may be problematic in a clinical practice; nevertheless, core criteria for the diagnosis of MCI include the evidence of concern regarding a change in cognition, impairment in one or more cognitive domains, preservation of independence in functional abilities and no evidence of a significant impairment in a social or occupational functioning (Albert et al. 2011). Whereas impairment in episodic memory is the most common clinical expression seen in MCI patients who subsequently progress to AD, other cognitive areas may be impaired, including executive functions (e.g., problem-solving, reasoning, planning, judgment), language functions (e.g., naming, fluency, expressive speech and comprehension), visuospatial skills and attention. Many validated clinical neuropsychological tests are available to assess these cognitive domains.

General definition of dementia as "a progressive cognitive decline of sufficient magnitude to interfere with normal social or occupational functions, or with usual daily activities" (McKeith et al. 2017) corresponds with core clinical criteria for AD-related dementia. Clinical evidence of progressive decline characteristic for dementia must include a presentation of a minimum two or more cognitive or behavioural (neuropsychiatric) symptoms that interfere with the daily functional ability that cannot be explained by major psychiatric disorder. The initial and most pronounced feature of AD-related dementia is an amnestic presentation with impaired ability to acquire and remember new information. Typical non-amnestic manifestations include linguistic deficits (especially impaired word-finding), visuospatial impairment (deficits in a spatial cognition like object agnosia, impaired face recognition, simultagnosia, alexia), and impaired

reasoning, judgment and problem solving as deteriorated executive functions (McKhann et al. 2011). Progressive alterations in personality and behaviour are observed simultaneously. As AD progresses to its last stage, physiological functions like swallowing, balance and bowel and bladder control are impaired, with severe complications such as immobility, malnutrition or aspiration with the high risk of pneumonia (which is the most commonly identified cause of death among elderly patients with AD).

3.1.1.2 Pathological findings

Alzheimer disease is considered to begin 20 or more years before symptoms arise, when microstructural alterations in the brain are initiated, yet without significant clinical expression. According to pathological findings, approximately 30% of cognitively normal elderly subjects meet neuropathologic criteria for AD despite the absence of apparent cognitive symptoms (Knopman et al. 2003) (Price & Morris 1999) (Savva et al. 2009). Conversely, recent pathological and clinical studies showed that the number of individuals (up to 30 %) who met the clinical criteria for AD did not have AD-related alterations in autopsy and in such cases different cause of dementia had to be considered (Nelson et al. 2011).

Well-recognized neuropathologic features of Alzheimer disease are abnormal forms of protein tau (neurofibrillary tangles – NFTs) and beta-amyloid plaques – changes that together with associated processes such as inflammation and oxidative stress, lead to neuronal loss along with observable brain volume reduction (Mirra et al. 1991) (Hyman 1997). Interaction of beta-amyloid (Aβ) aggregation with plaque development outside neuronal cells is believed to contribute to neuronal degeneration by deteriorating synaptic transmission, while the hyperphosphorylation and aggregation of tau protein with formation of NFTs interfere with axonal transport. The number of neurons containing neurofibrillary tangles in AD decreases over time, correlating with brain atrophy, which has been viewed as more accurate marker for assessment of cognitive impairment (de Jong et al. 2007). When the previous NINCDS-ADRDA criteria were defined, it was thought that actual symptoms presented by individuals with AD directly reflect the degree of damage to neurons in different parts of the brain; however, a growing number of studies revealed that an explicit correspondence between clinical expression

and the underlying pathology is not always observed (Jack et al. 2011). It has been described that various aspects of AD pathology appear to differently relate to clinical features and that amyloid and neurofibrillary pathology seem to develop on different time scales, rather than to occur simultaneously (Ingelsson et al. 2004).

Amyloid pathology is believed to develop first during the long presymptomatic phase, while the development of NFTs accelerates slightly before the appearance of the clinical stage of AD (Jack et al. 2009). Relatively high frequency (about 30%) of cerebral beta-amyloid positivity (Aβ+) shown in cognitively normal elderly adults approximately correspond with the prevalence of AD symptoms nearly a decade later (Rowe et al. 2010) (Jack et al. 2008b) (Aizenstein et al. 2008). Extensive number of neuritic amyloid plaques, apart from their evidence in the absence of any obvious symptoms, has been shown in AD brains independently of disease duration (Mirra et al. 1991) (Price & Morris 1999) (Ingelsson et al. 2004). Plaques are distributed unevenly in patches throughout the cortex with a significant intersubject variability (Braak et al. 1993). It should be noted, however, that increased Aβ deposition is seen also in disorders other than AD (e.g., amyloid angiopathy) (Albert et al. 2011). Likewise, evidence of abnormally phosphorylated tau protein as a solitary pathological sign is not disease-specific and may develop in hippocampi and elsewhere independently of other pathological processes in AD (Braak & Del Tredici 2011) (Nelson et al. 2009). Evidence of NFTs in the absence of amyloid neuritic plaques has been found in approximately 5% of elderly individuals, who therefore did not meet criteria necessary for the diagnosis of AD.

According to (Braak et al. 1993) accumulation of AD-related NFTs (as well as neuropil threads found in distal portions of dendritic processes) occurs in a specific pattern and relatively predictable sequence; degeneration is considered to be constrained to the entorhinal and transentorhinal cortex in the early AD stages (namely I-II), subsequently spreading into the hippocampus and other mesiotemporal areas, and eventually extending over the isocortical association regions (**Fig. 3.1**). Prior to the late stages (namely V-VI), only a relatively small total number of neurons is affected; however, involvement of transentorhinal and entorhinal cortex as structures crucial for continuous transmission of information from isocortex to hippocampus and

vice versa results in obvious cognitive symptoms. These late pathological phases are consistent with clinical presentation of severe cognitive alterations with unambiguous diagnostic picture.

It is expected that the co-occurrence of these two findings: at least a moderate number of amyloid plaques in certain regions of neocortex and the extent of the regional distribution of NFTs corresponding to Braak and Braak stage IV or higher (**Fig.3.1**) will continue to define neuropathological and pre-clinical entity of AD (Jack et al. 2011).

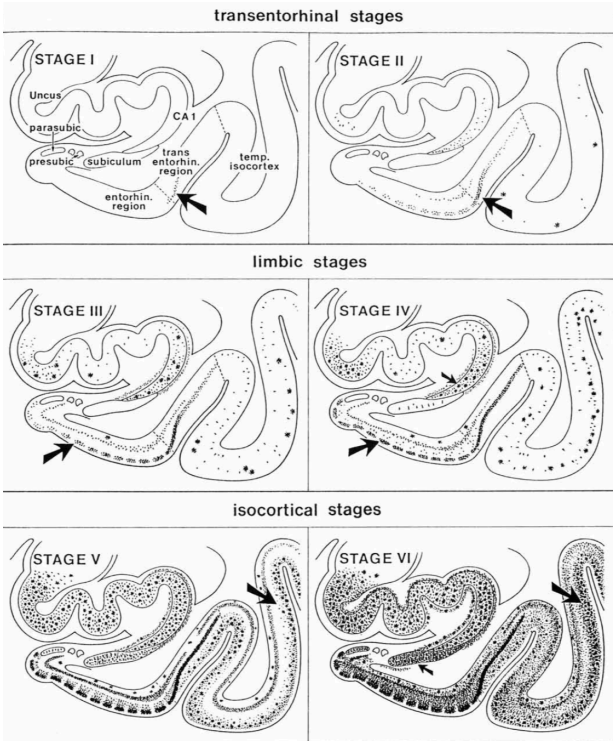

Fig. 3.1. Neurofibrillary changes in hippocampal formation, entorhinal and transentorhinal regions, and in the adjoining temporal isocortex. Development of changes from stage I to stage VI. Reproduced with permission from (Braak et al. 1993)

3.1.1.3 Diagnostic and prognostic biomarkers

Over the last decades a number of biological markers of various compounds of AD-related pathology has been studied and included in the diagnostic criteria. It should be noted that a growing number of studies validate prognostic value of ε4 allele of apolipoprotein E (APOE) gene involved in beta amyloid trafficking, which is otherwise a well-known major genetic risk factor for late onset AD (Payton et al. 2018) (Dang et al. 2018). If an autosomal dominant form

of AD is confirmed (mutations in genes APP, PS1, PS2,), then the symptomatic cognitive decline can be considered as prodrome to AD-related dementia, most likely in the cases of early onset AD (Albert et al. 2011).

Several major classes of biomarkers of AD-related pathophysiology have been described, based either on the process which they measure, or the type of clinical question they address (Hampel et al. 2010) (Albert et al. 2011). Importantly, they may serve either as a diagnostic support for the underlying etiology of clinical symptoms, or a prognostic tool to estimate the likelihood of cognitive functional progression to more severe stages of MCI or dementia. Conversely, if showing different regional patterns of alterations, biomarkers may indicate an alternative, non-AD etiology.

First category of measures, mapping and reflecting the evidence of Aβ deposits in the brain, include positive positron-emission (PET) amyloid imaging (see below in ***Neuroimaging biomarkers*** section) and cerebrospinal fluid (CSF) measure of low $A\beta_{42}$ (Jack et al. 2008b). The second group of biomarkers, more non-specific than markers of amyloid pathology is that of downstream neuronal degeneration or injury (Albert et al. 2011).

Direct measurement of tau depositions is considered to be a strong marker of the damage to neurons and synapses associated with AD and some clinical-pathological studies have revealed higher correlation rates between neurofibrillary pathology and cognitive impairment than between amyloid pathology and cognitive impairment (Gómez-Isla et al. 1997) (Bennett et al. 2004). Markers of tau accumulation include CSF measures of increased total tau or phosphorylated-tau (Blennow & Hampel 2003). It should be noted, however, that elevated CSF tau measures may also reflect general, non-specific neuronal and synaptic damage, and their presence may as well occur in other neurodegenerative disorders. Therefore, in line with diagnostic criteria, it is the combination of these two markers that is considered to be more informative in terms of AD-related pathology (Albert et al. 2011). Both tau measures and CSF $A\beta_{42}$ (as well as their ratio), have been further described as markers of progression of MCI to dementia (Albert et al. 2011).

3.1.1.3.1 Neuroimaging biomarkers

Ultimately, it is neurodegeneration that has been designated as a superior metric of AD severity (Nelson et al. 2011) (Savva et al. 2009). Neuroimaging markers of neuronal injury include a number of structural and functional measures (like brain atrophy and hypometabolism or hypoperfusion shown in a topographical pattern characteristic of AD) obtained with MRI or PET. MRI biomarkers of neuronal injury will be discussed separately in the following chapter **(3.2. Patterns in structural MRI)**.

In general, PET using ^{18}fluorodeoxyglucose (FDG) has been developed to evaluate neuronal glucose consumption, and as the main indicator of neuronal metabolism is used as a marker of neuronal damage (Reivich et al. 1979). PET using tracers for Aβ (amyloid imaging) is thought to be a marker of accumulation of the Aβ plaques that can be evaluated separately from structural changes in brain anatomy (Jack et al. 2008b).

FDG-PET is a measure of cerebral glucose metabolism reflecting neuronal activity, usually in a resting state without the need for cognitive activation. It can be therefore used as a marker of degeneration, detecting specific regional hypometabolism (Kuhl et al. 1982). For decades, a number of studies and trials have evaluated a characteristic profile of AD-related changes seen in FDG-PET, showing reduced FDG uptake predominantly in temporoparietal association areas including the precuneus and posterior cingulate cortex (Rice & Bisdas 2017) (Mosconi et al. 2008) (Hoffman et al. 2000). These alterations are closely associated with cognitive impairment as demonstrated in cross-sectional and longitudinal studies (Alexander et al. 2002) (Mosconi 2005) (Ossenkoppele et al. 2012). The potential prognostic accuracy of FDG in predicting progression to AD in MCI patients has been consistently demonstrated by a number of studies, confirming the pattern of hypometabolism in the most affected regions – medial temporal and inferior parietal cortex (Anchisi et al. 2005) (Sörensen et al. 2019). A number of authors have also evaluated alterations in FDG uptake attributed to pharmacodynamic drug effects (Hampel et al. 2010). Using FDG-PET in a combination with other validated markers of AD-related pathology (like CSF tau measures) to predict prognosis in MCI patients, is thought to further improve its prognostic value (Fellgiebel et al. 2007).

The most studied amyloid tracer is a11C-labelled thioflavin analogue known as Pittsburgh compound B (PIB) that crosses the blood-brain barrier and selectively binds to amyloid plaques

(specifically insoluble fibrillary forms of beta-amyloid 40 and 42) and doesn't bind to soluble amyloid forms (Lockhart et al. 2007) (Klunk et al. 2004). Marked retention of PIB have been shown diffusely in frontal, parietal, temporal as well as occipital cortex and striatum in patients with diagnosed AD (Klunk et al. 2004). It should be noted, however, that increased global PIB retention may be observed also in a significant number of elderly non-symptomatic individuals and a shift has been prompted towards the longitudinal assessment of the relationship between Aβ burden and cognitive decline, as amyloid positivity is thought to relate to preclinical AD (diagnostic criterium). Regardless of results confirming significantly higher rate of conversion to AD in MCI patients with positive PET measures, it has been additionally noted that only using this modality with other methods, like combination with structural MRI, could predict a significantly shorter time to progression (Jack et al. 2010).

3.1.2 Cerebrovascular and mixed dementia

Whereas AD accounts for an estimated 60-80% of dementia cases (Wilson et al. 2012); as any other syndrome, it can possibly have a number of causes, each related with distinctive symptoms and structural patterns. Many individuals with symptomatic dementia have brain abnormalities associated with more than one pathology. Historically, evidence of the other most common cause of dementia – vascular dementia (VaD, was used as an exclusion criterium for a diagnosis of AD. That guideline is no longer valid, consistent with the pathologic studies, which show that the brain changes of AD and VaD commonly coexist. Co-occurring neuropathology was discovered in about half of patients with AD (Brenowitz et al. 2017). VaD as a solitary diagnosis is considered to account for about 5-10 % of dementia cases (Brenowitz et al. 2017) (McKhann 2011). At the clinical level, confirmation of two or more causes of dementia leads to the diagnosis of mixed dementia. Recent studies suggest that mixed dementia is more common than previously recognized (Schneider et al. 2009) and its prevalence increases with age, with highest rates in the oldest old individuals (James et al. 2012) (De Reuck et al. 2018). Deteriorated executive functions like impaired judgment or ability to make plans or decisions are the most characteristic features in patients with dementia of cerebrovascular etiology, as opposed to memory loss typical for early stages of AD. Difficulties with gait and balance are also common.

3.1.3 Frontotemporal dementia

Frontotemporal dementia (FTD) or frontotemporal lobar degeneration (FTLD) accounts for less than 10 percent of dementia cases (National Institute on Aging 2018). It is a group of neurodegenerative diseases associated with accumulation of several proteins such as 3-repeat and 4-repeat tau, and TAR DNA-binding protein 43 (TDP-43), including behavioural-variant FTLD, primary progressive aphasia, Pick's disease, corticobasal degeneration and progressive supranuclear palsy, any one of which can result in frontotemporal disorder characterized with personality and behavioural changes and/or language impairment (Neumann & Mackenzie 2019). Majority of individuals with FTLD tend to develop symptoms at younger age than patients with AD; about 60% at age 45 to 60 (National Institute on Aging 2018). It has been shown that using FDG-PET to differentiate between AD and FTLD may result in greater accuracy than clinical assessment (Foster et al. 2007).

3.1.4 Dementia with Lewy bodies

Symptoms of dementia are also developed by patients with Lewy body disease (DLB, or Dementia with Lewy bodies). Misfolded alfa-synuclein is the main component of intracellular inclusions called Lewy bodies, that compromise of aggregated vesicles and proteins causing neuronal loss in specific brain regions. The revised DLB diagnostic criteria (McKeith et al. 2017) distinguish between diagnostic biomarkers and clinical features which include: fluctuating cognition with prominent variations in attention and alertness, altered executive functions, visuospatial impairment, sleep disorders (REM sleep behaviour disorder) and well-formed visual hallucinations that may be pronounced in early stages. Memory impairment may not necessarily be present early, but usually occur along the progressive course of disease. Diagnostic criteria also include one or more key features of parkinsonism: bradykinesia (defined as slowness of movement and decrement in amplitude or speed), rest tremor, or rigidity (McKeith et al. 2017) (Postuma et al. 2015).

About 5-10 % of individuals with dementia show evidence of DLB alone, however, the co-occurrence with AD pathology is more common (Alzheimer's Association. 2019 Alzheimers's Disease Facts and Figures. 2019). Because of essential differences in patient management and outcome, providing effective differential diagnosis is crucial. In the absence of one direct biomarker of DLB, several indirect methods were described as indicative, including

neuroimaging biomarkers like reduced dopamine transporter uptake (DAT) in basal ganglia (McKeith et al. 2017). Due to the fact that severe nigrostriatal dopaminergic degeneration typically occurs in DLB, but not in AD, the diagnostic accuracy appeared sufficiently high for DAT imaging to be clinically valid in distinguishing DLB from AD (McKeith et al. 2007). Generalized low uptake on SPECT/PET perfusion/metabolism scan with reduced occipital activity or the posterior cingulate island sign on FDG-PET imaging were proposed as supportive neuroimaging biomarkers (Lim et al. 2009) (O'Brien et al. 2014) (McKeith et al. 2017). Unlike in DLB, the occipital cortex in AD patients may retain its physiological glucose metabolism (Rice & Bisdas 2017). Likewise, in a clinical MR setting, relative preservation of medial temporal lobe structures on CT/MRI scan can be useful for separating DLB from AD (Harper et al. 2016); however, evidence of mediotemporal atrophy in DLB may suggest the co-occurring AD-related pathological process.

The accumulation of Lewy bodies in the cortex, alongside the accumulation of beta-amyloid plaques and tau tangles, also contributes to the symptoms of cognitive decline in advanced stages of Parkinson disease (PD). Recent studies show that signs of secondary dementia including frontal executive dysfunction in PD patients may be further associated with levodopa-induced dyskinesis (Yoo et al. 2019).

3.1.6 Normal pressure hydrocephalus (NPH)

Normal pressure hydrocephalus (NPH) is a clinical syndrome, first described by Adams et al. (ADAMS et al. 1965), manifested by the clinical triad of symptoms including gait disturbance, urinary incontinence and dementia. Whereas CSF pressure may be normal at one spinal tap, episodes of increased CSF pressure can occur, and hence NPH is also referred to as "intermittent pressure hydrocephalus". NPH is caused by excessive accumulation of CSF in the ventricular system due to an impairment of its flow and absorption. Roughly 50% of cases with NPH have a known cause (secondary or symptomatic NPH), such as meningitis, subarachnoid haemorrhage, or cranial trauma, while the remaining 50% of cases are idiopathic, usually presenting in the 7th decade of life (Damasceno 2015).

Idiopathic NPH is relatively common in the elderly population, with an estimated prevalence of 1.4% (comparing to 13% in AD) in people aged 65 years or older (Tanaka et al. 2009) (Hebert et

al. 2003), accounting for about 5-6 % of all dementias (Verrees & Selman 2004) (Damasceno 2015). Difficulties in differential diagnosis of NPH are common due to the fact that clinical manifestations of the triad (complete or incomplete) are often mimicked by other diseases; in particular they may be presented in VaD, PD, DLB, corticobasal degeneration (CBD), progressive supranuclear palsy, multiple system atrophy, medication side effects; or commonly seen in combination with other diseases (Damasceno 2015). In particular, there is an evidence for frequent co-morbidity of NPH and AD, which is reported from 31 to 75% (Golomb et al. 2000) (Leinonen et al. 2012) (Malm et al. 2013).

Unlike AD, NPH is considered to be potentially reversible cause of dementia, treatable by ventriculo-peritoneal (VP) shunt insertion. Results obtained from VP shunting vary widely (Bateman & Loiselle 2007) (Aygok et al. 2005) (Hamilton et al. 2010) (Klassen & Ahlskog 2011) and the postoperative response rate in NPH ranges from 10% to 90% in various studies. There are some longitudinal studies suggesting that the co-occurring moderate-to-severe AD-related pathology results in poor response to VP shunting (Hamilton et al. 2010). However, the issue of misdiagnosis cannot be excluded in some cases and it can be one of the possible explanations for poor response to shunting; hence some patients may present ventriculomegaly ex-vacuo rather than due to NPH (Klassen & Ahlskog 2011). Nevertheless, NPH with cognitive impairment as a prominent or initial symptom is considered to have worse prognosis after shunting. Improvement in gait and cognition after shunting has been observed in individuals that demonstrated prior typical NPH syndrome regardless of the co-occurrence of AD pathology (Golomb et al. 2000) (Bech-Azeddine et al. 2007). As have been mentioned, NPH-associated dementia is considered to be multifactorial, related to both cortical and subcortical changes, as well as to pressure-induced ischaemia or even vascular disease (Golomb et al. 2000) (Tullberg et al. 2002).

The classic triad of symptoms occurring in NPH is predominantly thought to be related to the compression of the subcortical WM tracts around the enlarged lateral ventricles (Ding et al. 2001). Whereas ventriculomegaly is a key diagnostic hallmark in radiological evaluation of NPH, the magnitude of ventricular enlargement and the extent of WM impairment often do not go along with the severity of NPH symptoms or response to shunting (Lenfeldt et al. 2011).

Accordingly, due to high rates of revised diagnoses of NPH, it has been confirmed that previously reported NPH-related ventriculomegaly cases with suspected double underlying pathology, may in fact refer to symptomatic expressions of other neurodegenerative process, further explaining unfavourable risk-benefit ratio for VP shunting (Espay et al. 2017).

3.2 Patterns in structural MRI

MRI has become one of the most powerful and versatile diagnostic tools available to clinicians and researchers. There has been tremendous growth in both technology and clinical usage since MRI first became available. In the last decades, structural neuroimaging has become widely available and recommended as part of the clinical evaluation in a number of different dementias (Hort et al. 2010) (Rascovsky et al. 2011). Correctly distinguishing between various causes of neurodegenerative diseases related with progressive cognitive decline is challenging but substantial for patients and their families to provide holistically adequate approach. Apart from excluding treatable causes of cognitive deficits, the role of imaging techniques has been established as a valuable support in providing information on specific pattern of changes related to different neurodegenerative processes, like offering positive predictive value for underlying disease pathology. Detailed descriptions of topographical MRI patterns used as markers of neuronal injury have contributed to better understanding of the pathogenesis of AD and other dementias. Neuroimaging is commonly used to assess disease progression and has been included in numerous studies and trials investigating progressive cognitive decline.

3.2.1 MRI basics

MRI relies on the physical principles of nuclear magnetic resonance and measures the magnetic properties of biological tissues. Hydrogen, is an atom present in water and fat; therefore, abundantly represented in the human body and particularly useful for the purpose of such measurements. Classical and quantum explanations of MRI as we know in a clinical setting start with magnetic property of hydrogen proton – called spin (or quantized angular momentum), which may be simplified to the concept of a rotation around its own axis. Spins are behaving like little magnets (magnetic dipoles) and in the absence of an external magnetic field their

orientation is random; when spins are placed in an external, static magnetic field (B0), they align with this magnetic field and start precessing around an axis parallel to the direction of B0, but with a random phase. The frequency of the precession (called the Larmor frequency (ω, measured in MHz)) is proportional to the magnetic field strength the hydrogen nucleus is experiencing (in Tesla); the gyromagnetic ratio (γ) is a constant specific to each specific nucleus or particle, measured in MHz/Tesla):

$$\omega = \gamma B$$

Spins can align either spin-up (parallel) or against (antiparallel) to the main magnetic field. More spins are aligned parallel (or more accurately in the spin-up condition – associated with lower energy state), and the sum of the protons precessing in the same direction around the direction of the external field is described as a net longitudinal magnetization (**Fig. 3.2**) When a patient is placed in the MRI scanner, most protons will align parallel to the magnetic field (B0, the Z axis).

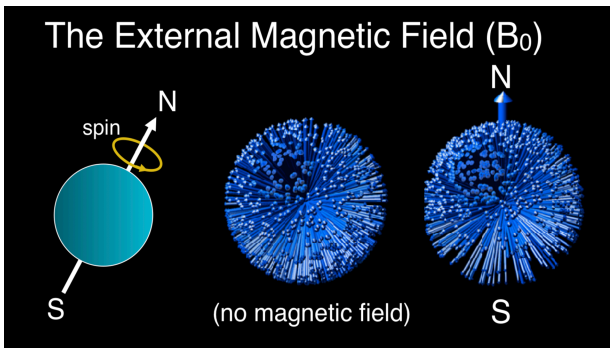

Fig. 3.2. The concept of net longitudinal magnetisation: The spin (and associated magnetic moment and angular momentum) is probabilistic in nature. Thus, each spin doesn't in fact align with the B, but rather exists in a probabilistic shape (cone) and spin-up and spin-down implies that probabilistic cone that faces up or down. The number of excess nuclei in external magnetic field (in lower vs. upper energy states) is proportional to B_0. These excess nuclei are the source of magnetization for all MRI experiments. Image adapted from http://users.fmrib.ox.ac.uk/~mchiew/teaching/

Hydrogen protons may be triggered by an orthogonal radiofrequency pulse (RF); resonance occur when RF is applied at the same frequency (Larmor frequency) – spins absorb energy in a process called excitation and start rotating at the same phase. Following the excitation pulse an additional net transverse magnetisation is produced in a plane perpendicular to the Z axis. When the RF pulse is switched off, the protons start returning to their original configuration, parallel to

the main magnetic field. The process by which the protons release the energy that they absorbed from the RF pulse is known as relaxation. Naturally occurring, two separate processes take place during this relaxation phase, characterised by two distinct time constants. While both times measure the spontaneous energy transfer by an excited proton, they differ in the final disposition of the energy (Dale et al. 2015). The recovery of the parallel magnetisation is characterised by the exponential time constant T1. T1 relaxation is the process by which the net magnetization returns to its initial maximum value parallel to B0 (longitudinal relaxation, spin-lattice relaxation). T2 relaxation is the process by which the transverse components of magnetization decay or dephase (transverse relaxation, spin-spin relaxation). During the relaxation phase protons emit RF energy, which in a form of a "signal" can be detected (read-out) by the MRI scanner, measured and transformed into an image. Gradient magnetic fields are applied to differentiate between signal from different locations by assigning different resonant frequencies to different spatial positions.

Due to the fact that protons have different relaxation rates depending on the tissue type, relaxation process is a fundamental aspect of MRI that provides the primary mechanism for image contrast. For example, tissues that consist mostly of water (like CSF), can be made to appear either bright (on T2-weighted images) or dark (on T1-weighted MRI brain images). Importantly, the RF pulses and magnetic fields used in MRI can be manipulated in numerous ways to modify the appearance of specific tissues for greater versatility and diagnostic utility.

3.2.2 MRI protocol

Validation of a systematic MR acquisition and reviewing protocols has become of a great importance in order to ensure the better reliability and reproducibility for any diagnostic process. Whereas specific protocols have been developed for clinical and scientific purposes (Jack et al. 2008a), a typical "dementia MRI protocol" in a clinical setting consists of an axial T1-weighted 3-D images, axial (and coronal) fluid attenuated inversion recovery (FLAIR), axial T2-weighted, axial susceptibility-weighted imaging, axial diffusion-weighted imaging (DWI), and an apparent diffusion coefficient (ADC) map derived from the diffusion scans (Asselin et al. 2019). Reviewing algorithm in the context of AD and other dementias should in the first place include assessment of the presence (or absence) of intra- or extra-axial lesions that are potentially

reversible and amenable to surgical intervention (tumors, arteriovenous malformations, subdural hematoma or hydrocephalus). Subsequent viewing protocol should include evaluation of other signal alterations within brain structure, with the following assessment of brain atrophy.

3.2.3 Vascular cognitive impairment and vascular dementia

The radiologic evaluation of signal alterations using T2-weighted imaging or FLAIR images can detect inflammatory demyelinating diseases, infections, toxic or metabolic processes which may be contributing to clinical manifestation of cognitive decline. Nevertheless, in the context of probable dementia, punctate or confluent regions of signal change within white matter (and/or deep grey matter) are highly indicative of vascular damage to the brain (Harper et al. 2014).

Designations of vascular cognitive impairment (VCI) and vascular dementia (VaD) are related to the entire spectrum of cognitive disorders resulting from vascular brain injury of both ischemic and non-ischemic origin. Pathophysiological findings underlying VCI include dysfunction of the neurovascular unit and mechanisms regulating cerebral blood flow (Gorelick et al. 2011). If T2/FLAIR signal changes are found in strategic locations, such as arterial territories, association areas and watershed carotid territories, it is assumed that VCI or VaD result from large vessel disease. Similarly, the evidence of lesions that are located bilaterally in thalamus imply small vessel disease (SVD), as well as the evidence of multiple lacunar infarctions in frontal WM and basal ganglia. T2 hyperintensities with corresponding T1 and FLAIR hypointensity in regions of a single deep perforating arteriole are indicative of small deep brain infarcts, especially when a rim of hyperintensity is present on FLAIR images, reflecting gliosis. Susceptibility weighted imaging is commonly used to detect cerebral microhemorrhages or microbleeds (CMBs), with small and rounded hypointensities that are radiological manifestations of focal leakage of blood-breakdown products from abnormal blood vessels. The location of these alterations is suggestive of underlying pathological processes: CMBs associated with hypertension are distributed mostly in deep brain regions, and CMBs associated with cerebral amyloid angiopathy (e.g., in AD) predominantly develop in cortical-subcortical regions; the co-occurrence of both phenomena is not uncommon in elderly subjects (Poels et al. 2011).

It is worth repeating that co-occurring neuropathology is found in as many as about half of patients with AD and the evidence of co-existing causes of cognitive impairment (including that of vascular origin) is no longer used as an exclusion criterium for a diagnosis of AD (Brenowitz et al. 2017). In the regard of commonly overlapping symptoms undermining clinical expression of cognitive deficits, discriminating the vascular contribution from neurodegenerative etiology has become a common clinical issue where MRI plays an unprecedented role.

3.2.3.1 Fazekas scale

The severity of T2/FLAIR hyperintensities located in cerebral white matter can be quantified by application of an established visual rating scales such as the age-related WM changes scale (Wahlund et al. 2001) or the Fazekas scale (Fazekas et al. 1987). Qualitative assessment of periventricular and deep white matter hyperintensity (WMH) burden using the Fazekas scale on FLAIR/T2 images involves WMHs grading from 0-3 (0: absent; 1: punctate foci; 2: beginning confluence; 3: large confluent areas) **(Fig. 3.3)**. WMHs are foci of WM damage caused by vascular impairment or micro-angiosclerosis and their confluence in at least two regions, and the beginning of confluence in a further two regions that involve at least a quarter of the total WM, is sufficient to diagnose SVD (van Straaten et al. 2003).

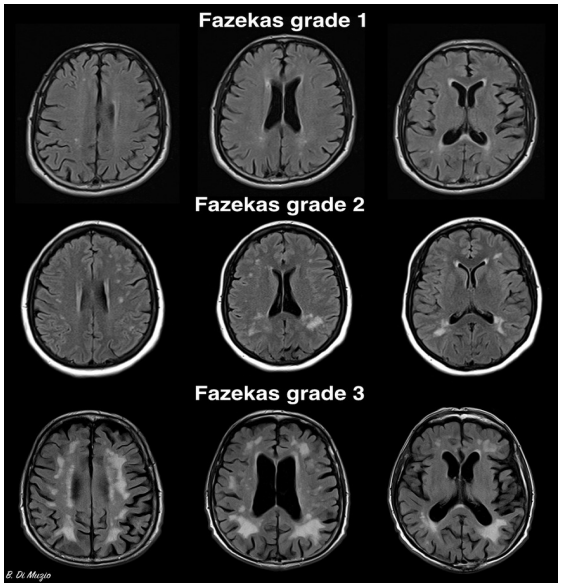

Fig. 3.3. Fazekas scale. Adapted from Radiopaedia.org, case courtesy of Dr Bruno Di Muzio, rID: 36927.

Although pathological studies suggest that WMHs may be primarily of ischemic nature as evoked by hypoperfusion, there is an emerging evidence that they may also reflect vascular deposition of beta-amyloid, particularly when distributed in posterior areas in patients with AD (Brickman et al. 2009). Nevertheless, age-related WMHs serve as robust radiological markers corresponding with cognitive decline, and when distributed in anterior brain regions, they are associated with deterioration in executive functions that is typical for normal aging. WMHs are found in 30-40% of all dementia patients (Asselin et al. 2019). Only minor cognitive decline has been observed in patients with the lower Fazekas score (Fazekas groups 1 and 2), whereas effect sizes in Fazekas group 3 seem to correspond with substantial deterioration in cognitive domains like social cognition, attention and memory (Kynast et al. 2018).

Regardless of the absence of consensus in the context of WMH association with AD, a growing number of studies confirm predictive value of increased total WMH volume in AD diagnosis, independently from amyloid positivity. Some of recent findings suggest that WMH volume rates may be associated with preclinical AD equally or more accurately than conventional AD biomarkers and cognitive tests (Provenzano et al. 2013) (Kandel et al. 2016). Nevertheless, current models emphasize that as the key manifestation of SVD, WMHs contribute to AD clinical presentation independently, regardless of an increasing awareness for its importance as a predictor of cognitive decline and dementia. Conversely, in the absence of MRI evidence of vascular damage, neurodegenerative etiology remains the most likely cause of cognitive decline and further evaluation of structural imaging should be focused on cerebral atrophy.

3.2.4 Cerebral atrophy assessment

While the properties of structural neuroimaging, such as excellent tissue contrast and high resolution allow for cerebral atrophy to be estimated accurately, visual assessment remains the primary method of scan interpretation in a clinical setting.

Global and regional brain atrophy is typically best identified on T1-weighted images; FLAIR and T2 images can be additionally used for the global evaluation. Coronal-oblique T1-weighted images are obtained in a plane orientated orthogonal to the long axis of hippocampi and parallel to the brainstem; images should be obtained with high resolution three-dimensional volume acquisition that can be reconstructed in all three planes. Thin-section coronal images enable the

reliable assessment of medial temporal lobe and hippocampal atrophy. Sagittal T1-weighted reconstructions are used for the evaluation of midline structures, as well as offer solid utility for rating parietal atrophy.

3.2.4.1 Visual atrophy rating scales

Several visual rating atrophy scores have been created to better utilise clinically relevant information and improve diagnostic accuracy in patients with cognitive deficits, using more structured approaches. Although primarily developed for research purposes, visual scales can be applied directly to a clinical set of images, usually without the need for additional software. A four-point or five-point scales are most commonly applied, with dichotomisation used to classify normal and abnormal scan appearance, where scale points 0 and 1 usually represent the degree of variation within the normal population, with points 2 and above describing pathological alterations (Harper et al. 2015). Visual scales that are widely used in a diagnosis of cognitive deficits focus on brain regions that are particularly susceptible to neuronal loss due to underlying pathology, and while offering the atrophy quantification at the individual level, they serve as potentially clinically applicable tools. The added value of combining scores from several visual rating in different brain regions may also increase the diagnostic value of these tools (Harper et al. 2016) (Yuan et al. 2019).

3.2.4.2 Focal lobar atrophy

Establishing diagnostic value of scales rating atrophy in patients with cognitive deficits is possible mainly due to the presence of patterns that are indicative of distinctive underlying processes, regardless of a certain degree of overlapping between conditions. Evidence of focal predominance in atrophy may serve as an initiating point narrowing the differential diagnosis (Harper et al. 2015).

3.2.4.2.1 Frontal lobe atrophy

In most cases, an asymmetrical pattern of atrophy or more anterior than posterior atrophy pattern, is associated with underlying FTLD pathology rather than AD pathology. Disproportionate frontal lobe atrophy is thus highly suggestive of FTLD (Harper et al. 2015). Clinical and anatomical differentiation within a broad syndrome category is related to a substantial variability

in the hemispheric distribution of atrophy, with predominantly extratemporal atrophy strongly asymmetric in Pick's disease group and relatively symmetrical in corticobasal degeneration – CBD, despite a clinical presentation suggesting asymmetrical correlation (Rohrer et al. 2011). Frontal atrophy in behavioural variant of FTD (bvFTD) may be either symmetrical or asymmetrical (with or without manifestation of additional temporal lobe atrophy) (Whitwell et al. 2013). Left posterior frontal and insular atrophy which may be limited to a subtle widening of the left sylvian fissure, is thought to be an anatomical discriminator in nonfluent forms of primary progressive aphasia – progressive non-fluent aphasia (Gorno-Tempini et al. 2011). In fact, each FTLD subtype pathological alterations may be associated with a variety of clinical presentations, although with different frequencies; clinical similarities therefore can arise from relatively distinct pathophysiological and neuroanatomical mechanisms (Gorno-Tempini et al. 2011) (Rohrer et al. 2011)

3.2.4.2.2 Temporal lobe atrophy

Distinctive patterns of neuroanatomic damage are characteristic for primary progressive aphasia subtypes: apart from left posterior fronto-insular regions affected in nonfluent forms, predominantly left anterior temporal regions are involved in the semantic dementia variant of FTD, and temporo-parietal regions in the logopenic variant (Gorno-Tempini et al. 2011). In general, asymmetric temporal atrophy is the key imaging feature in patients with dementia due to FTLD, but it can also be seen in patients with AD. Also, the presence of an anterior/posterior atrophy gradient in the temporal lobe is more suggestive of FTLD rather than AD (Harper et al. 2014).

Specifically, it is logopenic aphasia that has been found to be a result of AD pathology, contrary to the most of clinical syndromes associated with FTDL. It is characterised with the atrophy pattern extending from predominantly left temporal location to the posterior perisylvian and temporoparietal areas (Whitwell & Josephs 2012). In contrast to logopenic aphasia, posterior temporal structures are relatively preserved in semantic dementia, where atrophy is confined more anteriorly, and in the most severe form seen as ‘knife edge’ atrophy of the temporal pole, with selective loss of anterior fusiform gyrus volume (Gorno-Tempini et al. 2011). Conversely, the similar pattern of atrophy but located in right temporal lobe is most commonly detected in

bvFTD (Rascovsky et al. 2011). Initially significant asymmetry usually becomes less pronounced when bilateral temporal lobes become affected in the course progression of both bvFTD and semantic dementia (Harper et al. 2014).

3.2.4.2.3 Frontotemporal atrophy scales

Several frontotemporal atrophy scales that have been developed specifically for the differential purpose in the diagnosis of FTDL syndromes, were based on a postmortem staging scheme used to rate atrophy in FTD (Harper et al. 2015). The scale proposed by Davies et al., rating atrophy at the level of the anterior temporal lobe and the lateral geniculate nucleus, has been proven particularly useful in discriminating atrophy as the most important variable to predict prognosis in patients with bvFTD (Davies et al. 2006). The extended scale devised by Kipps et al, including additional atrophy rating of the posterior temporal lobe, appeared to be specifically sensitive to semantic dementia focal pattern of changes (Kipps et al. 2007). Later scales have been broadened to assess anterior atrophy more accurately, focusing on three regions — orbito-frontal, anterior cingulate and fronto-insular regions, all of them showing high potential for discriminating between neurodegenerative conditions (Davies et al. 2009) (Hornberger et al. 2010). In these studies, multiple brain regions emerged as relevant in the differential diagnosis of AD (temporal pole, anterior hippocampus, insula, orbitofrontal gyri), indicating the more diffuse pattern of atrophy (Harper et al. 2016).

3.2.4.2.4 Parietal and occipital lobe atrophy

The differential diagnosis for posterior cortical atrophy (PCA) in the parietal and occipital cortex involves CBD, DLB, and in the first place – AD, especially with co-existing mediotemporal lobe (MTL) atrophy. PCA is thought to be common in AD patients with typical and atypical clinical manifestation, and may assist in the clinical distinction of AD from other forms of dementia, particularly from FTLD. When combined with relative sparing of MTL, PCA seems to be characteristic for patients with atypical appearance (Koedam et al. 2011), especially in early-onset cases. Although mild hippocampal atrophy is usually present, atrophy of the posterior cingulum and the precuneus occurs to be the most characteristic finding in early-onset AD (Harper et al. 2014) (Lehmann et al. 2012). Less common causes of parietal atrophy may be associated with familial cases of FTDL with specific mutations, such as in patients with

progranulin mutation, in which apparent unilateral apparent frontoparietal atrophy extending into the temporal lobe has been described (Whitwell et al. 2012).

3.2.4.2.5 Visual rating of posterior atrophy

The Koedam scale measures PCA, assessed in sagittal, coronal and axial planes, focusing on the posterior cingulate sulcus, pre-cuneus, parieto-occipital sulcus and the cortex of the parietal lobes (Koedam et al. 2011). Separate scores are given in each imaging plane, separately for both hemispheres, and the highest score is acknowledged in the case of different scores in different planes. Based on a study population of AD and other dementias, the sensitivity and specificity of the Koedam scale for AD was 58% and 95%, respectively (Harper et al. 2015). When combined with MTL assessment, sensitivity of 73% and specificity of 87% has been reported for visual rating of PCA, confirming discriminative value in differentiating AD from FTD and normal ageing (Harper et al. 2014) (Koedam et al. 2011).

3.2.4.3 Focal hippocampal atrophy

Atrophy of the medial temporal lobe – the innermost part of the temporal lobe that includes the hippocampus, is the hallmark feature in the course of AD, and hippocampal atrophy has been incorporated in to diagnostic criteria as the most acknowledged and validated imaging biomarker of AD (Jack et al. 2011). Hippocampal atrophy in the preclinical stages was shown to predict the conversion to AD (Jack et al. 1999) (Wang et al. 2006) and the severity of cognitive deficits in MCI and AD appears to be correlated with the hippocampal volume (Sarazin et al. 2010).

Visual rating of MTL atrophy allows for distinguishing AD with high sensitivity and specificity when compared to control subjects (Westman et al. 2011). Less pronounced or absent atrophy of MTL structures, unusual in AD-related dementia, has been reported to be consistent with DLB (Harper et al. 2016). Nevertheless, if present in DLB patients, regional atrophy is suggestive of co-existing AD neuropathologic change and may predict a more rapid clinical course (Nedelska et al. 2015). Dopamine transporter imaging is therefore considered to be more efficient tool in distinguishing DLB from AD (Harper et al. 2014). Again, symmetrical pattern of MTL atrophy may also be seen in bvFTD along with frontal lobe pattern as the disease progresses.

3.2.4.3.1 Hippocampal sclerosis

Hippocampal atrophy accompanied with abnormal signal intensity (T2/FLAIR hyperintensity) is characteristic imaging feature of hippocampal sclerosis (HS) (Hanamiya et al. 2009). HS is the most common histopathologic abnormality found in adults with drug-resistant temporal lobe epilepsy (TLE) (Blümcke et al. 2013). The International League Against Epilepsy (ILAE) recognizes two main types of TLE: mesial temporal lobe epilepsy arising in the hippocampus, the parahippocampal gyrus and the amygdala, and lateral temporal lobe epilepsy arising in the neocortex at the outer lateral surface of the temporal lobe. The term HS is used to histopathologically define the pattern of selective neuronal cell loss with concomitant astrogliosis in the hippocampal formation (including the dentate gyrus) (Blümcke et al. 2013). Histopathologic subtypes of HS with examples of MRI findings in histopathologically verified types of TLE-HS are shown and described in detail in **Fig 3.4.** We further evaluate the effect of HS on hippocampal volumes in our study (**subchapter 4.4**)

It is worth mentioning, however, that the percentage of TLE-related reported MRI findings can vary notably from 25% to approximately 70% in a clinical setting, with highest scores found when patients were referred to tertiary epilepsy centers (Blümcke et al. 2013). When described in nonepileptic elderly patients, HS-like patterns of cell damage may be possibly related to anoxic or ischemic injury and neurodegeneration (Nelson et al. 2011).

3.2.4.3.2 Mediotemporal atrophy scales

MTL rating scales were initially created for the use with MRI as well as CT imaging (De Leon et al. 1997). In 1992 Scheltens et al. proposed a visual rating scale that has been incorporated in the research criteria for the diagnosis of AD (Dubois et al. 2007). The Scheltens scale has been applied in many studies and has served as the basis for additional scores, which have also been widely used.

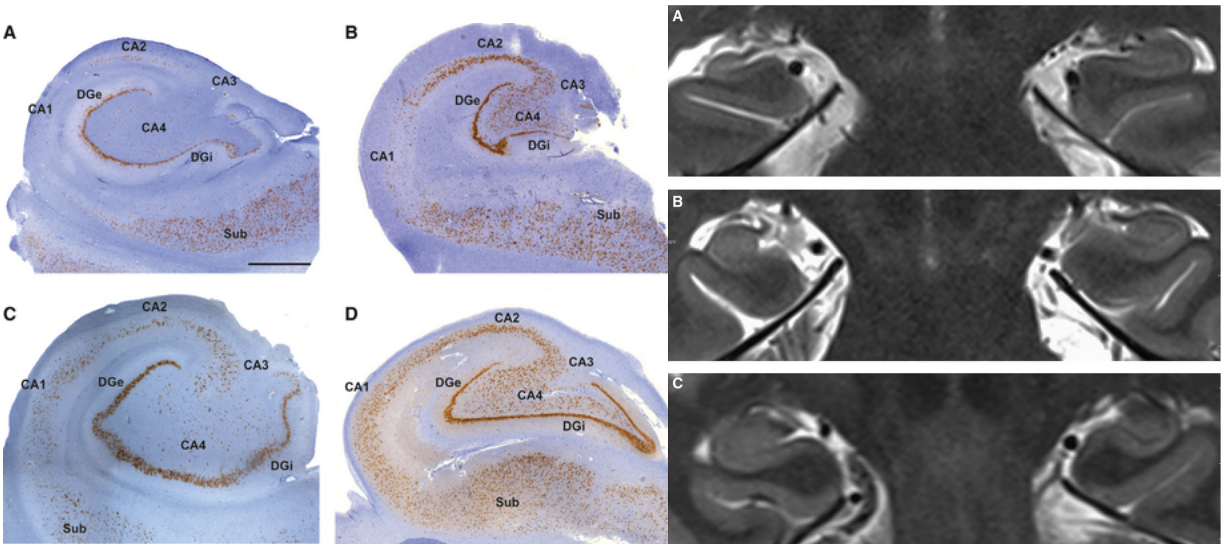

Fig. 3.4. *On the left*: Histopathologic subtypes of HS in patients with TLE. (**A**) ILAE HS type 1 shows pronounced preferential pyramidal cell loss in both CA4 and CA1 sectors (CA- cornu ammonis). Damage to sectors CA3 and CA2 is more variable, but frequently visible. Variable cell loss is also seen in the dentate gyrus, with abundant granule cell loss in the internal limb in this sample, and a transition with preservation of cells in the subiculum. (**B**) ILAE HS type 2 (CA1 predominant neuronal cell loss and gliosis): This is a rarer and atypical HS pattern characterized by neuronal loss primarily involving CA1 compared with other subfields where damage is often not really detectable by visual inspection (**C**) ILAE HS type 3 (CA4 predominant neuronal cell loss and gliosis): This is characterized by restricted cell loss mostly in CA4. (**D**) No HS, gliosis only: Microscopic inspection does not reveal significant cell loss in any of the hippocampal subregions (no-HS). DGe/DGI, external/internal limbs of dentate gyrus; Sub, subiculum. *On the right:* 3T MRI findings in histopathologically verified types of TLE-HS. Presurgical MRI findings in TLE patients with histopathologically classified HS on the right side (left on panel). (**A**) ILAE HS type 1. (**B**) ILAE HS type 2. (**C**) ILAE HS type 3. In these specific examples, volumetric loss is severe in ILAE HS type 1, moderate in ILAE HS type 2, but not detectable in ILAE HS type 3. Adapted with permission from (Blümcke et al. 2013).

The qualitative assessment of focal atrophy using the Scheltens scale is based on rating three hallmark features of MTL: the width of the choroid fissure, the width of the temporal horn of lateral ventricle and the height of the hippocampus (Scheltens et al. 1992) (**Fig. 3.5**). The score is graded from 0 to 4, where 0 means no hippocampal atrophy; 1: isolated widening of choroid fissure; 2: additional widening of temporal horn; 3: moderate loss of hippocampal volume; 4: marked widening of the choroid fissure, enlargement of the temporal horn and the severe loss of hippocampal volume and internal structure. Diagnostic sensitivity and specificity of MTL atrophy for AD were 81 and 67% in the original study, or much higher in numerous consecutive

reports using Scheltens scale in a clinical setting (Westman et al. 2011). The score of 2 for individuals older than 75 years of age is considered to be normal.

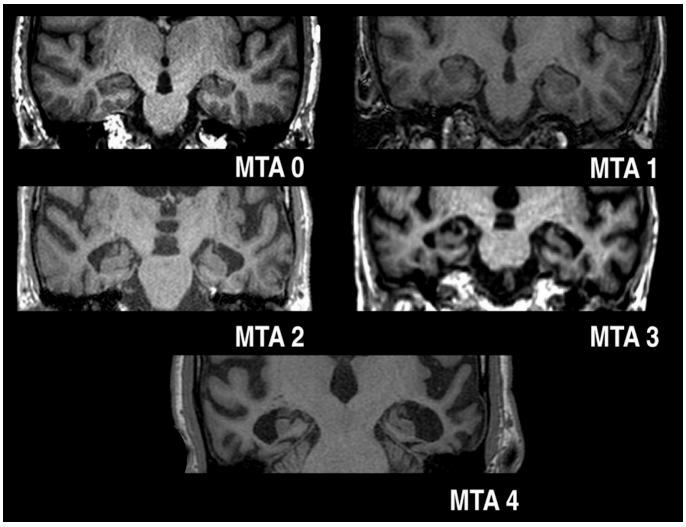

Fig. 3.5. Scheltens scale. Adapted from Radiopaedia.org, case courtesy of Dr Bruno Di Muzio, rID: 42027

The Scheltens scale is used a part of the extended rating scale proposed by Galton et al., that additionally incorporates medial non-hippocampal structures, as well as anterior and lateral regions; the complete Galton scale has been reported as helpful in a differential diagnosis (Galton et al. 2001). Later improvements on the clinical utility of the Scheltens scale include calibrated visual rating system using reference images for calibration of atrophy ratings in several discrete brain regions, including the entorhinal and perirhinal cortex (Urs et al. 2009). Further adaptations enable rating of MTL atrophy with the use of the axial plane images (Kim et al. 2014) or short inversion time inversion recovery images (Kaneko et al. 2012).

3.2.4.4 Generalised atrophy

Symmetrical generalised atrophy is commonly observed in AD and DLB, and may also accompany WM alterations in patients with VaD. Global brain atrophy without focal lobar volume loss is a typical finding on structural MRI studies in normal ageing, as one of the features associated with the accumulation of multiple age-related structural changes. These changes are highly heterogeneous in individuals and result in a variety of clinical cognitive manifestations (Harper et al. 2014). Assessment of these non-specific changes to determine whether they are

early indicators of neurodegenerative disease is challenging, because the findings in a normally aging brain can overlap with pathological findings in dementias.

Gradual decline of brain volume occurring in later decades of life may be visualized on MRI as dilatation of the cortical sulci that can be associated with cortical and subcortical grey matter (GM) as well as WM loss. A typical widening of the sylvian fissure, the basal cisterns, the ventricles and the interhemispheric fissures, along with increasing prominence of the perivascular spaces is commonly observed in older patients. In a normally aging brain the frontal lobes are usually affected first (related to deterioration of executive findings), followed by the parietal lobes atrophy and enlargement of the lateral ventricles with relative sparing the temporal horns; any change in the temporal horns is therefore suggestive of pathological finding in neurodegenerative disease.

The finding of ventricular enlargement that is disproportionate to cerebral atrophy may be suggestive of NPH. Ballooning of frontal horns and widening of temporal horns without evidence of hippocampal atrophy, accompanied by periventricular hyperintensities that are not attributable to microvascular ischemic changes or demyelination, are MRI (or CT) signs of NPH that may be decisive for the diagnosis and selection of shunt-responsive patients (Damasceno 2015). Further NPH-related features include thinning and elevation of the corpus callosum, with callosal angle between 40º and 90º (**Fig 3.6**) and aqueductal or fourth ventricular flow void. Ventricular enlargement can be measured with Evans index, which is the ratio between the maximal width of the frontal horns and the maximal width of the inner table of the cranium at the level of the frontal horns; or by an equivalent measure. In case of Evans index>0.3 ventricular enlargement is considered disproportionate and not entirely attributable to cerebral atrophy.

In NPH the ventricles are disproportionately more dilated than the cortical sulci, which are narrow or obliterated at the high convexity and midline, with local narrowing of the subarachnoid space surrounding the medial and outer brain surface (Fig. **3.6**) (Damasceno 2015) (Hashimoto et al. 2010). On this basis, the finding of dilated ventricles accompanied with relatively enlarged basal cisterns and Sylvian fissures may be misleading and challenging in the context of evaluation cerebral atrophy and differential diagnosis.

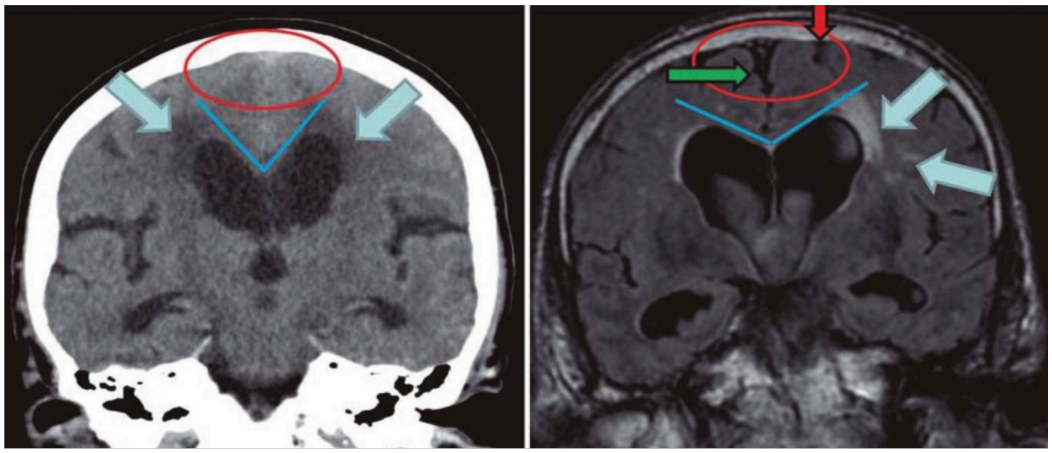

Fig. 3.6. Coronal head CT (left) and MRI (right) at the level of the posterior commissure: in the left image, the CSF spaces over the convexity near the vertex are narrowed (red circle), as are the medial cisterns - these are typical findings of NPH. On the right image, however, the CSF spaces over the convexity near the vertex (red arrow) and the medial cisterns (green arrow) are widened, a finding consistent with brain atrophy. The blue lines in both images indicate the callosal angle: an angle less than 90º is typical of NPH (left image), while an angle greater than 90º is typical of brain atrophy (right image). The blue arrows indicate periventricular signal alterations; the unilateral occurrence of these alterations (right image) suggests they are probably due to vascular encephalopathy. The abnormalities seen in the left image may well represent transependymal CSF changes due to NPH. Reproduced from (Damasceno 2015) (In turn citing from (Kiefer & Unterberg 2012), with permission.

3.2.4.4.1 Visual rating of global cortical atrophy

The qualitative assessment of global cortical atrophy on axial FLAIR images can be performed with the use of the Pasquier scale, also known as the global cortical atrophy (GCA) scale. The GCA scale is grading sulci diameters and gyri volumes in frontal, parieto-occipital and temporal regions, as well as assess ventricular system size (Pasquier et al. 1996). A visual rating scale developed by O'Donovan et al to assess ventricular enlargement has been used in a study distinguishing between AD and DLB with the use of the GCA scale, with scores confirming similar, general atrophy pattern in both groups of patients (O'Donovan et al. 2013). Practical implications associated with specifying multiple regions of interest (ROIs) has led to the development of the simplified scale to be primarily used as a component part of a larger diagnostic assessment (Harper et al. 2015). Comparing with other atrophy scales, GCA scale remains considered to be more confounded by age, as a result of extensive character of brain coverage, and the use of age-specific cut-offs may be needed to be improve a diagnostic value of the scale (Scheltens et al. 1997).

Rates of change in whole-brain volumes have been found to correlate with changes in cognitive performance, supporting their validity as markers of disease progression. Previous longitudinal studies that used time between initial and follow-up examination to model disease progression found whole-brain atrophy rates of 0.4–0.7% for cognitively normal older individuals and of 0.6–2.2% for AD patients (Dicks et al. 2019). It has been observed that these rates measured in AD (prior to developed dementia), have been estimated at 1.4–2.2% per year, whereas rates of atrophy during normal aging (for a mean age of 70 years) do not usually exceed 0.7% per year (Frisoni et al. 2010). However, contrary to the assumptions of many previous studies, whole-brain atrophy is not a linear (simply age-related) phenomenon and appears to accelerate in late onset AD during the transition stages to the MCI and AD dementia (Jack et al. 2008c).

3.2.5 Morphometric methods

As already reviewed, structural imaging can provide clinically useful information in patients with cognitive decline. Whereas gross atrophic changes can be assessed visually, a number of more advanced neuroimaging techniques such as volumetric quantification or automated classifier algorithms appear to be extensively reported in AD-related research and clinical trials (Harper et al. 2015). The design of brain morphometric studies depends on multiple aspects that can be categorized variably, due to the possibility of analysing brain properties at different scales (e.g., in the whole brain, regions of interest, cortical or subcortical structures), or even between different modalities. Furthermore, studies can be longitudinal (within the same brain, measured at different times) or cross-sectional (across brains). And finally, the data can be subjected to a wide range of distinctive approaches and tools for image processing and analysis steps.

3.2.5.1 Rates of change in whole-brain volume

Mapping of the dynamic change in cerebral atrophy, associated with a measurement of global brain volume over time, can be achieved by a number of methods; some of them serve as on-site developed techniques (Josephs et al. 2008), some are applied on a larger scale with the use of software packages (Sluimer et al. 2010). Some of these packages are commercially available or under General Public License (GNU), like Structural Image Evaluation, using Normalisation, of Atrophy (SIENAX), part of FSL (FMRIB Software Library (Smith et al., 2002) (http://www.fmrib.ox.ac.uk/analysis/research/siena/) (described in **Chapter 4.1.1 – Methods**).

3.2.5.2 Voxel-based morphometry (VBM)

Whereas whole-brain atrophy is not specific to AD (or even to neurodegeneration), it is the pattern of GM loss or cortical thinning that has been found to be more disease specific and correlating cross-sectionally and prospectively with clinical symptoms (Frisoni et al. 2010) (Apostolova & Thompson 2008). GM atrophy modelled as a function of time in patients with abnormal baseline amyloid has been shown to occur faster in temporal lobes in AD dementia, while frontoparietal areas seem to be involved also in prodromal AD when GM volumes were modelled with age (Dicks et al. 2019).

The most popular morphometric method that can simultaneously visualize group differences or statistical effects on GM (and WM), throughout the whole brain is known as Voxel-based morphometry (VBM) (Ashburner & Friston 2000) (Good et al. 2001). VBM was primarily developed to investigate voxel-wise differences in the local GM volume between several populations, or in one population related to one clinical score. While measuring structural differences among populations, VBM is sensitive to differences derived from a comparison of the local composition of various brain tissue types (e.g., GM, WM, CSF), while removing positional and large-scale volume differences, down to a specified spatial scale (Ashburner & Friston 2001). This approach is unbiased, and requires no a priori information about the location of these possible differences in the GM. VBM is available for many of the major neuroimaging software packages, like Statistical Parametric Mapping (SPM) or FSL (FMRIB Software Library, http://www.fmrib.ox.ac.uk/fsl, more detailed description is covered in **Chapter 4.1** Methods) and it provides an efficient tool to test or generate specific hypotheses about brain changes over time.

In general, image registration is the process of transforming different sets of data into one coordinate system, and this step is necessary for any kind of inter-subject comparison. In order to compare the structural MRI brain images on a voxel-wise basis, they first need to be transformed into a standard space (usually Montreal Neurological Institute template MNI152 – a standard space average of 152 brains), which involves the use of non-linear registration (Andersson et al. 2007). The classical VBM approach initially segments the brain into three tissue classes – GM, WM and CSF, then aligns GM individual maps to a common space and averages the data of all

subjects while retaining information on the variability of each study group. GM images are smoothed to reduce the confounding effects of individual morphological differences while retaining the global disease associated changes (Apostolova & Thompson 2008).

The local differences in GM density (or volume) can be subsequently statistically analysed across scans at the voxel level via general linear modeling (GLM) techniques and further interpreted in anatomical terms (e.g., as GM atrophy). VMB has been proven to be a useful method in assessing GM volume changes when comparing AD patients with healthy controls (Baron et al. 2001), especially when correlated with poor cognitive performance (Kim et al. 2011b).

Nevertheless, the interpretation of the results obtained with the traditional voxel-wise techniques was considered to be problematic and the approach criticised for its limitations. Possible bias has been associated with difficulties to determine if the observed local differences in GM distribution effectively mirror reduced cortical thickness or reflect different gyrification patterns resulting from the misalignment of the gyri and sulci (Douaud et al. 2007). The newer generation of VMB approaches addresses this issue by modulating the voxel intensity of the spatially normalized GM maps to correct for local expansion (or contraction) due to the non-linear component of the spatial transformation. As a result, the final modulated voxel contains the same amount of GM as in the native pre-registered grey matter map (Douaud et al. 2011) (Apostolova & Thompson 2008). However, even with the improved design, the amount of spatial smoothing used in VBM remains the limiting factor in the interpretation of results. Digital filtering of GM maps is a step necessary to counterbalance the inter-individual differences in images that allows for easier detection of systematic, global disease-induced effects as opposed to individual variability; nevertheless, it occurs at the expense of blurring of focal changes (Apostolova & Thompson 2008).

3.2.5.3 Tensor/deformation-based morphometry (DBM)

Whereas VMB is still currently widely used, some other alternatives exist. Deformation-based morphometry (DBM) is a fully automated, voxel-based method that can objectively analyze local expansion or shrinking of brain tissue in any brain area (Ashburner et al. 1998). DBM evaluates

information contained within the vector field generated by the nonlinear warping of an individual MRI scan to a reference template (Lau et al. 2008). In contrast to VBM, DBM does not require segmentation of the brain into different tissue compartments and the statistical analyses are not performed on the registered voxels but on the deformation fields used to register them (which requires multivariate approaches) or derived scalar properties. One common variant, referred to as Tensor-based morphometry (TBM), is based on the Jacobian determinant of the deformation matrix. Color-coded Jacobian maps, which show the local expansion or compression factor at each point in the image, indicate local volume loss or gain relative to a reference image (Hua et al. 2008).

The biggest advantage of DBM with respect to VBM is its ability to detect subtle changes in longitudinal studies. TBM has been shown to be useful at the very early stages of dementia before severe cognitive decline emerges, as well as in longitudinal studies where the progression of MCI to AD has been predicted (Hua et al. 2008). DBM/TBM allows for efficient analysis of large datasets; nevertheless, its limitations include the long computation time required to produce the results and the special expertise required for the analysis (Tuokkola et al. 2018).

3.2.5.4 Surface-based morphometry (SBM)

Alternatively, numerous studies have adopted surface-based morphometry (SBM) and utilized primarily surface-based morphometric tools. FreeSurfer (http://surfer.nmr.mgh.harvard.edu) is the most popular software that has been primarily developed to generate surface representations of the cerebral cortex. It runs on a wide variety of hardware and software platforms, and is open source.

Historically, evolution of FreeSurfer started with improvements of models focused on topological accuracy (of both the GM/WM boundary, as well as the pial surface to measure cortical thickness and volume) (MacDonald et al. 2000), through deformable surface approach (Fischl et al. 2001), with subsequent focus on corrections of topological defects to obtain accurate surface models. Practically, FreeSurfer uses the 3D T1-weighted images to locate the pial and WM surface of the cortex and the distance between these surfaces reflects the vertex-wise thickness of cortical areas.

FreeSurfer surface models have been proven to provide an excellent basis for the analysis of the properties of the cerebral cortex (but not for subcortical and ventricular structures – for this purpose further wide array of image analysis tools and algorithms have been developed) (Fischl 2012). Besides good performance, FreeSurfer owes its popularity to possibility of its integration with other toolkits, such as the extensive FMRIB software library (FSL) (Smith et al. 2004). Numerous studies on cognitive deficits have adopted SBM approach to assess morphometric parameters, such as cortical thickness to detect atrophy patterns in normal aging (Salat et al. 2004), MCI, AD and other dementias (Möller et al. 2016). Recently proposed machine learning-based method with a use of SBM classifier showed high sensitivity and specificity for both discriminating AD from normal controls and prediction of disease progression (Lee et al. 2018).

3.2.6 Computational anatomy and diffeomorphometry

Development of computational anatomy (CA) techniques for brain morphometry have been at the forefront of neuroimaging studies of neurodevelopment and neurodegeneration (Ceritoglu et al. 2013). At the heart of these techniques is the modeling of anatomical structures considering their complexity and the large variation between individuals. CA methods include newer metrics and more subtle descriptors to create maps of structural differences throughout the brain without manual interaction with images (Apostolova & Thompson 2008). The metric structures in CA are related to morphometrics, with the distinction that CA focuses on an infinite-dimensional space of coordinate systems transformed by a diffeomorphism, hence the central use of the terminology diffeomorphometry. The diffeomorphometry metric of CA measures how far two diffeomorphic changes of coordinates are from each other, which in turn induces a metric on the shapes and images indexed to them (Miller et al. 2014).

Diffeomorphic registration, since its introduction in the 90's (Christensen et al. 1996) has been playing an important role in computational procedures for constructing correspondences between dense coordinate systems such as ANTS – Advanced Normalization Tools (Tustison et al. 2014) or LDDMM – The Large Deformation Diffeomorphic Metric Mapping (Miller et al. 2002). VBM approaches are built on many of these principles.

3.2.7 Assessment of subcortical structures – different approaches

The oldest image analysis approach for structural MRI applied in dementia research is the region of interest (ROI) technique that measures the total volume of specific brain structures. It depends on manual delineation of the regions or structures of interest on each consecutive image slice, followed by calculating the overall volume of the structure, which is then used for statistical analysis (Apostolova & Thompson 2008). Manual evaluation of subcortical structures, such as the hippocampi (de Leon et al. 1993) (Korf et al. 2004) and the amygdala (Horínek et al. 2007) has been shown to be a sensitive but time-consuming and operator-dependent technique to assess subcortical atrophy. Additionally, analyses using this approach require an accurate *a priori* hypothesis and well-established tracing protocol, therefore they often tend to be limited to one or two structures of interest. Trained specialists performing manual segmentations of subcortical structures need to rely on a prior knowledge of shape, image intensities and shape-to-shape relationships (Patenaude et al. 2011).

In recent decades, automatic segmentation approaches, specifically tuned for detecting and localizing subcortical atrophy have become widely available (Chupin et al. 2009) (Patenaude et al. 2011). While many quantitative MRI studies on subcortical GM nuclei have defined a single measure of structural volume, the shift has been prompted towards methods obtaining specific information about subregions of atrophying structures (Ceritoglu et al. 2013). This approach is considered to be particularly useful in determining whether MRI morphometric results correlate with neuropathologic or clinical features, and with other structural changes, as well as to more precisely define the sub/regional distribution of volume loss (discussed in more detailed in **Chapter 4.1.2 -4.1.3**).

Statistical shape models have been established as a robust segmentation tools, starting with early 2D models to widespread utilization of 3D models, and associated with breakthroughs in automatic detection of shape correspondences (Heimann & Meinzer 2009). The subcortical segmentation in methods utilizing Active Shape Model (ASM) or Active Appearance Model (AAM), which relies on learning anatomical information (vertices/control points or intensity distribution) from pre-segmented training datasets, can be handled in the Bayesian framework by solving a maximum a posteriori estimation problem. An implementation of this method, called FIRST (FMRIB's Integrated Registration Segmentation Toolkit), is distributed with FSL

package (described in **subchapter 4.1.1**). When analysing differences in subcortical structures shape between different groups, it is possible to show the *location* of changes in these structures, additionally to changes in their overall *volume.* Further differences in vertex locations provide a direct, local measure of geometric change in a structure between groups that, unlike VBM, is not dependent on tissue classification methods or arbitrary smoothing (Patenaude et al. 2011).

Besides ASM and AAM methods, numerous other approaches apply automated segmentation of subcortical structures. These approaches can be surface-based, volumetric-based or frequently – the combination of different methods.
Likewise, CA methods have also been used to demonstrate localized shape differences in subcortical structures in multiple neuroimaging studies. Analyses based on LDDMM framework have been proved to be particularly useful for studying changes in subcortical nuclei in normal aging, AD and other conditions (Qiu et al. 2008) (Ceritoglu et al. 2013). Many authors proposed combined approaches, such as FreeSurfer subcortical labeling in the LDDMM template-based segmentation (Khan et al. 2008), or the use of LDDMM in SBM pipeline (Miller et al. 2012). Numerous complementary analyses (VBM, ROI-based, and surface-based hippocampal shape analysis) have shown correlations between regional atrophy and their scores for episodic memory (Sarazin et al. 2010).

3.2.8 Machine learning-based utility of atrophy patterns

Reassuming, patterns of brain atrophy measured using MRI have been successfully utilized as biomarkers of AD. On this basis, it is worth to conclude that in recent years, there has been a growing interest in machine learning techniques for brain image analysis that can further aid the diagnostic process in AD and other dementias. Development of the classifiers for AD-specific atrophy similarity measure has become a novel approach for the prediction of dementia risk and for the evaluation of AD trajectories on the individual subject levels (Lee et al. 2018). However, due to complex and variable patterns of brain atrophy, defining a proper similarity measure between individuals is a challenging process, and automatic methods for AD classification require a large number of structural data. For this purpose, MR volumes provided by Alzheimer's Disease Neuroimaging Initiative (ADNI) are commonly utilized (Cuingnet et al. 2013).

In short terms, any supervised machine learning algorithm is “trained” to produce a desired output from a set of input (training) data. The classification algorithm is therefore used to learn the mapping function from the input to the output and the goal is to approximate the mapping function so well that with the introduction of new input data output can be easily predicted. Classification methods in imaging data provide a general framework to classify individual subjects, using arbitrary features defined e.g., on the 3D cortical surface or volumetric features (Lee et al. 2018). Numerous supervised machine learning frameworks have successfully demonstrated the discriminating power of cortical and subcortical atrophy patterns for AD diagnosis (Cho et al. 2012). Likewise, also semi-supervised learning approaches (in a learning procedure using unlabeled data in conjunction with labeled data for improving the classification performance) have been used to show early AD conversion prediction in MCI subjects (Moradi et al. 2015). Support vector machine (SVM) is a relatively common learning model of classification for brain image analysis in AD (Cuingnet et al. 2013). It allows to capture complex multivariate relationships in the data and SVM classifiers have been reported to show high sensitivity and specificity in discriminating AD from healthy controls (Klöppel et al. 2008) (Vemuri et al. 2008) and other dementias, such as FTLD (Davatzikos et al. 2008).

3.3 Patterns in DTI data

As shown in the previous part of the proposed thesis, structural MRI studies appear to have high sensitivity and specificity in the diagnosis of AD. The ongoing research on a variety of other advanced MRI approaches is continually providing further insight into the pathomechanism of the disease. Among those, diffusion tensor imaging (DTI) permits a quantification of water diffusion in the brain in a manner that reflects the tissue microstructure. In particular, DTI provides information about the direction and the magnitude of water diffusion within tissues, and various parameters that are related to different aspects of the tissue microstructure can be used to quantify diffusion. Hence, it has become a promising approach for the identification of biomarkers of distinctive disorders that affect the central nervous system (Szabó et al. 2012) (O'Dwyer et al. 2011) (Hattori et al. 2012a). Notably, a number of studies supported a growing role of DTI and tensor-derived parameters in the assessment of microstructural WM integrity in MCI and AD. Parts of the following subchapter has been previously reviewed by (Stěpán-Buksakowska et al. 2012).

3.3.1 DTI basics

The main concept of DTI is based on measuring differences in the magnitude of diffusion of water molecules within the brain (Basser & Pierpaoli 1996) (Moseley et al. 1990). The basic measured quantity is the diffusivity or apparent diffusion coefficient (ADC) that is expressed in units of mm^2/s. Diffusion can be otherwise described as isotropic (the same in all directions, e.g., approximately in CSF) or anisotropic (when varies with direction). The nature of water diffusion in WM fibre tracts is highly anisotropic and the utility of DTI relies in the detection of in vivo microstructural WM alterations by taking advantage of this feature. Beaulieu et al. described the essential role of the membranes as predominantly responsible for the anisotropy of molecular diffusion in WM tracts by experimentally eliminating a dominating role of fast axonal transport, axonal cytoskeleton of neurofilaments and microtubules, and local susceptibility-difference-induced gradients (**Fig.3.7**) (Beaulieu 2002). Moreover, anisotropy seems to be additionally modulated by the degree of myelination of the individual axons.

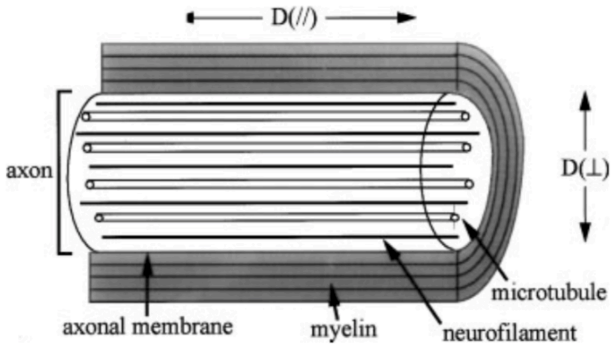

Fig. 3.7. A simplistic schematic of the longitudinal view of a myelinated axon. Myelin, the axonal membrane, neurofilaments and microtubules (associated with axonal transport) are all longitudinally oriented structures that could hinder water diffusion perpendicular to the length of the axon and cause the perpendicular diffusion coefficient to be smaller than the parallel diffusion coefficient. Reproduced with permission from (Beaulieu 2002).

In GM, where the measured apparent diffusivity is largely orientation-independent (i.e. isotropic, or more precisely – with a minor degree of anisotropy), the scalar ADC is usually adequate to characterize the diffusion of molecules (Basser & Jones 2002). Conversely, while ADC is insufficient to characterize the orientation-dependent water mobility in WM, a more complex model of *diffusion tensor* has been proposed to describe the variability of diffusion in each voxel (volumetric pixels).

Mathematically, the diffusion tensor can be described as a 3×3 symmetric, positive-definite matrix and can be modelled by an ellipsoid that represents an isosurface of (Gaussian) diffusion probability (**Fig. 3.8**). The diffusion ellipsoid can be characterized by 3 orthogonal (mutually perpendicular) eigenvectors that represent the orientations of the main axes and 3 eigenvalues ($\lambda 1$, $\lambda 2$, $\lambda 3$) that refer to the magnitude of the diffusion along each axis. The major eigenvector of the diffusion tensor points in the principal diffusion direction (the direction of the fastest diffusion).

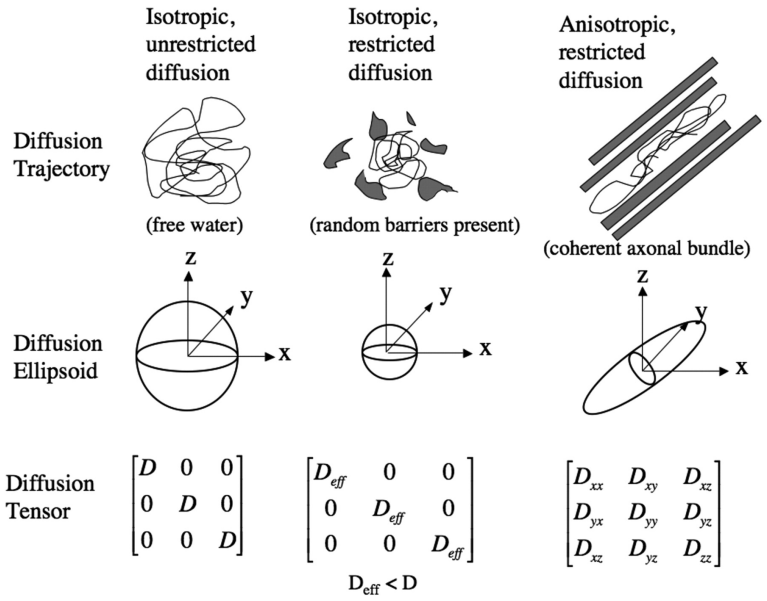

Fig. 3.8. The diffusion ellipsoids and tensors for isotropic unrestricted diffusion, isotropic restricted diffusion, and anisotropic restricted diffusion. Reproduced with permission from (Mukherjee et al. 2008).

In order to measure diffusion using MRI, magnetic field gradients are applied to create an image that is sensitized to diffusion in a particular direction (with the use of the standard gradient coils, in MR spin-echo image acquisition scheme). By employing magnetic field gradients prior to and after the 180° rephasing pulse, the first gradient dephases all spins, while the second gradient rephases only those spins that remained stationary. Conversely, spins that diffused in a direction parallel to the diffusion gradient cannot be completely rephased due to a different magnetic field during the second gradient. This results in a local signal attenuation. In more colloquial terms – diffusion weighting is achieved by introducing extra gradient pulses that "cancel out" stationary water molecules and cause a random phase shift for molecules that diffuse (O'Donnell & Westin 2011). By repeating this process of diffusion weighting in different, multiple directions, a 3D diffusion model (the tensor) can be estimated. The signal loss can be measured by solving Stejskal-Tanner equation (Stejskal 1965) (Le Bihan 1995) and visualised as darker voxels in MR images – voxels of WM tracts parallel to the applied gradient direction appear dark in the diffusion-weighted image for that direction. To calculate the tensor, at least 6 diffusion-weighted images (acquired by non-collinear motion probing gradients) and at least one non-diffusion-weighted image need to be obtained (Ni et al. 2006) (**Fig. 3.9**).

Diffusion-weighting by a pair of strong gradient pulses is associated with a number of imaging parameters unique to diffusion imaging, such as the magnitude (b-value), orientations, as well as the number of the least diffusion-weighted images (so-called b = 0 images). The majority of DTI studies use b-values in the range of 700–1000 s/mm^2 (Tournier et al. 2011).

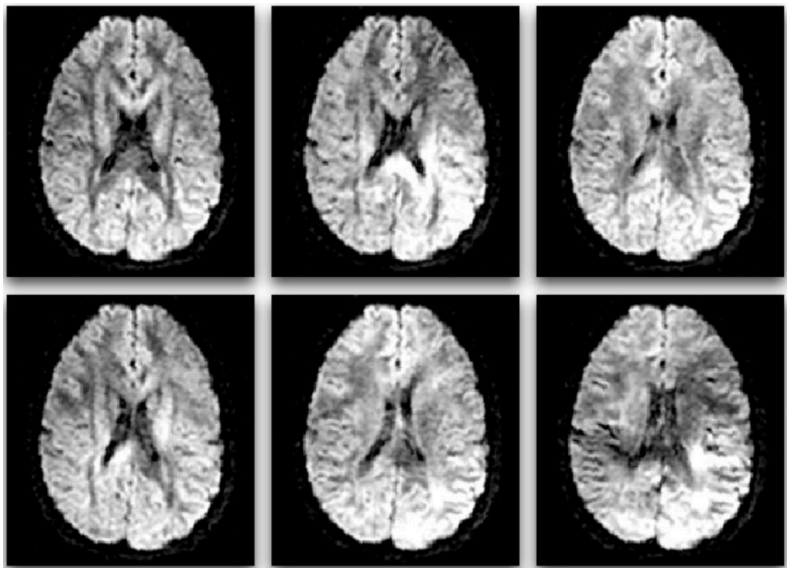

Fig 3.9. Six diffusion-weighted images (the minimum number required for tensor calculation). In diffusion MRI, magnetic field gradients are employed to sensitize the image to diffusion in a particular direction. The direction is different for each image, resulting in a different pattern of signal loss (dark areas) due to anisotropic diffusion. Reproduced with permission from (O'Donnell & Westin 2011).

3.3.1.1 Diffusion tensor parameters

One of the greatest advantages of DTI lies in its utility in evaluating the complex nature of WM microstructure with the use of several relatively simple quantitative measurements that can be derived from the tensor (Le Bihan et al. 2001). The average of the tensor's eigenvalues – referred to as the mean diffusivity (MD), describes the overall extent of water diffusion in a voxel. MD is orientation-independent and can serve as a marker of WM ultrastructure. The measure of diffusivity parallel to the principal diffusion direction (λ1, L1, also called the axial diffusivity – AD, or longitudinal diffusivity – LD) is equal to the largest eigenvalue. The perpendicular diffusivity measure (PD, also called the radial diffusivity – RD) is equal to the average of the two

smaller eigenvalues (λ2+λ3)/2). LD is thought to be a putative axonal damage marker; whereas RD is considered to be sensitive to the degree of restriction that diffusing water molecules experience due to the presence of axonal membranes and myelin (Song et al. 2002) (Song et al. 2003). Both these measures can be roughly interpreted as diffusivity parallel to and perpendicular to WM fibre tracts, most effective in regions of coherently oriented axons with little effect of fibre crossings. The fractional anisotropy (FA) is the most widely used tensor-derived measure, considered to be a measure of WM integrity. FA provides information on the directionality of the diffusion tensor, reflecting WM ultrastructure determined by axonal fibre packing, as well as degree of myelination and axon diameter (Beaulieu 2002). While FA literally measures the *fraction* of the diffusion that is *anisotropic* (that ranges from 0 to 1) (Basser & Pierpaoli 1996), it constitutes a normalized variance of the eigenvalues:

$$FA = \frac{1}{\sqrt{2}} \frac{\sqrt{(\lambda_1 - \lambda)^2 + (\lambda_2 - \lambda)^2 + (\lambda_1 - \lambda)^2}}{\sqrt{\lambda_1^2 + \lambda_2^2 + \lambda_3^2}}$$

In case of all 3 eigenvalues being equal in size (λ1= λ2= λ3, the same amount of diffusion in all directions – e.g., CSF) FA is 0. If one eigenvalue is much larger than the other two (λ1> λ2=/> λ3 that indicate one direction of preferred diffusion, e.g. parallel to WM fibres) FA becomes closer to 1 (Basser & Pierpaoli 1996). In practice, acquiring more diffusion directions can result in a more precise estimation of this diffusion tensor: based on Monte Carlo simulations, it has been established that minimally 20 gradient directions for FA and at least 30 gradient directions are required for robust MD calculation (Jones 2004).

3.3.1.2 Tensor maps and maps of diffusion metrics

There are several methods to visualize the large amount of data obtained with DTI in a clinical setting or for further analyses. Tensor-derived metrics can be displayed as 2D color or grey-scale images; the major and minor eigenvalues may also be displayed in this fashion. The color scheme that is most commonly used to represent the orientation of the major eigenvector has been established in a following manner: blue is superior-inferior, red is left-right, and green is anterior-posterior (Pajevic & Pierpaoli 1999) (**Fig.3.10**). The image intensity can be modulated, e.g. with the fractional anisotropy image.

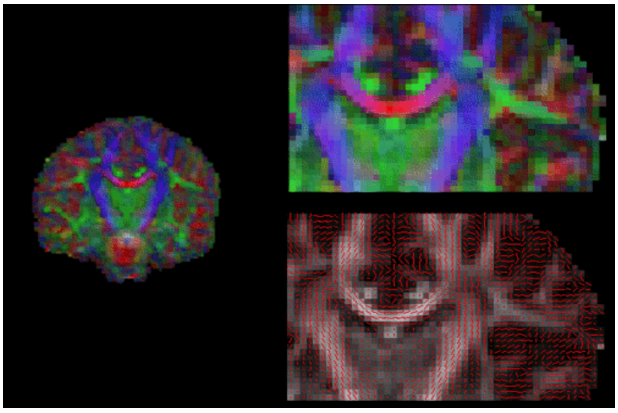

Fig.3.10. Example of visualizing the principal tensor direction with the use of FSLView (part of FLS FSL software package – FMRIB Software Library, http://www.fmrib.ox.ac.uk/fsl). Reproduced from http://ftp.nmr.mgh.harvard.edu/pub/dist/freesurfer/tutorial_packages/OSX/fsl_501/doc/fslview/dti.html.

3.3.2 Advanced diffusion imaging methods

It is important to note that all tensor-derived parameters are indirect measurements, based on the oversimplified diffusion tensor (DT) model that assumes there is a unique orientation of the fibers in each voxel, the direction of which is represented by the tensor's main eigenvector (Tournier 2014). Whereas this assumption is valid in homogeneous WM regions, where fibres have predominantly the same orientation (therefore diffusion can be adequately described with the use of DT), this model may not be sufficient in case of crossing fibers – regions in which the fibers orientation is not unique, i.e. when the fibers are interdigitating, curving, bending or diverging (Tournier et al. 2007).

This limitation has led to the development of new techniques that address this issue and that attempt to estimate the component fibres either discretely or as a fibre orientation distribution (FOD). This can be achieved with the use of multi-tensor approaches, spherical deconvolution, constrained spherical deconvolution, or from the angular dependence of the diffusion profile (Lazar 2010). Different functions have been proposed to express this angular dependence, including the Orientational Distribution Function (ODF) (Tuch 2004).

Multi-tensor and deconvolution methods routinely employ a High Angular Resolution Diffusion Imaging (HARDI) acquisition, where data is acquired on a spherical shell in the diffusion space (i.e., the q-space) and diffusion-weighted images are obtained for a large number of different encoding direction (e.g., over 60) at a single b-value that is usually higher (Tournier et al. 2007).

High order techniques such as diffusion spectrum imaging (DSI) or Q-ball imaging (QBI) (**Fig. 3.11**) can estimate ODF from HARDI data in several distinctive mathematical manners. ODF can be also estimated with the use of the diffusional kurtosis (DK) approximation of the diffusion signal that is decomposed into two components representing the Gaussian and non-Gaussian diffusion contributions, respectively (Lazar et al. 2008). Diffusion kurtosis imaging (DKI) characterizes the departure from Gaussian diffusion using a fourth order tensor (the kurtosis tensor) that requires a relatively limited number of diffusion measurements and b values no higher than 2500 s/mm^2. Nevertheless, the method has several limitations, such as less accurate estimation of the fibre directionality when fibres are crossing at small angles (Lazar et al. 2008) (Lazar 2010) (**Fig. 3.11**).

3.3.3 White matter tractography

To date, numerous algorithms have been developed to generate 3D representations of axonal fibres that estimate the connectivity patterns between different brain regions from the continuity in the local estimates of fibre direction at each voxel. These techniques are referred to as WM/fibre tractography and can be generally classified in deterministic, probabilistic, and global optimization algorithms.

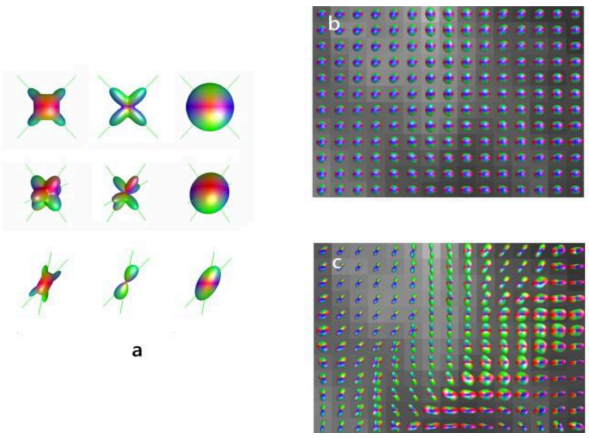

Fig. 3.11. ODF reconstructions using QBI and DK-ODF methods for different fibre configurations: (a) ODF reconstructions of two and three simulated fibers crossing at large angle (top two rows) and of fibers crossing at 30 degrees (bottom row) using DK-ODF, Q-ball, and diffusion tensor methods (from left to right). The original fibre directions are indicated by lines. (b) Diffusion tensor and (c) DK-ODF maps of the intersection between fibres. Reproduced with permission (Lazar 2010).

The *deterministic* algorithms create a unique trajectory (propagation direction) for each starting point or seed, resulting in a path that connects two distinctive brain regions. This process includes seed selection, fibre trajectory termination and fibre selection strategies (described in **Fig. 3.12**) (Lazar 2010). Conversely, the *probabilistic* algorithms characterize the uncertainty in fibre path estimation by generation of multiple possible trajectories for a seed point. Essentially, these algorithms connect the seed point with a set of voxels (in different brain locations) using weights that define the relative connectivity (Friman et al. 2006) (Lazar 2010) (Parker et al. 2003). Finally, *global optimization* algorithms generate the most optimal path between two brain regions by minimizing a cost function describing the features of the path to the underlying diffusion signal (Kreher et al. 2008).

Overall, WM tractography is considered to be a more postprocessed representation of DTI data than visualization of tensor maps and maps of metrics; however, although useful in tract visualization, all these methods are computationally demanding and more prone to errors – especially in voxels that contain crossing fibres (Lazar 2010). The limitations include the requirements of user-defined ROIs and threshold values, which affect the number of fibers tracked and the degree of noise effects.

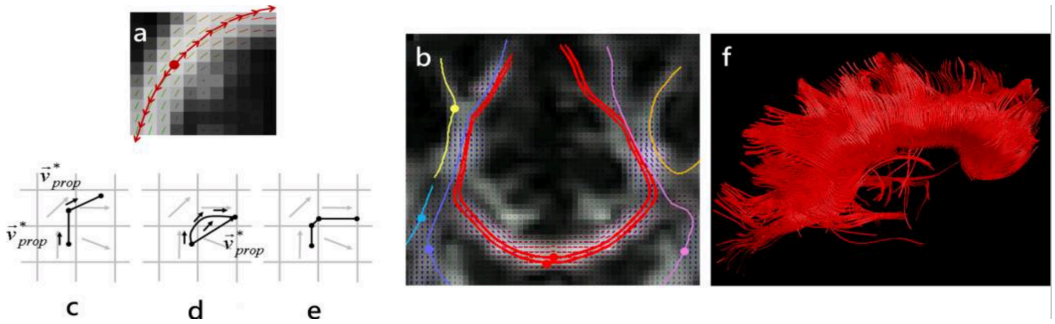

Fig. 3.12. (a) and (b): Fiber trajectories are obtained by following fiber direction estimates from voxel to voxel; the trajectory is initiated in both forward and backwards vector field directions starting at a "seed" point (indicated by a dot) ; (c)–(e) Several strategies may be used to step along the trajectory including a constant step size with the propagation direction estimated at the beginning of the step (c) or along the step (d), or a variable step size (Fiber Assignment by Continuous Tracking – FACT, (e)); (f) Tractography reconstruction of the corpus callosum obtained from seeds situated in the mid-sagittal region of the tract. Reproduced with permission from (Lazar 2010)

3.3.4 Tract-based Spatial Statistics (TBSS)

Remaining issues of reproducibility and inter-subject comparisons of diffusion parameters can be partially resolved with the use of whole-voxel techniques. As WM fibres lose integrity due to underlying pathological processes that affect axonal density and homogeneity, changes in the diffusion characteristics of water molecules can be reflected in distinctive diffusion tensor-derived metrics.

Tract-Based Spatial Statistics (TBSS) is an automated method that allows for performing multi-subject statistical testing on these diffusion-related parameters; misalignment issues are solved with restricting analysis to the core of the fibre bundles, represented by the local maxima of FA (Smith et al. 2006) – described in more detail in **subchapters 4.3** and **4.4**. TBSS aims to improve the sensitivity, objectivity and interpretability of multi-subject analyses, as it combines advantages of voxel-based approaches (enabling evaluation of the whole brain without an a priori predefining voxels or tracts of interest) with advantages of tractography-based approaches (estimating FA from relevant voxels). Moreover, while tractography measurements are derived from averaging values over all voxels within an individual WM tract, which can possibly exclude discrete areas of difference, TBSS can quantify DTI-based WM alterations throughout the entire brain without an a priori hypothesis, and at the same time detect different patterns of abnormality within individual tracts. This doctoral thesis includes two studies that further demonstrate the utility of TBSS approach in defining patterns of WM alterations in AD and NPH (subchapter **4.2** – partially, **subchapter 4.3**), as well as in TLE (**subchapter 4.4**).

3.3.5 DTI patterns in AD and MCI

DTI patterns in AD and MCI – approaches:

Numerous studies have revealed altered diffusion metrics in AD, and over the years, different approaches have been used to evaluate these parameters. Earlier investigations tended to restrict the analysis to certain brain regions (Bozzali et al. 2002) (Choi et al. 2005) – an approach that is highly hypothesis-driven, and cross-study comparisons are difficult. Progressively, conventional ROI approaches have been further extended to the whole brain using VBM style analysis (Teipel et al. 2012) (Xie et al. 2006) (Medina et al. 2006) or *TBSS approach* restricted to the core of the

fibre bundles (Smith et al. 2006). TBSS analysis was employed in our studies and is further described in **subchapters 4.3 and 4.3.**

Despite the undisputed merits of these studies, it has been argued, that in order to identify disease-specific markers, the patterns of various diffusion parameters should be judged together with the spatial pattern of the combination of these parameters. Standard approaches based on the GLM framework are not well suited for this purpose, because the information referring to the different diffusion parameters is combined only at the point of interpretation. Model-free, exploratory data analysis methods offer a solution to this issue, by fusing data before statistical analysis in order to characterize multimodal variances across space (Teipel et al. 2007). *Linked independent component analysis (ICA)* that has been proposed to obtain independent components of multimodal variability automatically balances the information content of different modalities, finding subject loadings that produce statistically independent and non-Gaussian spatial maps across the modalities (Groves et al. 2011). In our study, modified to a single modality group, as described in **subchapter 4.2**, we set out to identify the spatial pattern of the diffusion parameter motif characteristic of AD, using linked ICA to decompose the data containing various diffusion parameters in the WM skeleton representing the core of the fibre bundles.

DTI patterns in AD and MCI – findings:

Consistent with previous pathological and structural MRI findings, diffusion studies have shown an inhomogeneous pattern of WM abnormalities in AD and MCI that originate in the medial temporal region, subsequently spreading over wider temporal, parietooccipital and frontal regions. Regardless of significant role of these studies in revealing the pathological cascade underlying AD, differences in diffusion patterns across clinical groups remain challenging to interpret. The key issue that has been widely discussed is whether deteriorated connectivity within certain fibres and regions is primary due to WM changes following the specific pattern of atrophy through myelin breakdown and axonal damage, or secondary, due to perikaryal degeneration (Wallerian degeneration). Changes in distinctive WM regions (especially in extra-temporal locations) have been reviewed in more detail (Stěpán-Buksakowska et al. 2012):

3.3.5.1 Fornix

In AD and MCI patients, decreased FA and elevated MD have been naturally observed in the fornix (Kantarci et al. 2010) (Nowrangi & Rosenberg 2015), which is an important outflow tract of the hippocampus. Fornix is also known to contain afferent fibres to the hippocampus from structures in the diencephalon and basal forebrain (Zarei et al. 2010) and has been historically described as an essential component of the Papez circuit (limbic structures). These projections are known to play an essential role in memory functions (especially memory consolidation), and damage to the isolated fornix has been associated with anterograde amnesia. Explicitly, alterations in the hippocampus, fornix, and other diencephalic structures result in the inability to form declarative (semantic and episodic) memories.

Whereas neurodegenerative changes of the fornix have been consistently associated with the cognitive impairment in AD patients, DTI studies have shown that the integrity of the fornix may be compromised already in its early phases, and thus may be an early indicator of the disease progression from preclinical (i.e. asymptomatic) to clinical (i.e. symptomatic) stages (Nowrangi & Rosenberg 2015). Cross-sectional DTI analysis by Mielke *et al*. and longitudinal analysis of the same cohort by Nowrangi *et al*. showed significant difference in fornix integrity that has correlated across cognitive scores in both MCI and AD, supporting its role as a potential indicator of AD progression (Mielke et al. 2009) (Nowrangi et al. 2013). Interestingly, according to some studies, degeneration of the fornix in AD seems to precede degeneration of the hippocampus (Douet & Chang 2015) (Fletcher et al. 2013).

3.3.5.2 Corpus callosum (splenium vs genu)

Interhemispheric disconnections occurring due to atrophy of the highly myelinated corpus callosum (CC – the major WM network consisting of corticocortical fibres) significantly correspond to cognitive impairment, and numerous early DTI studies have examined global or regional CC changes in AD and MCI patients (Cho et al. 2008) (Mielke et al. 2009) (Rose et al. 2006) (Kavcic et al. 2008) (Bozzali et al. 2002) (Lee et al. 2010) (Stricker et al. 2009) (Chen et al. 2009) (Duan et al. 2006) (Zhang et al. 2007) (Di Paola et al. 2010). Whereas most of these studies focused directly on investigating FA and MD alterations in the genu and the splenium of CC (rarely in the middle CC), some of them measured AD-related parameters globally in all CC regions. In a meta-analysis by Sexton *et al.*, it has been confirmed that AD-related changes in FA

and MD are characteristic for both the splenium and the genu; nevertheless, alterations in the splenium appear to be more significant (Sexton et al. 2011).

Diffusion parameters have been widely evaluated in CC not only of patients with established AD but also in patients with MCI (Stahl et al. 2007) (H. Cho et al. 2008). Nevertheless, discrepancies between the studies concerning the conversion rate from normal aging to MCI, and from MCI to AD have been shown. Some studies showed significantly reduced FA in in AD but not in MCI (Zhang et al. 2007). Whereas other authors reported that CC is involved in both AD and MCI groups, more prominent WM impairment shown in AD were suggestive to be related specifically to AD progression (Chen, Lin, et al. 2009) (Chen, Chen et al. 2009). Likewise, there are studies on CC that suggest the role of diffusion metrics in distinguishing MCI patients when compared to normal controls (Wang et al. 2009).

Importantly, different pathological models have been suggested to account for callosal WM microstructural alterations in the course of progressive cognitive manifestations in MCI and AD. The callosal genu and anterior midbody form the inter-hemispheric connection of prefrontal regions (prefrontal association cortices) that are known to be involved in the later stage of AD pathology evolution (Braak et al. 1993), and atrophy in anterior sections of CC seems to account for general deficits in executive functions and attention in AD (Di Paola et al. 2010). On the other hand, the splenium links two-thirds of the higher-order processing areas of the lateral temporal lobes (i.e., temporal pole, superior and inferior temporal gyri) and of the parietal lobes, which, together with MTL structures, are primarily involved in the cortical degeneration of AD (Braak & Braak 1997) (Schmahmann & Pandya 2007). Clinically, the callosal reductions in posterior sections are therefore thought to interfere with the functioning of the large cortical networks, including those involved in memory functions that are impaired early in the course of AD (Di Paola et al. 2010).

Lee *et al.* hypothesized that both degenerative and cerebrovascular processes in AD additively affect the anterior CC (genu), whereas the main WM degenerative process occurs essentially in the posterior CC (splenium) (Lee et al. 2010). Similarly, it has been proposed that the selective vulnerability of posterior cerebral WM distinguishes AD patients from healthy subjects, while

anterior and middle WM integrity may be relevant to cognitive decline in both healthy and AD subjects, supposedly due to the additional vascular impact (Kavcic et al. 2008).

Importantly, it has been observed that the reduced volume of CC posterior segments correlates with GM temporal atrophy (Di Paola et al. 2010) and these findings are highly suggestive of the process that assumes secondary WM atrophy due to cortex degeneration – referred to as Wallerian degeneration. The alternative retrogenesis theory assumes that diminished WM integrity is the result of myelin breakdown (that occurs in reverse order to myelogenesis), suggesting that WM degeneration is a direct consequence of AD pathology (Bartzokis 2004) (Reisberg et al. 1999). It has been hypothesized that regions which become myelinated later in brain development (including neocortical association and allocortical fibres) are characterized by a smaller number of oligodendrocytes that support a greater number of axons in comparison to regions that become myelinated earlier. Thus, oligodendrocytes in these regions of widespread networks are particularly employed in the metabolic sense and associated WM fibres become more susceptible to pathological processes, such as oxidative stress (Zhang et al. 2009). According to the retrogenesis model, pathways with small diameter fibres that myelinate later in normal development are the first to be affected by the AD degenerative process (Bartzokis 2004), and pathways with large diameter fibres that myelinate first in development (such as primary motor fibres) are the last to be affected by AD (Stricker et al. 2009). The retrogenesis hypothesis might thus better explain WM atrophy in regions where neuronal disruption may not solely account for Wallerian degeneration. It has been demonstrated that the genu of the CC is a region characterised with the high density of small diameter fibers that myelinate later in neurodevelopment (Aboitiz et al. 1992), whereas fibers of the splenium of the CC myelinate earlier. In conclusion, corpus callosum appears as a model structure in which atrophy seems to result from both Wallerian degeneration (in posterior subregions) and the myelin breakdown process (in anterior subregions) (Di Paola et al. 2010). Evidence favouring the Wallerian degeneration or the retrogenesis processes in other various AD-related regions remains widely disputed, and likewise, both models are often proposed to account for WM alterations.

3.3.5.3 Cingulum (posterior vs. anterior)

The common findings in DTI studies on MCI and AD include posterior cingulum – an important hub for information transfer between the parahippocampal gyrus and the prefrontal cortex (O'Dwyer et al. 2011) (Sexton et al. 2011). WM fibres projecting from the posterior cingulum to the entorhinal cortex have been shown to be involved in the cognitive network closely related to memory function. Consistently with pathological and other neuroimaging studies, many authors have shown decreased FA in the posterior cingulum (Kiuchi et al. 2009) (Rose et al. 2006) (Zhang et al. 2007), along with increased MD (Nakata et al. 2009). It has been hypothesized that the integrity of fibres connecting the medial temporal lobe with the posterior cingulum is diminished even at an early stage of AD (Zhang et al. 2007). Likewise, Kiuchi *et al.* found that FA values in the bilateral posterior cingulum bundles in MCI subjects were significantly decreased when compared to controls; however, no significant differences were demonstrated between MCI and AD subjects (Kiuchi et al. 2009). These findings might lead to the assumption that alterations in the posterior cingulum precede the onset of dementia, indicating measures in this region as a possible marker of the earliest stages of AD. Other studies; however, found significant changes in the posterior cingulum in AD, but not in MCI (Cho et al. 2008).

Not only posterior cingulum, but also anterior cingulum – an important frontal association tract connecting regions repeatedly implicated in cognitive control is thought to play an important role in studies on early cognitive deficits (Metzler-Baddeley et al. 2012). Lower FA in the anterior portion of the cingulum have been also reported in association with disease progression to AD (Mielke et al. 2009). A possible explanation is the partial effect of WMHs in the anterior region, related to the common presence of vascular-induced changes, which may influence these results (Lee et al. 2010).

3.3.5.4 Uncinate fasciculus, superior and inferior longitudinal fasciculus

Many studies that focused on assessing differences in diffusion parameters across AD, MCI, other dementias and normal aging have reported WM abnormalities in several association tracts, such as the superior longitudinal fasciculus (SLF), inferior longitudinal fasciculus (ILF), uncinate fasciculus (UF) or inferior occipitofrontal fasciculus (Damoiseaux et al. 2009) (Kiuchi et al. 2009) (Kantarci et al. 2010) (Stricker et al. 2009) (Taoka et al. 2006) (Zhang et al. 2009). Components of SLF – connecting temporo-parietal regions with frontal regions, and ILF –

connecting temporal and occipital lobes, appear to play an important role in memory, attention and executive functions. (Historically, the SLF and arcuate fasciculus (AF), connecting cortical regions involved in language comprehension and production, were viewed as synonymous. More recently, four components of the SLF have been described as follows: components that connect frontal and opercular areas with the superior parietal lobe (SLF-I), the angular gyrus (SLF-II), the supramarginal gyrus (SLF-III), and the superior temporal gyrus (SLF-IV - previously viewed as the AF) (Dick & Tremblay 2012)). As previously suggested, alterations in late-myelinating fibres that connect cortical structures affected consecutively in the course of AD may reflect both Wallerian degeneration and retrogenesis process.

Deteriorated integrity of SLF and ILF seen in pathological processes in MCI (Cho et al. 2008) and AD (Stricker et al. 2009) may possibly indicate another biomarker for disease progression. It has been hypothesized that WM changes are more likely to occur earlier in the ILF than in the SLF, because the ILF contains connections between structures affected earlier in the AD neuropathological process; in contrast, the SLF components primarily connect the parietal and frontal lobes, which are affected later in the disease process than medial temporal lobe structures (Stricker et al. 2009). Likewise, diminished integrity of the UF connecting the prefrontal regions with the medial temporal lobe has been commonly reported in AD (Damoiseaux et al. 2009) (Kiuchi et al. 2009) (Taoka et al. 2006) (Zhang et al. 2009) and MCI patients (Kiuchi et al. 2009).

3.3.6 DTI in NPH

As previously reviewed, widespread areas of altered WM have been found and described in AD (Teipel et al. 2012) (Kincses et al. 2013). Likewise, regional microstructural WM alterations were also found in NPH when compared with controls (Hattori et al. 2012a) (Kanno et al. 2011) (Hattingen et al. 2010). Despite the pathological evidence for frequent co-morbidity of NPH and AD (Golomb et al. 2000) (Leinonen et al. 2012) (Malm et al. 2013) and regardless of a substantial role of diffusion MRI in differential diagnosis of AD and other dementias, to date, only a few studies compared diffusion parameters between AD and NPH (Hong et al. 2010) (Kim et al. 2011a) (Kanno et al. 2011) (Hattori et al. 2012b) (Hattori et al. 2011).

Most of the previous investigations restricted the analysis to certain brain regions (Hong et al. 2010) (Kim et al. 2011a) (Hattori et al. 2012b) (Hattori et al. 2011), an approach that is reasonable, but highly hypothesis-driven, and methodological issues appear to compromise the generalizability of the results for the cross-study comparisons. The use of DTI approach in hydrocephalus was first mentioned in the study on acute dementia (Assaf et al. 2006). Consistently with neuropathological studies (Ding et al. 2001) (Del Bigio et al. 2003), differences in diffusion parameters in WM fibres are believed to occur mainly as a result of dilated horns of the lateral ventricles in NPH (Hong et al. 2010), raising an interesting issue on the extent of WM alterations. In this context, further DTI studies focused on a whole-brain analyses, including the use of VBM analysis (Kanno et al. 2011). To overcome the registration issues common for VBM-style approaches, analyses restricted to the core of the fibre bundles, (represented by the local maxima of FA) have been recommended as particularly convenient for this purpose (Smith et al. 2006). Accordingly, several studies have employed Tract Based Spatial Statistics (TBSS) analysis in NPH patients (Hattori et al. 2012a) (Hattingen et al. 2010) (Scheel et al. 2012), however – to date of the publication, NPH-related WM alterations were compared only to healthy controls and no comparisons to other dementia types were carried out previously. In the context of possible difficulties that may occur when NPH is distinguished solely with the use of structural imaging and atrophy patterns (**Fig.3.6**, discussed in **subsection 3.2.4.4** *Generalised atrophy*), we hypothesised that comparing whole brain WM integrity in AD and NPH would result in two distinctive spatial patterns of diffusion parameters. This study is described in **subchapter 4.3**.

3.3.7 DTI in temporal lobe epilepsy (TLE)

Underlying pathological findings in TLE – the most prevalent type of focal epilepsy, include neuronal loss and gliosis in hippocampus (Bronen et al. 1991). Widespread GM abnormalities are also frequently reported to extend to the parahippocampus and entorhinal cortex (Dawodu and Thom 2005), amygdala (Hudson et al. 1993), thalamus, and multiple cortical regions 30/05/2019 09:32:00. Although TLE is considered to be a GM disorder, changes in WM fibres that reflect altered underlying brain connectivity seem to have important implications in terms of seizure generation and propagation (Concha et al. 2009) (Deleo et al. 2018).

Consistently, it has been shown that WM changes associated with TLE are not restricted to the affected MTL and involve a larger epileptogenic network (Thivard et al. 2005) (Deleo et al. 2018), possibly reflecting the underlying seizure-related WM alterations. Numerous neuroimaging studies on unilateral TLE revealed temporal and extra-temporal WM changes (Gross 2011) (Schmidt and Pohlmann-Eden 2011) (Liu et al. 2014) (Bao et al. 2018). To date, several studies used TBSS to evaluate WM changes in TLE patients compared to healthy controls (Liu et al. 2014) (Sanches et al. 2017) (Sone et al. 2018) (Tsuda et al. 2018); however, most of the reported TLE-related WM alterations were described without consideration of affected side or neglecting the possible discrepancies resulting from lateralization of brain function. We hypothesized that right and left TLE (RTLE and LTLE) have different spatial patterns of WM changes that can be differentiated and interpreted with the use of multiple diffusion parameters. In the study presented in **subchapter 4.4** we compared global microstructure of fibre bundles with regard to seizure associated WM alterations – in both right and left TLE, addressing some of the methodological issues of previous studies.

4 Experimental part

In this part, methodology and results of the included studies are described and discussed. The chapter contains four studies (**subchapters 4.1-4.4**), each divided into Methods, Results, Discussion and Summary sections.

4.1 Structural MRI patterns in AD

In this study, we aimed to obtain both the global and regional specific information about the degenerative processes characteristic for AD. The content of this chapter has been published in the following paper:

- Štěpán-Buksakowska I, Szabó N, Hořínek D, Tóth E, Hort J, Warner J, Charvát F, Vécsei L, Roček M, Kincses ZT. Cortical and subcortical atrophy in Alzheimer disease: parallel atrophy of thalamus and hippocampus. *Alzheimer Dis Assoc Disord. 2014* Jan-Mar;28(1):65-72.

4.1.1 Methods

A total of 12 subjects diagnosed with AD (mean age: 75.08 years, range 61 to 87 years) and 13 healthy controls (mean age: 69.92 years, range 55 to 83 years) were included in this study. No significant age difference was found between the two study groups ($P<0.05$). All AD patients were recruited by a neurologist from the Memory Disorders Unit, Department of Neurology (University Hospital Motol, Prague, Czech Republic). The clinical diagnosis was made according to NINCDS-ADRDA guidelines (McKhann et al. 1984) (Dubois et al. 2007). According to EFNS guidelines (Hort et al. 2010) patients were diagnosed with mild to moderate AD (scores between 16 and 26 on the Mini Mental State Examination). Mean Mini Mental State Examination score was 19.41 (range, 15 to 24). Half of the patients had score between 19 and 22, and only 16% of patients had score 15.

Thirteen age-matched and sex-matched subjects with normal cognition were recruited from family members of patients, and from advertisement responders. All subjects underwent

neurological and neuropsychological evaluation. Exclusion criteria for patients and controls included illicit drug use and any major neurological or psychiatric disorder other than AD. All subjects (or guardians, in case of demented patients) provided written informed consents; approval for the study was obtained from the local ethical committee.

Image Acquisition

All subjects were examined with a GE 3.0T HDX MR scanner. T1-weighted 3-dimensional Brain Volume (BRAVO) sequence (TR/TE = 10.9/4.6, FOV 24x24 cm^2, 352x224 matrix, 1.0 mm slice thickness, whole-head coverage, flip angle 13 degrees) was performed with a standard 8-channel head coil, and foam pads were used to prevent head motion.

Comparison of the Total Brain Volume

The total brain volume was calculated with SIENAX (Structural Image Evaluation, using Normalisation of Atrophy) (Smith et al. 2002), part of FSL (Smith et al. 2004). SIENAX starts by extracting brain and skull images from single whole-head input data (Smith et al. 2002). The image is then corregistered to the standard Montreal Neurological Institute template (MNI152 – a standard-space average of 152 brains) with a constrained affine transformation (brain image used for estimating initial and final translations and rotations, skull image is used to optimize scaling and skew). The determinant of this transformation matrix is the v-scaling factor, which represents the relative scaling of individual skull to the MNI152 skull. This factor was shown to have a strong linear relationship with the intracranial volume derived from T2-weighted images (Fein et al. 2004). Then, tissue-type segmentation with partial volume estimation was carried out (Zhang et al. 2001) in order to calculate total volume of brain tissue (including separate estimates of volumes of GM and WM). Volumetric comparisons were performed using the Statistical Package for Social Sciences (SPSS 17 for OS X, SPSS Inc., http:// www.spss.com).

Voxel-wise Analysis of the Cortical Atrophy

We employed an "optimised" VBM-style protocol (Ashburner & Friston 2000) (Good et al. 2001) using FSL (Smith 2002). Non-brain regions were removed from all structural images (Smith 2002), and tissue-type segmentation was carried out by FAST4 (FMRIB's Automated

Segmentation Tool 4) (Zhang et al. 2001). The resulting GM partial volume images were registered to a standard space (MNI152) using linear transformation (Jenkinson et al. 2002), followed by a nonlinear registration (Andersson, JLR et al. 2007). More precisely, the resulting images were averaged to create a study-specific template, to which the native GM images were then nonlinearly reregistered. The registered partial volume images were then modulated to correct for local expansion or contraction by dividing by the Jacobian of the warp field. The modulated segmented images were then smoothed with an isotropic Gaussian kernel with a sigma of 3mm. Finally, voxel-wise GLM was applied using permutation-based nonparametric testing. Thresholding was carried out with a threshold-free cluster enhancing technique (Smith & Nichols 2009). Images were thresholded at $P<0.05$ and corrected for multiple comparisons.

Volumetric Analysis of the Subcortical Structures

All acquired images were processed and analysed with the tools of the FSL software package (FMRIB Software Library, http://www.fmrib.ox.ac.uk/fsl) (Smith et al. 2004). Automatic segmentation of subcortical structures (hippocampi, thalami, and amygdalae) was carried out with FMRIB's Integrated Registration Segmentation Toolkit (FIRST), which benefits from the principles of Active Shape and Appearance Models (ASM and AAM) applied within the Bayesian framework (Patenaude et al. 2011). In this approach, prior information about the shape and signal intensities were gained as shape and appearance models from a training set of 336 manually labelled T1-weighted images. In the first step, shapes of subcortical structures were parameterized by means and eigenvectors, and a deformable model was used to construct tessellated surface meshes. Once the shape model based on vertex location was created, image intensities were sampled for each vertex along the surface normal and a multivariate Gaussian distribution was used to model the relationship between shape and intensity. The advantage of using the AAM in a Bayesian framework is that of elimination the need for other empirical weightings between intensity and shape (Patenaude et al. 2011). The posterior probability of the shape on changing intensity features was maximized (Zarei et al. 2010) when the model was fit to the new acquired images. The volume of the segmented structures was standardized to the total intracranial volume (more precisely with the v-scaling factor estimated by SIENAX) and compared across groups with a nonparametric Mann-Whitney U test. The normalized size of the

various subcortical structures was correlated in patients and controls separately. Age and sex were used as covariates.

Focal Shape Changes of the Subcortical Structures

As described above, the shape-deformable model was fit to the individual subcortical structures, resulting in the construction of 3D surface meshes. The number of vertices was maintained across all subjects and the point correspondence was preserved. The surface meshes were registered in a 2-stage process to a common space in a MNI152 template (6DOF: rotations and translations) with FLIRT (FMRIB's Linear Image Registration Tool) (Jenkinson et al. 2002). To evaluate local subcortical changes (shape alterations) between AD patients and healthy controls, a multivariate vertex-wise F statistics test was performed at each vertex (Patenaude et al. 2011). Images were thresholded at $P<0.05$. Vertex analysis on subcortical structures showed significant gross volume change, thus, no correction for multiple comparisons was applied.

4.1.2 Results

Changes in Total Brain Volume

The SIENAX analysis showed reduced total brain volume in AD patients (normality of the data was violated based on the Kolmogorov-Smirnov test, hence non- parametric Mann-Whitney U test was used: $P<0.007$). The total GM as well as the total white matter was also reduced in AD patients (Mann-Whitney U test: $P<0.04$ and $P<0.007$, respectively) (**Fig. 4.1**).

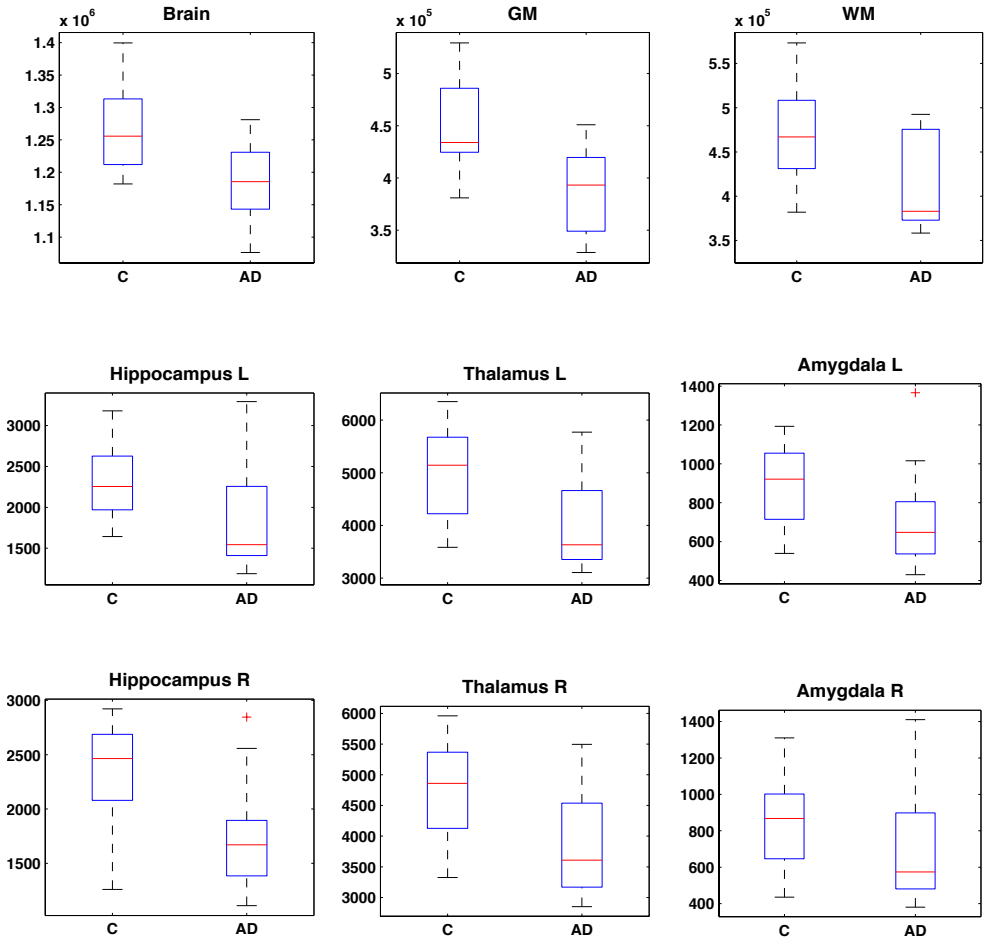

Fig. 4.1. Volumetric alterations in AD. Top row represents the total brain volume, total GM and WM volume in controls (C) and in AD patients. Significant differences were found in all 3 comparisons. In the lower 2 rows the thalamic, hippocampal, and amygdalar volumes are represented on the right (R) and on the left (L). Differences were significant for the bilateral thalami and hippocampi. On the box-plot the central mark is the mean, the boxes represent the 25th to 75th percentiles, and outliers are depicted as red crosses. Data are presented in mm^3.

Localized Cortical Grey Matter Atrophy

VBM analysis showed GM atrophy in AD patients in the bilateral medial temporal structures (hippocampus, parahippocampal gyrus, and amygdala), temporal cortical structures on both sides, but dominantly on the left (temporal pole, superior, middle and inferior temporal gyri), and of the bilateral praecunei and the left parietal regions (inferior parietal lobule, intraparietal sulcus) (**Fig. 4.2**).

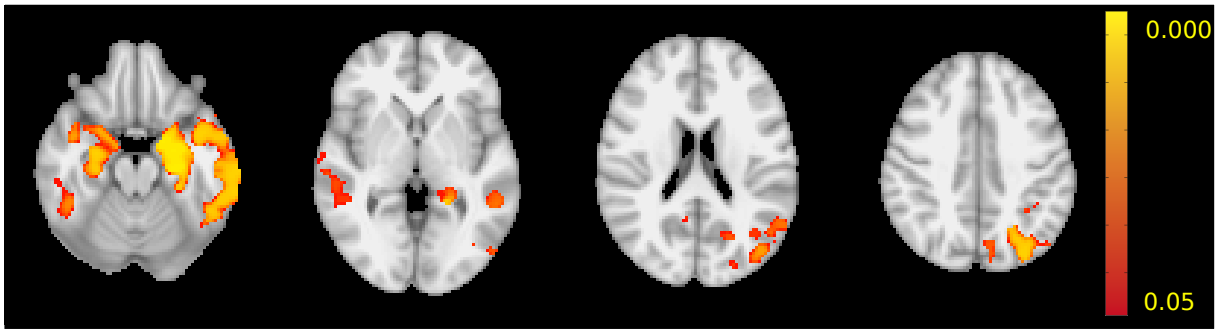

Fig 4.2. Localized GM atrophy in Alzheimer's disease. Significant GM atrophy is depicted in red-to-yellow representing P-value. Statistical images are overlaid on standard brain (MNI152).

Subcortical Atrophy

The size of the bilateral thalami, hippocampi, and amygdala were compared between AD patients and controls. As the Kolgomorow-Smirnof test indicated that the normality assumption was violated, a nonparametric Mann-Whitney U test was performed, which showed significantly smaller thalami and hippocampi on both sides (right thalamus: $P<0.015$; left thalamus: $P<0.015$; right hippocampus: $P<0.0071$, left hippocampus $P<0.0317$) (**Fig. 4.1**). The sizes of both amygdalae were also smaller, but the difference was not significant ($P>0.53$).

The vertex-based analysis of the focal subcortical atrophy showed local shrinking of size in antero-ventromedial and antero-medio-dorsal regions of the thalami in AD patients (**Fig. 4.3**).

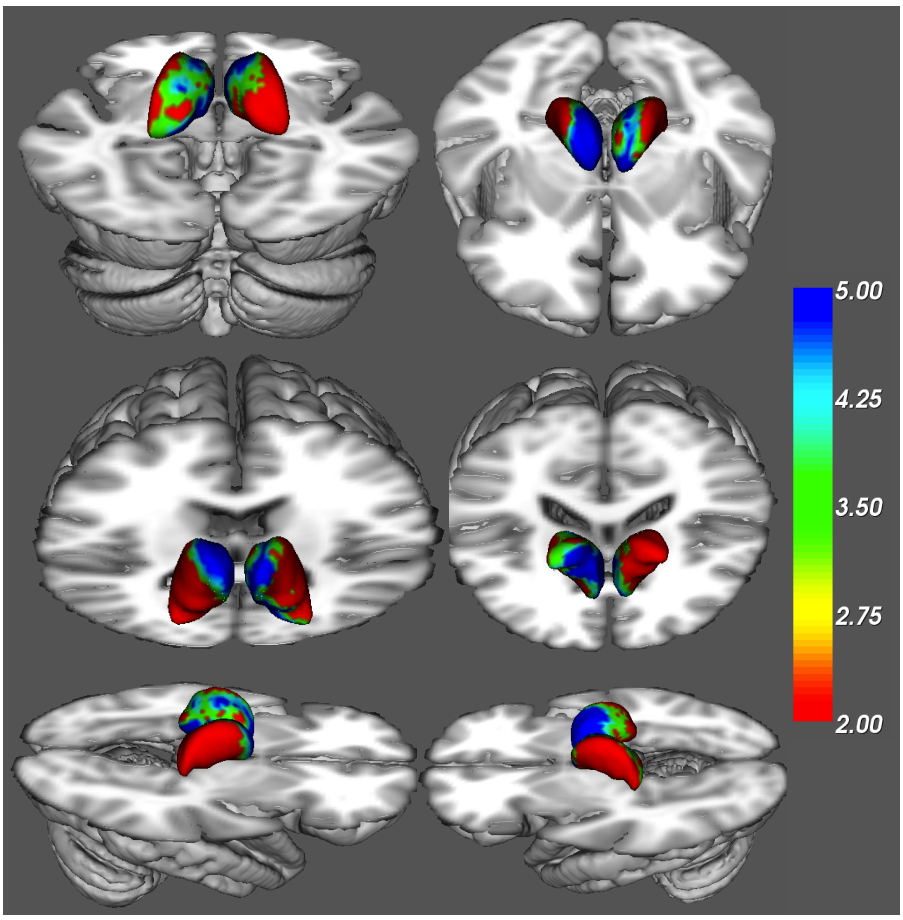

Fig. 4.3. Vertex analysis results for the bilateral thalami. The thalami are colour-coded by F-statistic values thresholded at P<0.05 uncorrected. The following viewpoints are depicted: superior-posterior (top-left), superior-anterior (top-right), inferior-anterior (mid-left), inferior-posterior (mid-right), right (bottom-left), left (bottom-right).

In the case of the hippocampi, the left hippocampus showed localized atrophy at the medial side of the body (**Fig. 4.4**). On the right side, however, the hippocampal atrophy did not show any focality.

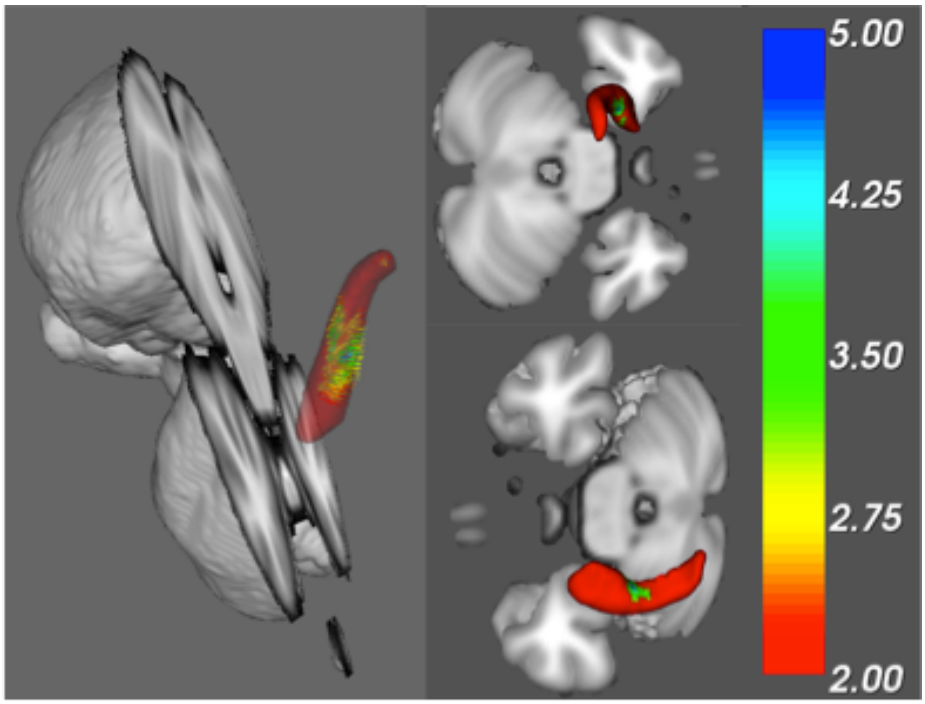

Fig. 4.4. Vertex analysis results for the left hippocampus. The hippocampus is color-coded by F-statistic values thresholded at P<0.05, uncorrected. The vectors represent the mean difference between the groups (Alzheimer disease and controls). Views from posterior-superior, anterior-superior, and right aspect are included.

Correlation of the Subcortical Volumes

In AD patients the volume of the hippocampi correlated with the size of the thalami on both sides (R=0.91, P<0.0003 for the right and R=0.913, P<0.0002 for the left side, corrected for multiple correlations, age and sex as covariate) (**Fig. 4.5**). In addition, the size of the amygdalae correlated significantly with the volume of the thalami (left: R=0.887, P<0.0006, right: R=0.799, P<0.0055; corrected for multiple correlations, age as covariate). The size of the left amygdala also correlated with the size of the left hippocampus (R=0.828, P<0.0031; corrected for multiple

correlations, age as covariate). No similar correlations were found in normal controls regarding subcortical volumes (**Fig. 4.5**).

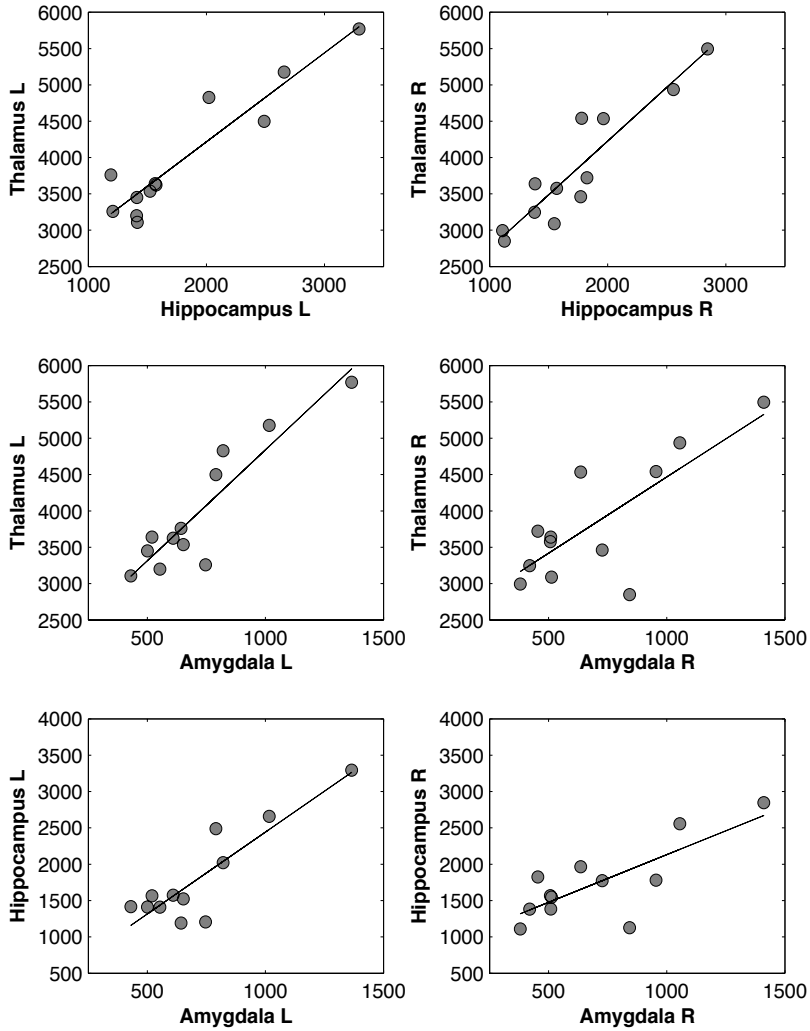

Fig. 4.5. Correlation of thalamic, hippocampal, and amygdalar volumes. Note the correlation of the right hippocampus and amygdala was not statistically significant. Volumes are represented in mm^3.

4.1.3 Discussion

In this study, we carried out an integrative evaluation of brain atrophy in AD. The brain volume loss included WM and GM. While the neocortical atrophy was distributed over widespread regions, it also showed regional specificity, incorporating the mesiotemporal lobe and some posterior structures such as the praecuneus. Similarly, atrophy of the bilateral thalami and hippocampi was identified and was shown to be regionally specific. Furthermore, subcortical structure sizes were highly correlated in patients, but not in controls.

Grey as well as white matter atrophy contributed to the loss of total brain volume. The loss of neocortical GM confirmed the expected pattern of AD-related atrophy (Karas et al. 2003) (Kinkingnéhun et al. 2008), with the most substantial volume reduction seen in the bilateral temporal regions extending to the parietal area. The diminished cortical volume in more posterior brain area (including bilateral praecuneus), also showed significant atrophy, larger on the left side. Whereas posterior cerebral atrophy is considered to be typical in early onset AD when combined with relative sparing of MTL (Koedam et al. 2011b) (Karas et al. 2007), it is thought to be common in AD patients with typical clinical manifestation and MTL atrophy; our results confirm these findings.

In addition to the reduced total brain volume and the VBM-identified focal cortical loss, the atrophy of the subcortical GM structures was confirmed in the FIRST analysis. Apart from reduced hippocampal and thalamic volumes, the vertex analysis displayed the regional atrophy in anteromedial and anterodorsal regions of bilateral thalami and in the medial area of the left hippocampus. Our results in this respect are in line with those previously published with the same methodology (Patenaude et al. 2011) and consistent with the results presented by Zarei *et al.* that showed reductions in the anterodorsal region of thalami (Zarei et al. 2010). As suggested by Zarei, in agreement with neuropathologic studies (Xuereb et al. 1991) the volume reduction of anterior parts of the thalamus may be caused by the degeneration of the anterodorsal nuclei and additionally the mammilo-hippocampal tracts within the anterior internal medullar lamina. The impairment of connections between anterior thalamus and hippocampus (direct via fornix and indirect via mamillary bodies) is considered to be associated with AD-related memory loss

(Zarei et al. 2010) along with the disruption of WM tracts leading from anterodorsal nuclei to the retrosplenial area (Kaitz & Robertson 1981).

Focusing on the regional hippocampal atrophy in AD patients, previous MRI studies revealed a reduction of volume related mainly to the CA1 subregion, considered to correspond to the medial aspect of the head and lateral aspect of the body (Frisoni et al. 2008) (Scher et al. 2007) (Xie et al. 2009). In our study, FIRST analysis confirmed loss of overall hippocampal volume and, consecutive vertex analysis showed inward deformation across the medial zone of the left hippocampal surface. Local changes of the medial hippocampal surface may be related to the atrophy of the subiculum (lying roughly beneath the deformed surface), assuming the correspondence of delineated areas on the hippocampal surface to underlying subregions (Csernansky et al. 2005). However, it should be clearly stated that local displacement of vertices in any superficial region does not necessarily indicate volume reduction directly under that surface. Therefore, in the current study, an indirect effect of volume loss in a CA1 subregion on the contralateral hippocampal side cannot be explicitly excluded.

However, of more significance than the atrophy of individual structures, we found that the volumes of the subcortical structures were correlated in AD patients, but not in healthy controls. Zarei et al showed the spot of thalamic atrophy in the anterodorsal surface, similar to what was found in our study, where the thalamus connects to the hippocampus through the fornix (Zarei et al. 2010). Similarly, the amygdalae are known to be connected to the hippocampi (Colnat-Coulbois et al. 2010). These results might suggest the atrophy of these structures is not independent, but that primary neurodegeneration in one of the structures could lead to secondary degeneration of regions connected to it. Authors of pathologic studies formulated a similar hypothesis: Xuereb et al found the anterodorsal nucleus of the thalamus to be the most affected structure by the pathologic process in AD (Xuereb et al. 1991). The connectivity profile of the anterodorsal nucleus and the anterior nuclear group raises an interesting issue. These anterior nuclei are connected to the medial limbic portion of the temporal lobe on the one end, and to the cingulate gyrus on the other (Zarei et al. 2010). Interestingly, the anterodorsal nucleus constitute only a thin lamina of cell layers around the anteroventral nucleus, representing a small portion of the anterior nuclear group within the thalamus. Thus, it is unlikely that the degeneration of this nucleus itself could account for the overall reduction of volume (Zarei et al. 2010). As significant

cell loss was observable only in the anterodorsal nucleus, the gross thalamic atrophy might be explained by a change in the glial cell populations or a loss of synapses that characterize all the dorsal nuclei – in large numbers (Xuereb et al. 1991). In our study, the focal atrophy in thalami appeared to be more widespread, extending to medio-dorsal regions bilaterally and larger in the right thalamus, where changes are also widespread antero-ventro-medially.

In a previous study, Cherubini et al found reduced volume of the bilateral thalami and hippocampi similar to our results (Cherubini et al. 2010). However, although the hippocampal microstructure investigated by diffusion MRI was found to be altered, neither the fractional anisotropy nor the mean diffusivity was altered in the thalamus (Cherubini et al. 2010). In this study, we found that the volumes of the subcortical structures were correlated in AD patients, but not in healthy controls. These results might lead to the conclusion that the atrophy of these structures is not independent, but that the primary neurodegeneration of one structure could trigger secondary degeneration of connected regions. It should be noted that our findings do not necessarily imply a causal relationship; they might simply indicate a similar rate of atrophy in the hippocampus and the thalamus. Further, longitudinal studies on parallel structural and functional connectivity should bring new insight to our understanding of the dynamics of brain atrophy; in particular, they may clarify the relation between thalamic and hippocampal atrophy.

In the last decades, global and regional hippocampal atrophy has been investigated with the application of numerous distinctive volumetric methods. The primary aim of the rapidly evolving refined algorithms is to provide empirical parameterisations of hippocampal shape variability in order to enable robust cross-sectional analysis between patients and controls (Shen et al. 2011). The main inconvenience of basic statistical shape models is that shape descriptors / coefficients cannot directly visualize localized cross-sectional changes in hippocampal volume reduction. This is because these coefficients are not directly associated with the deformed area, but only to a mode of this deformation; therefore, additional information is required to enable such visualization (Shen et al. 2011).These limitations are omitted in the applied FIRST method, with the use of the Bayesian approach for vertex-based analysis; once conditional probabilities allow the expected intensity distribution to change with the proposed shape, there is no need for additional empirical descriptors (Patenaude et al. 2011). Furthermore, contrary to the VBM approach, which is based on tissue-type / locally averaged GM segmentation, in the FIRST

analysis no such information is needed, as it is based purely on differences in vertex locations that determine structure boundaries. Even more conveniently, no further arbitrary smoothing or any other boundary correction is required in vertex analysis, as vertex coordinates of underlying meshes are used directly to localize focal geometrical changes (Patenaude et al. 2011). In contrast to FIRST analysis, no thalamic atrophy was detected in our VBM analysis. Lower GM-WM contrast and misregistration issues in the thalamic regions may be responsible for the differences.

The essential drawback of the vertex analysis (as well as any other segmentation method for subcortical structures) as described above, is that cross-sectional assessment of the focal shrinkage in subcortical volume is only indirectly related to the underlying subregional atrophy and that global atrophy does not necessarily appear in the form of significant focal atrophy (Patenaude et al. 2011) (Zarei et al. 2010). In general, methods based on vertex-wise features are considered to be sensitive to noise (Cho et al. 2012). Moreover, our study certainly suffers from the limitation that only a relatively low number of patients were recruited.

4.1.4 Summary

To evaluate AD-related brain atrophy in an integrative manner we have consecutively performed several analyses incorporating distinctive morphometric methods, each bringing complementary information about AD-related atrophy patterns. Correspondingly with the *whole-brain atrophy* (including total GM and WM loss) that distinguished patients from elderly age-matched controls, we confirmed that it is the *regional pattern of GM atrophy* that appears to be its main component of discriminative value.

Likewise, obtaining specific information on subcortical structures shape, rather than solely measuring their overall volume can help in the interpretation of AD-related changes. Moreover, of more significance than the atrophy rates of individual structures, we found that the volumes of the subcortical structures were correlated in AD patients, but not in healthy controls. Similar rate of atrophy in the hippocampi and the thalami together with their specific focal structural changes found in patients may be suggestive of non-independent sequence of neurodegenerative processes resulting in the atrophic pattern as presented.

4.2 DTI patterns in AD

In this study, we set out to identify the spatial pattern of the diffusion parameter motif characteristic of AD. We used linked ICA to decompose the data containing various diffusion parameters in the WM skeleton representing the core of the fibre bundles. The results of these analyses were summarized in the following article:

- Kincses ZT, Hořínek D, Szabó N, Tóth E, Csete G, Stěpán-Buksakowska I, Hort J, Vécsei L. The pattern of diffusion parameter changes in Alzheimer's disease, identified by means of linked independent component analysis. *J Alzheimers Dis. 2013*;36(1):119-28.

4.2.1 Methods

A total of 16 subjects diagnosed with AD (median age ± SD: 77.5 ± 6.71 years) and 17 healthy controls (median age ± SD: 74 ± 8.4 years) were enrolled in the study. Age and gender were not significantly different in the two groups (age: Mann-Whitney test: $U = 84.5$, $z = -1.84$, $p = 0.063$; gender: χ^2 (2, $n = 33$) = 3.51, $p = 0.72$). All the AD patients were recruited by a neurologist from the Memory Disorders Unit, Department of Neurology, University Hospital Motol, Prague, Czech Republic. Clinical diagnosis was made in accordance with the EFNS guidelines (Hort et al. 2010). Participants were evaluated by a neurologist who obtained medical history from the patient and caregiver, and performed the Mini-Mental State Examination (MMSE), Hachinski Ischemic Scale, and a neurological examination. Research assistants and study coordinators gathered other data including Geriatric Depression Scale, Activities of Daily Living, and additional personal and family history.

All participants were administered a comprehensive neuropsychological evaluation. The psychometric battery covered the following cognitive areas: 1) verbal memory measured with the Auditory Verbal Learning Test trials 1–6 and Delayed Recall trial, Free and Cued Selective Reminding Test; 2) non-verbal memory measured with the Rey-Osterrieth Complex Figure Test-

the Immediate Recall condition; 3) visuospatial function measured with the Rey-Osterrieth Complex Figure Test-the Copy condition; 4) executive function measured with the Trail Making Test B and Controlled Oral Word Association Test; 5) attention and working memory measured with the Backward Digit Span and Trail Making Test A; and 6) language measured with the Boston Naming Test.

Most of the subjects were either on a cholinesterase blocker or NMDA receptor blocker medication (4 rivastigmine, 9 donepezil, 1 memantine). Control subjects with normal cognition were recruited from among the family members of the patients and from the group who responded to an advertisement. All participating subjects underwent neurological and neuropsychological evaluation. The mean MMSE score was 20.18 (range: 14–25) for patients and 29.29 (range: 24–30) for controls. Concomitant diseases, such as hypertension, diabetes, and hypercholesterolemia were evenly represented in the two study groups. The exclusion criteria for patients and controls included illicit drug use and any major neurological or psychiatric disorder other than AD. All the subjects involved (or their guardians in the cases of demented patients) provided their written informed consent; approval for the study protocol was given by the local medical-ethical committee.

Data acquisition

MR imaging was carried out on a 3T GE MR scanner. 3D spoiled gradient echo images (FSPGR: TE: 4.1 ms, TR: 10.276 ms, matrix: 256×256, FOV: 25×25 cm, Flip angle: 15°, in-plane resolution: 1×1 mm, slice thickness: 1 mm) and 30 direction diffusion weighted images with 5 non-diffusion-weighted reference volumes (TE: 93.8 ms, TR: 16000 ms, matrix: 96 × 96, FOV: 23×23 cm, Flip angle: 90°, in-plane resolution: 2.4×2.4 mm slice thickness: 2.4 mm, b: 1000 s/m2, NEX: 2, ASSET) were acquired for all subjects.

Image analysis

Diffusion data were corrected for eddy currents and movement artefacts by 12 degrees of freedom affine linear registration to the first non-diffusion-weighted reference image (Jenkinson & Smith 2001). Diffusion tensors at each voxel were fitted by the algorithm included in the

FMRIB's Diffusion Toolbox (FDT) of the FMRIB's Software Library (FSL v. 4.0, http://www.fmrib.ox.ac.uk/fsl; (Smith et al. 2004)). FA, MD, and diffusivity parallel (λ1) and perpendicular ((λ2 + λ3)/2) to the principal diffusion direction were computed for the whole brain. In order to reduce the possible errors arising from misalignment of the images, we used the Tract Based Spatial Statistics (TBSS) method (Smith et al. 2006). For all subjects, the FA data were aligned into a common space chosen to be the best target from all FA images, using the non-linear registration tool FNIRT (FMRIB's Non-linear Image Registration Tool) (Andersson, JLR et al. 2007), which uses a b-spline representation of the registration warp field (Rueckert et al. 1999). A mean FA skeleton was derived from the mean FA image, which represents the centres of all tracts common to the group. The aligned FA data for each subject were then projected onto this skeleton and thresholded at 0.2 FA. Similarly, to FA, the MD, axial, and radial diffusivity images were also warped to the thresholded mean FA skeleton image. For computational reasons, images were downsampled to an isotropic resolution of 2 mm. The resulting images were fed into the linked ICA.

Linked independent component analysis

Linked ICA is an exploratory data analysis approach for the fusion of information from several different imaging modalities. The approach was described in detail earlier (Groves et al. 2011). The main aim of the analysis is to identify combined group level features of the multimodal data that reflect a biophysically plausible form of variability. The resulting components consist of *subject loading*, which indicates how much the given combination of *modalities* across *space* is expressed in individual subjects. The original, full version of the analysis decomposes the multimodal data from different modality groups with identical spatial organization in a modality group over modalities. In the current analysis, we used a restricted version of the approach, with only a single modality group of different diffusion parameters in the FA skeleton. The decomposition results in a trilinear factorization of the data:

$$y_{n,t,r} = \sum_{i=1}^{L} X_{n,i} W_{t,i} H_{i,r} + E_{n,t,r} \qquad (1)$$

where in an n voxel space, $X_{n,i}$ is the spatial map for component i, $W_{t,i}$ is the modality weighting for component i in modality t, and $H_{i,r}$ is the weight for component i in subject r. Uncorrelated Gaussian residuals are assumed, with the modality-dependent noise precision λ_t :

$$E_{n,t,r} \sim N(0, 1/\lambda_t). \qquad (2)$$

To adapt to different scalings of the signal in each modality, an automatic relevance determination (Wipf & Nagarajan) prior is used on the modality courses (W).

The matrices are optimized to find estimates of the generative model of Eq. 1 such that the spatial maps are maximally non-Gaussian. The spatial patterns were converted to pseudo-Z-statistics by accounting for the scaling of the variables and the SNR in that modality. Images were thresholded at the pseudo-z-value of 3.1 or 2.3.

4.2.2 Results

We decomposed the combined data of 16 patients and 17 controls with linked ICA into six independent components. Out of the six components, only two showed different subject loadings in the two investigated groups (IC 0: $p < 0.044$, IC 3: $p < 0.0027$).

The subject loadings were not correlated with the cognitive function of the patients as measured by the MMSE.

IC 0 was dominated by axial diffusivity (39%), but to a smaller degree, MD (27%), FA (14%), and perpendicular diffusivity (20%) also made significant contribution.

In the spatial map, increased axial diffusivity was found in patients in several regions where fibres are crossing: forceps major and minor and corona radiata, superior longitudinal fascicle and corona radiata (in **Table 4.1** both of these structures are indicated). Smaller clusters were found with similar diffusion alterations in the parahippocampal (putative cingulum bundle) and paraamygdalar WM, fornix, uncinate fasciculus, and in the thalami (**Fig. 4.6**). Importantly fibres of the internal capsule were spared.

Increased axial diffusivity was accompanied by increased MD in most of the regions described above. Additionally, some smaller clusters of increased MD were detected in juxtacortical WM. Similarly, increased perpendicular diffusivity was found in patients in similar regions identified with the axial diffusivity alterations. The peak of statistical significance in case of perpendicular diffusivity was in the close vicinity that of axial diffusivity, but in most of the cases not right on the same spot.

Decreased FA was detected in two larger clusters in the forceps major bilaterally (right: x = −28 mm, z=12mm, Z_{FA} =−6.1, Z_{MD} =3.79, y=−60mm, Z_{RD} =6.73; left: x=26mm, y=−52mm, z=10mm, Z_{FA} = −4.26, Z_{MD} = 4.11, Z_{RD} = 5.66). Some smaller clusters were detected in the juxtacortical WM. IC 3 was also dominated by axial diffusivity (52%) and MD (29%). FA and perpendicular diffusivity had only minor contribution (3% and 15% respectively).

The spatial map of increased axial diffusivity indicated a small cluster in the left parahippocampal WM (putative cingulum bundle; x = −26 mm, y=−32mm, z=−16mm, Z_{MD} =2.75, Z_{AD} =2.39). A few single voxel size differences were found in various bilateral, frontal and temporal regions (**Fig. 4.7**).

The spatial map of the MD (increased in patients) depicted a left precuneal juxtacortical WM cluster (x=−18mm, y=−62mm, z=30mm, Z_{MD} = 2.83), a left cluster in the left cingulum bundle — the same spot as indicated by the axial diffusivity. Small clusters of increased MD were found in the anterior temporal WM (possibly inferior longitudinal fascicle) bilaterally (left: x=−40mm, y=−10mm, z=−30mm, Z_{MD} =2.4; right: x=40mm, y=−10mm, z=−28mm, Z_{MD} = 2.54). A few single voxel differences were detected in the frontal, parietal, temporal, occipital WM, bilateral anterior commissure, and in the left thalamus.

The component did not indicate differences in FA or perpendicular diffusivity.

Axial diffusivity	Side	X	Y	Z	FA	MD	L1	L23
Forceps minor, anterior corona radiate	L	−22	8	32	–	3.86	**5.71**	–
Forceps minor, anterior corona radiata	R	16	14	30	–	5.35	**6.98**	4.48
Forceps major, posterior corona radiata	L	−24	−40	26	−3.9	18.8	**13.7**	16.4
Forceps major, posterior corona radiata	R	24	−38	32	–	7.47	**9.85**	3.1
Corona radiata	L	−26	−24	34	–	–	**8.09**	–
Inferior fronto-occipital fasciculus versus posterior thalamic radiation	L	−30	−32	12	–	–	**4.95**	–
Superior longitudinal fasciculus corona radiata	R	34	−42	28	–	4.35	**5.39**	–
Uncinate fasciculus	L	−36	−4	−24	–	–	**4.21**	–
Corona radiata	R	28	−14	16	–	–	**4.91**	–
External capsule	R	36	−12	24	–	–	**4.87**	–
Superior longitudinal fasciculus	L	−26	−38	26	−3.1	17.3	**13.7**	14.4
Inferior longitudinal fasciculus	R	38	−24	−4	–	3.35	**3.66**	–
Anterior limb internal capsule	R	16	12	0	–	4.85	**4.83**	–
Anterior limb internal capsule	L	−18	8	6	–	–	**3.63**	–
Paraamygdalar white matter	L	−28	−12	−8	–	3.92	**4.61**	–
Paraamygdalar white matter	R	28	−10	−10	–	3.8	**4.64**	–
Cingulum	L	−28	−40	−8	–	14.1	**9.95**	12.5
Fornix	L	−2	8	−2	–	3.46	**5.29**	–

Table 4.1. Significant clusters in component #0. Side of the cluster (L-left, R-right), standard space coordinates in mm, z values for fractional anisotropy (FA), mean diffusivity (MD), axial (L1) and perpendicular (L23) diffusivity are given in the consecutive columns. The indicated peak statistical significances are based on axial diffusivity (the associated z values are indicated in bold).

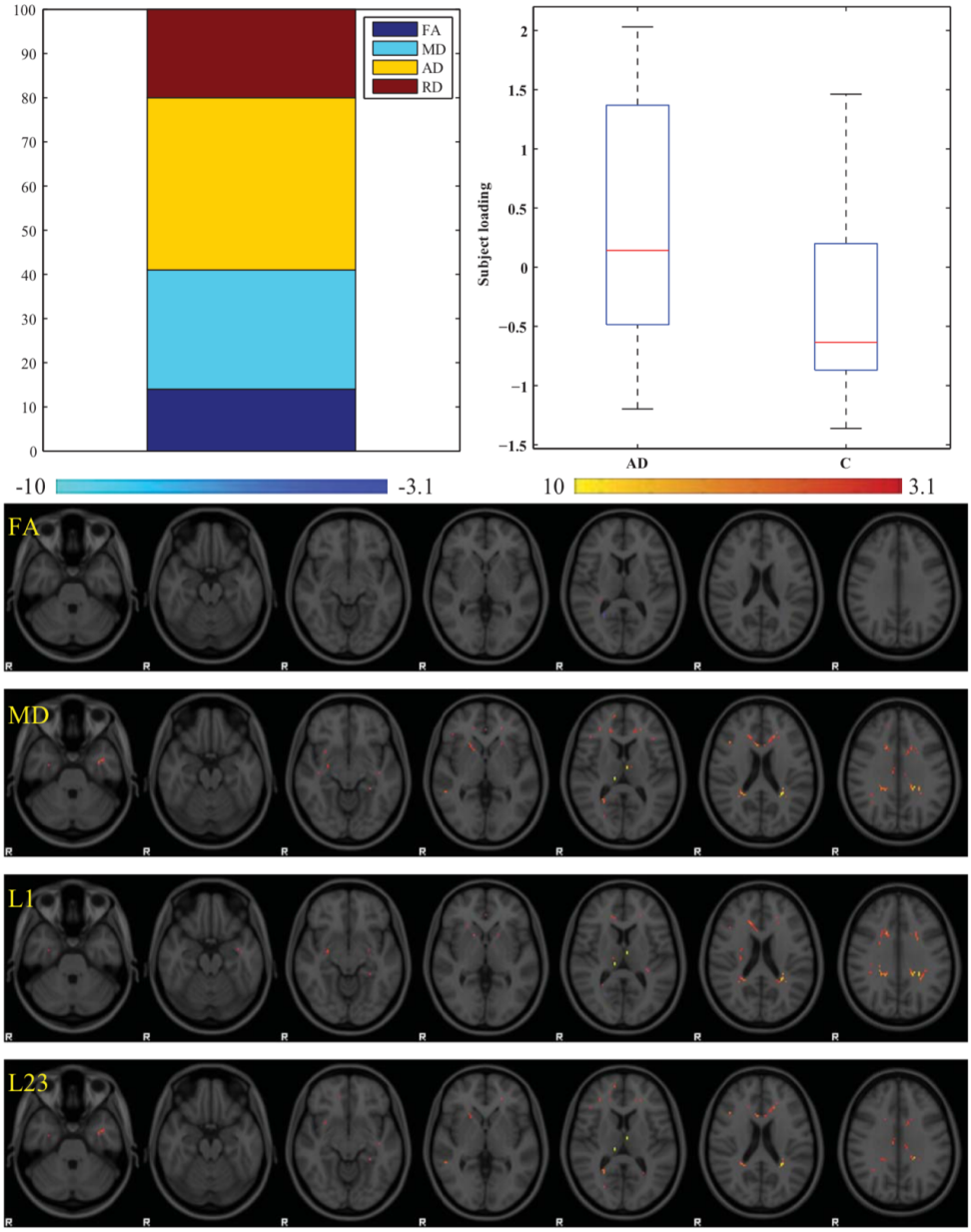

Fig. 4.6. Summary graph of component #0. Subject loadings were different between AD patients and healthy controls (p<0.044, higher in patients, top-right boxplot). The component was mainly driven by the axial diffusivity (top-left barplot). Statistical images are overlaid on MNI152 standard brain. Blue-to-light blue colour signifies a reduction, red-to-yellow an increment of the given parameter (FA, fractional anisotropy; MD, mean diffusivity; L1, axial diffusivity; L23, perpendicular diffusivity). Images are thresholded at z = 3.1. Colour bars reflect pseudo-z values.

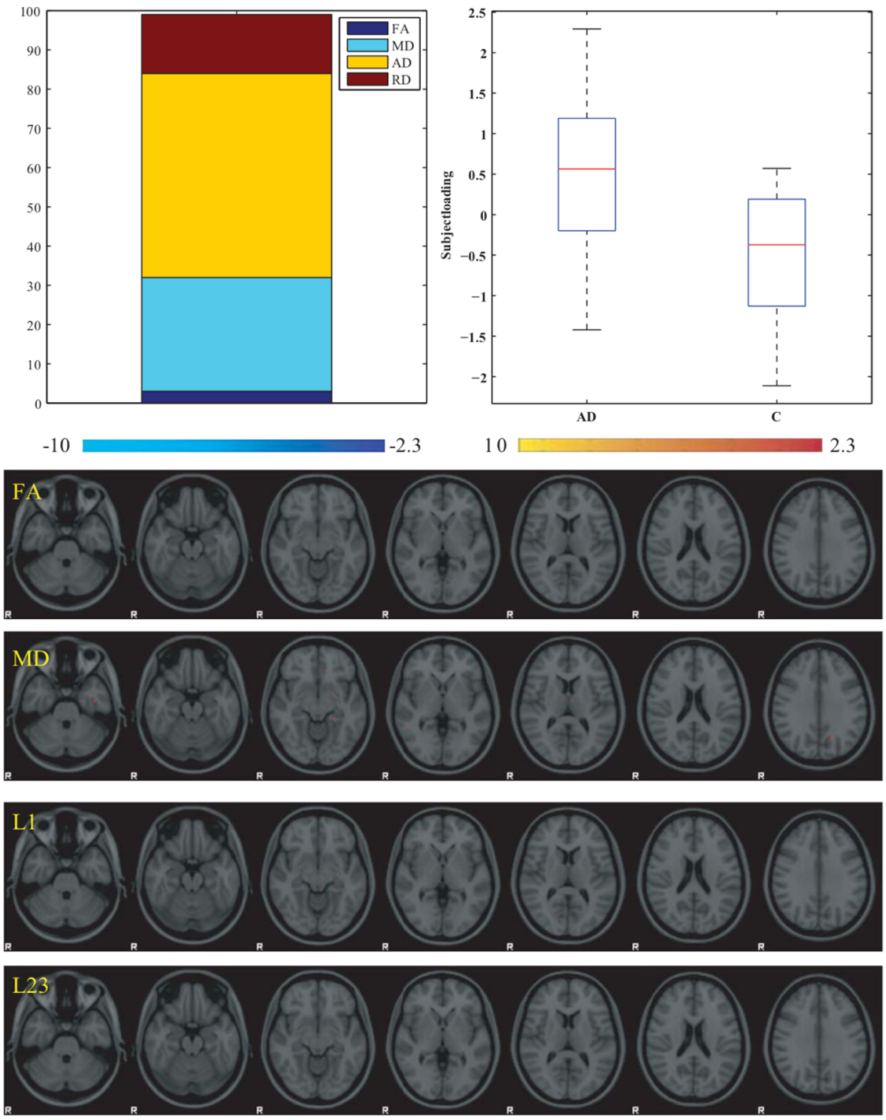

Fig. 4.7. Summary graph of component #3. Subject loadings were different between AD patients and healthy controls ($p < 0.0027$, higher in patients, top-right boxplot). The component was mainly driven by the axial diffusivity (top-left barplot). Statistical images are overlaid on MNI152 standard brain. Blue-to-light blue colour signifies a reduction, red-to-yellow an increment of the given parameter (FA, fractional anisotropy; MD, mean diffusivity; L1, axial diffusivity; L23, perpendicular diffusivity). Images are thresholded at z = 2.3. Colour bars reflect pseudo-z values.

4.2.3 Discussion

In the current study we used multivariate analysis to identify the motif of diffusion parameter changes in AD. One of the most crucial findings of this analysis was that diffusion alterations in

AD are dominated by increased axial diffusivity. The increased axial diffusivity, which was paralleled by increased mean and perpendicular diffusivity, was found in the intersection of major WM fibres bundles such as forceps major and minor, corona radiate, and superior longitudinal fascicle. Importantly, the alterations spared the internal capsulae. Similar changes were found in the medio-temporal structures.

There are two models of WM disintegration in AD. The retrogenesis model posits that WM disintegration is the reverse of the myelogenesis (myelinogenesis) (Reisberg et al. 1999).

The small-diameter fibres that are myelinated last in the neocortical association and the allocortical fibres are the first to be affected during the progression of the disease (Bartzokis 2004). An alternative hypothesis considers that the WM disintegration is related to the Wallerian degeneration due to cortical neuronal degeneration (Coleman 2005). Our results, which revealed WM disintegration in the association fibres as well as in parahippocampal WM, indicate that the two hypotheses might exist in parallel.

Similar data on AD patients were earlier analysed by Groves et al. with linked ICA in the seminal paper describing the method (Groves et al. 2011). However, that analysis was different in additionally considering the GM atrophy besides the microstructural alterations measured with diffusion MRI. Hence, in their analysis, the components described complex variations of the GM and WM, which were expressed in the same way in individual subjects. With that, they hypothesized that WM disintegration is related to cortical atrophy or at least co-occurs with similar dynamics in patients (Wallerian degeneration model). While this is reasonable, it might also be necessary to consider GM atrophy-independent microstructural changes (retrogenesis model). In their analysis component #2 of the flat, concatenated and linked ICA identified widespread cortical atrophy and co-occurring WM disintegration. In contrast, component #11 of the Groves analysis identified FA and MD alterations mainly in the callosal fibres without cortical atrophy. In our analysis, neocortical association fibres and the medial temporal WM were also affected, which may point to the validity of both models. However, it should be emphasized that late myelinating fibres connect to the medio-temporal structures (Brun & Englund 1986).

While it is generally accepted that the primary pathology is in the GM, it has also become clear that the cognitive dysfunction in AD is also related to disconnection (Gunning-Dixon & Raz 2000). This has been confirmed in several *in vivo* human diffusion (Liu et al. 2011) and functional MRI studies (Delbeuck et al. 2003) (Greicius et al. 2004), in human (Stokin et al. 2005) and animal (Desai et al. 2009) histological investigations. Moreover, it is known that amyloid-protein aggregates can also be found in the WM (Roher et al. 2002) and regionally specific myelination abnormalities can be detected prior to the development of tau and amyloid pathology in an animal model of AD. It was reported recently that the amyloid-$_{42}$ oligomer inhibits myelin formation *in vivo* (Horiuchi et al. 2012). Oligodendrocytes have been demonstrated to be susceptible to amyloid (Zeng et al. 2005) and oxidative stress (Deng et al. 2004), factors that are crucial in the pathogenesis of AD (Kincses et al. 2010).

Thus, diffusion MRI-detected parameter alterations have frequently been described in AD. While the reported spatial distribution of such alterations is variable, most is probably the consequence of methodological differences; callosal and medio-temporal disintegration are often reported features (Xie et al. 2006) (Stricker et al. 2009) (Salat et al. 2010) (Damoiseaux et al. 2009) (Zhang et al. 2007) (Rose et al. 2006). Furthermore, correlation of cognitive performance with diffusion parameters was recently investigated with univariate approaches (Bosch et al. 2012) (Huang & Auchus 2007) (Fellgiebel et al. 2008). In a recent TBSS study investigating several cognitive measures, only memory composite was correlated with FA when AD and mild cognitive impairment patients were analysed together but not for AD patients separately (Bosch et al. 2012). Similarly, in our study no correlation was found between the expression of the components in individual subjects (subject loadings) and the MMSE scores. It is important to point out MMSE is a general measure of cognitive performance and does not test a single specific cognitive function which could be correlated with a focal structural alteration.

Previous studies have indicated that the different patterns of the diffusion parameter alterations may be associated with different pathological changes in the white matter. The alterations of axial and radial diffusivity in mouse models of multiple sclerosis have been suggested to relate to axon or myelin damage, respectively (Sun et al. 2007) (Song et al. 2005) (Budde et al. 2008). One mouse model study revealed a decreased FA in transected nerves, the FA returning toward the normal in the course of axonal regeneration. Additionally, the FA and axial diffusivity

correlated significantly with the total axon count (Lehmann et al. 2010). In the optic nerve of mice, a significantly decreased axial diffusivity was observed 3 days after retinal ischemia without any detectable changes in radial diffusivity, which was consistent with histological finding of significant axonal degeneration without demyelination. Consistent with the histological finding of myelin degeneration, an increase in radial diffusivity was observed 5 days after ischemia (Song et al. 2003). The myelin content in the post-mortem human brain, prior to and after fixation, was predicted by the changes in radial diffusivity, together with FA and MD (Schmierer et al. 2008). A further possibility behind the increased axial diffusivity might be the selective degeneration of the weaker of the crossing fibres (Douaud et al. 2011). In the current study, the identified components were most strongly influenced by the axial diffusivity. This might suggest that axonal loss is the key pathological process. On the other hand, other diffusion parameter changes were also significantly included in the independent components. At this stage, the pathological relevance of these findings cannot be unanimously concluded. While it is crucially important to understand the pathological relevance of the diffusion alterations in AD, if further studies could confirm the results and extend these findings in longitudinal investigations, diffusion MRI could be a potential biomarker in studies testing putative neuroprotective treatments.

4.2.4 Summary

In this study we made use of a model-free analysis approach of linked independent component analysis to identify a motif of diffusion parameter alterations exemplifying AD. Analysis revealed six independent components, two of which demonstrated differences between patients and controls. Component #0 was dominated by axial diffusivity but significant alterations in fractional anisotropy and mean and radial diffusivity were also detected. Alterations were found in regions of crossing of major WM pathways, such as forceps, corona radiata, and superior longitudinal fascicle, as well as mediotemporal WM. These results lend support to the coexistence of WM disintegration of the late myelinating associating fibres and Wallerian degeneration-related disintegration, in accordance with the retrogenesis and Wallerian hypothesis.

4.3 DTI patterns in AD and NPH

In this study we compared whole brain WM integrity in AD, NPH and normal aging. We hypothesised that these conditions have different spatial patterns of WM alterations reflected in diffusion measures that can differentiate them. The content of this chapter has been published in the following study:

- Hořínek D, Štěpán-Buksakowska I, Szabó N, Erickson BJ, Tóth E, Šulc V, Beneš V, Vrána J, Hort J, Nimsky C, Mohapl M, Roček M, Vécsei L, Kincses ZT. Difference in white matter microstructure in differential diagnosis of normal pressure hydrocephalus and Alzheimer's disease. *Clin Neurol Neurosurg. 2016* Jan; 140:52-9.

4.3.1 Methods

Forty-eight patients participated in this study: 17 subjects diagnosed with NPH (average age 76.18 years, SD 8.38), 14 subjects diagnosed with AD (78.92 years, SD 6.31) and 17 healthy controls (74.06 years, SD 8.11) (**Table 4.2**). Subjects with idiopathic NPH were recruited from among patients attending the Department of Neurosurgery of Central Military Hospital, Prague and were diagnosed by an experienced neurosurgeon – according to the clinical diagnostic criteria of probable NPH, including gait disorder, dementia and urinary incontinence (ADAMS et al. 1965). Patients with any other neurologic disease, psychiatric disorder or history of head trauma were excluded from the study. All 17 NPH patients underwent gait speed test on 10-m track, get-up and go test, diagnostic lumbar infusion test and neuropsychological evaluation. All patients underwent VP shunting procedure. In cases of uncertain results of lumbar infusion test, the 120-h external drainage test was additionally performed before VP shunting. The NPH patients were those that had a positive postoperative clinical response. Patients with negative response to lumbar infusion test or external lumbar drainage, respectively, were excluded from this study. Definitive diagnosis of NPH was assessed after symptomatic improvement following VP shunt insertion. MRI scanning was carried out previous to the VP shunting.

The control subjects were recruited among the healthy volunteers (from family members of patients and from the group who responded to the advertisement), with no history of neurological or psychiatric disorder.

There were no differences between the age of the groups. All AD patients were recruited by a neurologist from Memory Disorders Unit, Department of Neurology (University Hospital Motol, Prague, Czech Republic). The clinical diagnosis was made according to NINCDS-ADRDA and respecting new EFNS guidelines (Hort et al. 2010). The study protocol was approved by local institutional ethics committee and informed consent was obtained from all subjects (or their guardians).

MR imaging was carried out on a 3T GE Signa HDx MR imaging system (GE Medical Systems, Milwaukee, WI) in the Central Military Hospital, Prague. All sequences were acquired using 8-channel head coil. The MRI protocol included T1-weighted 3D BRAVO sequence (TR: 10.9, TE: 4.6 ms, matrix: 352 × 224, FOV: 24 × 24 cm, flip angle: 13°, in-plane resolution: 0.68 × 1.07 mm^2, slice thickness: 1 mm). T2-weighted and FLAIR images were acquired, as a part of the diagnostic workup, to exclude patients with significant vascular lesions and other causes of dementias. Diffusion images were obtained with a diffusion-weighted single-shot echo-planar imaging (b = 1000 s/m^2 for 30 non-collinear diffusion directions with 5 non- diffusion-weighted reference volumes, TR: 16,000 ms, TE: 89 ms, matrix: 128 × 128, FOV: 24 × 24 cm, flip angle: 90°, in-plane resolution: 1.8 × 1.8 mm^2, slice thickness: 2.4 mm).

	NPH	AD	Control group
Number of subjects	17	14	17
Age (±SD)	76.18 ± 8.38	78.92 ± 6.31	74.06 ± 8.11
Female/male	8/9	8/6	10/7
MMSE score	24.28 ± 2.92	19.4 ± 3.0	30 ± 0

Table 4.2. Sociodemographic data of the subjects. Data are represented as mean ± standard deviation. NPH, normal pressure hydrocephalus; AD, Alzheimer's disease; MMSE, Mini Mental State Examination.

Image analysis

Raw diffusion data were visually inspected and data with major movement artefact were excluded from further analysis. Then DTI images were corrected for eddy currents and motion artefacts by 12 degree of freedom (12DOF) affine linear registration to the first non-diffusion-weighted reference image (Jenkinson & Smith 2001). Diffusion tensors at each voxel were fitted using the FMRIB's Diffusion Toolbox (FDT, FSLv.4.0, www.fmrib.ox.ac.uk/fsl). Fractional anisotropy (FA), mean diffusivity (MD), and diffusivity parallel ($\lambda 1$) and perpendicular (($\lambda 2 + \lambda 3$)/2) to the principal diffusion direction (RD – radial diffusivity) were computed for the whole brain. In order to reduce the possible errors arising from misalignment of the images, we used the Tract Based Spatial Statistics (TBSS) method (Smith et al. 2006). All subjects' FA data were aligned into a common space that was chosen to be the best target from all FA images (an algorithm included in the TBSS package), using the nonlinear registration tool FNIRT (http:// fsl.fmrib.ox.ac.uk/fsl/fslwiki/FNIRT), which uses a b-spline representation of the registration warp field. A mean FA skeleton was derived from the mean FA image that represents the centres of all tracts common to the group. Each subject's aligned FA data was then projected onto this skeleton and thresholded at 0.2 FA. The resulting data were fed into voxel-wise cross-subject statistics. Modelling and inference using standard general linear model (GLM) design set-up was accomplished using permutation-based cluster analysis (5000 permutation) (Nichols & Holmes 2002) as implemented in FSL; the design was encoded for group membership. For statistical inference Threshold-Free Cluster Enhancing (TFCE) approach was used (Smith & Nichols 2009).

In case of all AD and NPH patients' data – the lateral ventricles, the 3rd ventricle and the Sylvian fissures were masked manually on the high-resolution T1-weighted images. The CSF volumes estimated from these masks were fed into TBSS analysis to reveal voxel-wise correlation between the CSF volumes and diffusion metrics. A separate group-specific skeleton was used for each group.

Back-projection of the results into native FA space

In order to detect possible misregistrations, TBSS results from group comparison and correlation were back-projected to the original FA map with the "tbss deproject" algorithm of FSL. The results of the back-projection were checked visually for registration artefacts.

4.3.2 Results

Registration problems

Back-projection of the group comparison TBSS results showed that the registration failed around the thalami, affecting also the internal capsule in NPH patients. No other region showed misregistration in NPH patients and there was no misregistration in AD patients. We found no misregistrations in the results of the TBSS correlation. The misregistered regions were excluded from the results.

White matter microstructure alterations in NPH patients compared to controls

White matter microstructure as evaluated by group level voxel-wise FA differences in the centre of WM fibre bundles was significantly altered in NPH patients as compared to normal controls. Higher FA values were found in the cortico-fugal fibres arising from the frontal and parietal cortex. Reduced FA was found over the corpus callosum, most prominently in the splenium. Additional WM regions with significantly lower FA were found in the left parietal lobe and left temporal pole (**Fig. 4.8**).

MD was higher in NPH patients compared to controls over the majority of WM fibre bundles except the juxtacortical white matter. In particular, higher MD was observed in the bilateral optic radiation where FA was reduced in NPH patients.

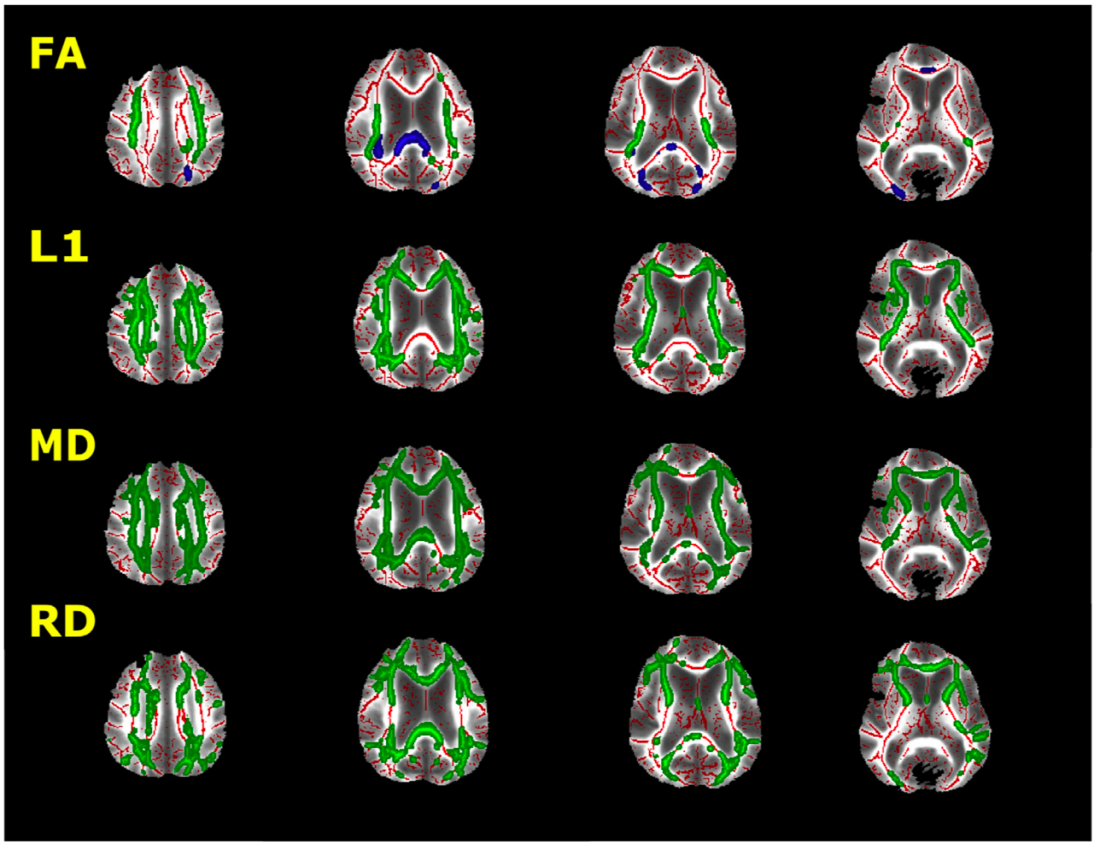

Fig. 4.8. WM alterations in NPH compared to controls. WM fibre tracts with higher FA, λ1 (L1), MD and RD in NPH patients are depicted in green, and tracts with lower FA are depicted in blue. Misregistered areas are excluded. Significant clusters were thickened in order to obtain better visualisation. Results are overlaid on the mean FA skeleton thresholded at 0.2. Images are thresholded at $p < 0.05$, corrected for multiple comparisons.

An increase of λ1 was also found in widespread regions, highly overlapping with MD changes, but not in regions where FA was reduced, e.g., in the corpus callosum and in the optic radiations. On the other hand, the increase in RD was widespread, but not seen in the cortico-fugal fibres where FA was found to be increased (**Fig. 4.8**).

White matter microstructure alterations in AD patients compared to controls

No significant FA differences were found between AD patients and normal controls.

MD was higher in AD patients in the left parieto-temporal WM. However, when lowering the statistical threshold, the differences were found to be bilateral and were also seen in the frontal WM (**Fig. 4.9**).

The λ1 was increased throughout widespread WM of the frontal, parietal and temporal lobes, as well as in the brain stem, but not in the occipital lobe.

RD was not altered in AD patients.

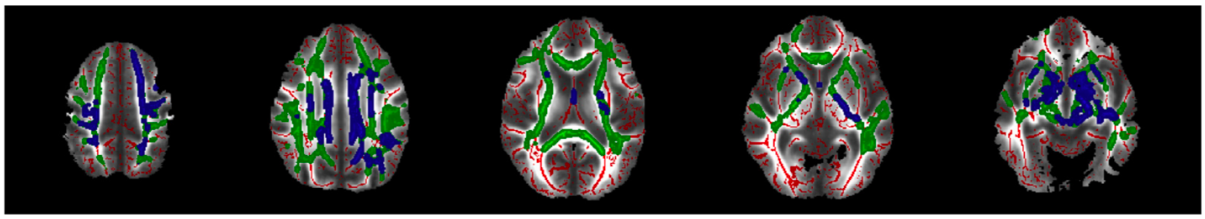

Fig. 4.9. WM alterations in AD as compared to normal controls. Higher λ1 in AD patients are shown in green. Blue regions depict higher MD in AD patients. Images are shown without misregistered areas, thresholded at $p < 0.05$ and corrected for multiple comparisons.

Comparison of white matter microstructure in NPH and AD

FA was found to be higher in NPH patients in the cortico-fugal white matter tracts similar to what was found when comparing NPH patients with normal controls. Similarly, reduced FA was found in the splenium of the corpus callosum in NPH patients (**Fig. 4.10**).

The MD was higher in NPH patients in the bilateral cortico-fugal fibres in the frontal and parietal WM. There were no tracts having lower MD in NPH than in AD patients.

Higher λ1 (L1) was found in AD patients predominantly on the right side of the splenium of the corpus callosum, while λ1 was higher in NPH patients in the bilateral cortico-fugal fibres in the frontal and parietal WM.

RD was higher in NPH patients than in AD patients in the right parietal and frontal WM adjacent to the anterior and posterior horn of the lateral ventricle.

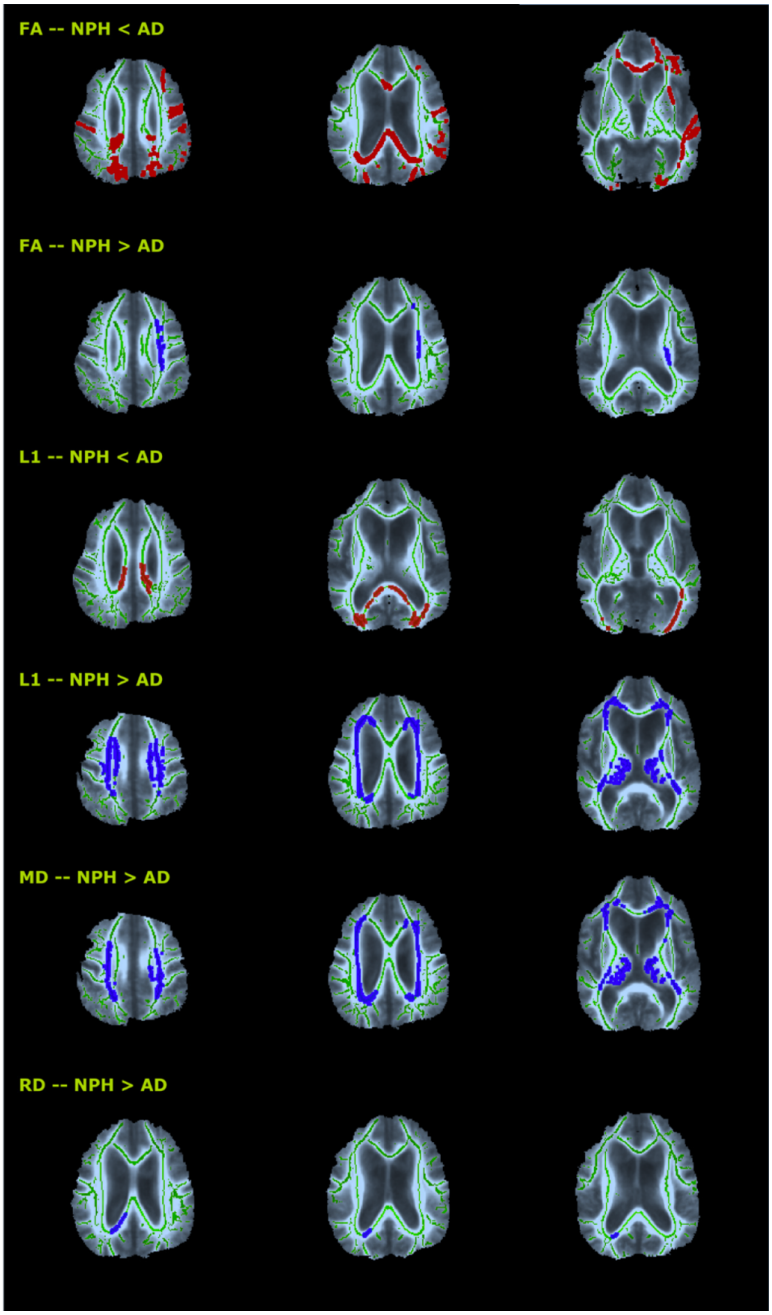

Fig. 4.10. Differences in diffusion parameters between NPH and AD patients. Blue thickened clusters indicate higher parameters in NPH patients, while red region higher parameters in AD. Images are overlaid on the mean FA image. The WM skeleton thresholded at 0.2 is shown in green. Images are shown without misregistered areas, thresholded at $p < 0.05$ and corrected for multiple comparisons.

Diffusion alterations related to ventricular size

In AD patients, negative correlation between volume of lateral ventricles and FA in the left frontal WM near the anterior horn, as well as between the volume of Sylvian fissure and RD in the right splenium of corpus callosum were found. Also, there was a positive correlation between the volume of Sylvian fissure and RD in the right part splenium of corpus callosum localised postero-laterally from the previous one. There was no correlation between the volume of the 3rd ventricle and the diffusion parameters (**Fig. 4.11**).

In NPH patients, a positive correlation between volume of 3rd ventricle and FA in bilateral frontal WM – especially on left side – near the anterior horn of lateral ventricles and a negative correlation with RD in the splenium of corpus callosum was found. There was no correlation between the volume of either lateral ventricles or the Sylvian fissures and the diffusion parameters.

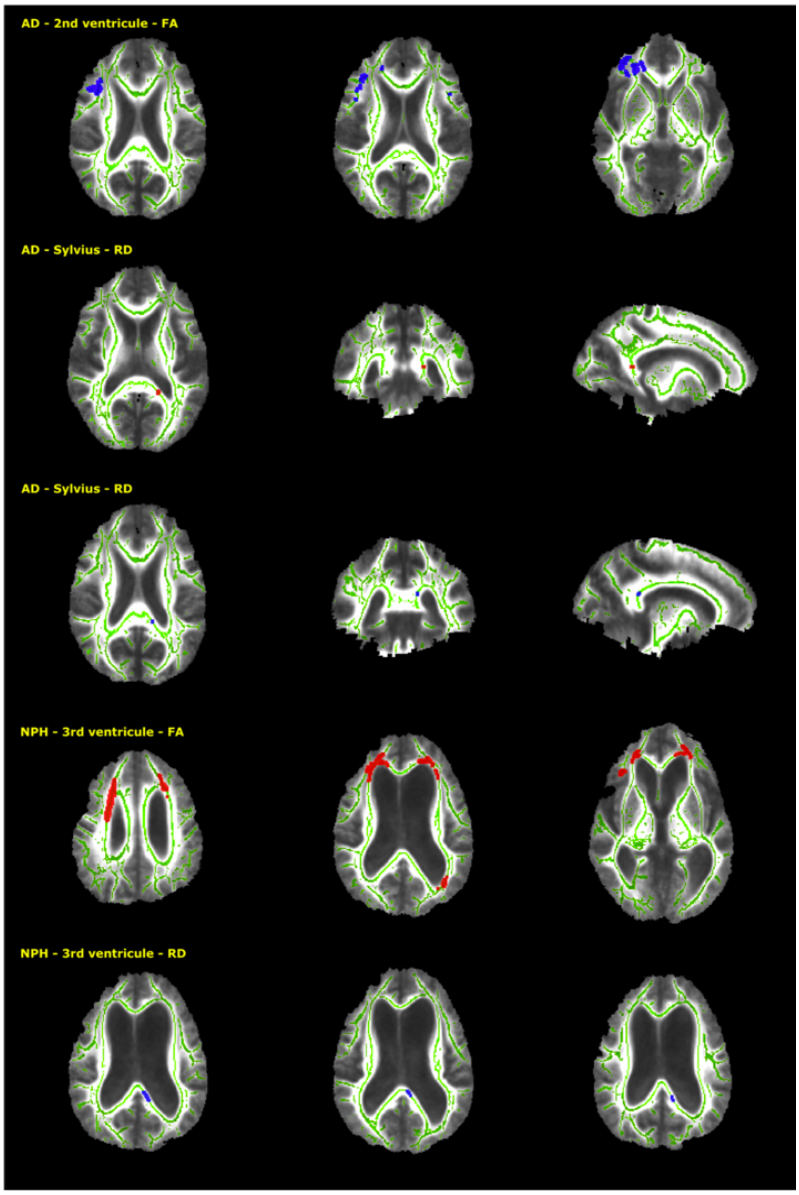

Fig. 4.11. CSF space correlation with WM diffusion parameters in patients. Results are overlaid on the mean FA skeleton thresholded at 0.2. Images are thresholded at $p<0.05$, corrected for multiple comparisons. Negative correlations are depicted in blue, positive correlations are depicted in red. In the first row FA shows negative correlation to the 2nd (lateral) ventricle volume in AD. In the second and third row RD shows positive and negative correlation to the Sylvian fissure volume in AD, respectively. In the fourth row FA shows positive correlation, in the fifth row RD shows correlation to the 3rd ventricle in NPH.

4.3.3 Discussion

We found that there are measurable differences in WM microstructure in NPH as compared to AD and normal controls. The most characteristic changes in NPH were the increased FA in the cortico-fugal tracts adjacent to the lateral ventricles, along with increased MD and axial diffusivity. In contrast, posterior callosal WM pathways had reduced FA paralleled with increased RD. Furthermore, increased lateral ventricular volume negatively correlated with the FA of the frontal WM in AD and 3rd ventricular volume positively correlated with the FA of the frontal and parietal periventricular WM in NPH.

Our results are basically in line with previous DTI studies on NPH. Hattori et al. (Hattori et al. 2012a) in a combined TBSS- and ROI-based investigation found increased FA in the internal capsule and in corticospinal tracts, along with decreased FA in the periventricular WM and posterior parts of the splenium. Also using the combined TBSS and ROI approach, Hattingen et al. (Hattingen et al. 2010) reported significantly lower FA and higher MD values in corpus callosum, along with higher FA and MD values in the periventricular corticospinal tract. Accordingly, Kanno et al. (Kanno et al. 2011) in a VBM-style analysis showed increased MD in the periventricular regions and lower FA in the corpus callosum and the subcortical regions. Recently, similar results were also presented in NPH patients before VP-shunting (Scheel et al. 2012). Moreover, our results are also broadly consistent with a recent DTI study on a rodent model of hydrocephalus (kaolin-induced), in which regionally heterogonous diffusion alterations were also detected in the WM fibres (Yuan et al. 2012).

The reduction of FA in the corpus callosum and posterior periventricular WM fibres in NPH can be explained with mechanical pressure on the callosal and periventricular fibres caused by ventricular enlargement to the extent it that may cause axonal degeneration (Ding et al. 2001). Furthermore, it appears that induced CSF effusion into the periventricular WM due to increased pressure (resulting in extracellular edema) also significantly contribute to the altered diffusion parameters (Medina & Gaviria 2008). A further explanation could be that the enlargement of the ventricles may cause predominantly antero-posterior stretching of WM fibres in the body of corpus callosum and cranio-caudal stretching of the fibres in the splenium. In either case, the

stretching is perpendicular to the main fibre direction in the corpus callosum – and that can possibly lead to reduced FA and increased RD (Hattori et al. 2011).

We propose two alternative hypotheses for the increased FA that may be seen mainly as a result of the increase of axial diffusivity (λ1) in the periventricular cortico-fugal fibres. One possibility is that the increased mechanical pressure arising from the reduced CSF turnover may stretch the ventricles and compress the WM fibres, which in turn will reduce the winding of the fibres within a voxel, resulting in increased water diffusivity in the main direction – parallel to fibres. Alternatively, the degeneration of crossing fibres that are running through the corpus callosum (the region where reduced FA was found) will reduce the perpendicular diffusivity. However, since no reduction of the RD was measured here, this second hypothesis seems less likely.

As previously reviewed (in **subsection *3.2.4.4* *Generalised atrophy*** and **subsection 3.3.6** *DTI patterns in NPH)* AD is considered to be the most important differential diagnosis for NPH and is often found as NPH comorbidity. Our study reported higher MD in parieto-temporal WM in AD patients when compared to controls, consistently with the pattern known from previous DTI studies (Sexton et al. 2011). Likewise, higher MD values in NPH patients indicate reduced axonal fibre calibre along with increased amount of extracellular space, occurring as a result of increased CSF diffusion into interstitial periventricular space due to increased CSF production and decreased brain perfusion (Hattori et al. 2011) (Ivkovic et al. 2012). In our study these regional changes were more significant for the left hemisphere; however, they were displayed also on the right when the statistical threshold has been lowered.

In our study, no significant change in FA was detected in AD patients. That is in contrast to former TBSS analyses on AD patients that reported FA reductions in various locations. Some of these studies however used a more liberal statistical threshold (Salat et al. 2010) (Liu et al. 2011), or much higher gradient directions to define diffusion parameters (Damoiseaux et al. 2009). Nevertheless, while no significant FA differences were found between AD patients and normal controls, we reported an increase of λ1 – axial diffusivity in the temporal, parietal and frontal lobes in AD patients. Increased λ1 can be explained by increased extra-axonal space due to reduced axonal density and faster diffusion parallel to axons (Sun et al. 2008). According to

Kim et al. (Kim et al. 2006), λ1 changes may simply describe axonal damage occurring secondarily to Wallerian degeneration.

The results of the present study are broadly consistent with the findings described in **subchapter 4.2** - *DTI patterns in AD.* Correspondingly to the present analysis, in our previous study - using a model free approach, we found that the increased λ1 accounted for the main component of the pattern in diffusion alterations in AD patients. These findings have lent support to the agreement on the coexistence of WM disintegration of the late myelinating associating fibres and secondary degeneration-related disintegration, in accordance with the retrogenesis and Wallerian degeneration hypotheses (**Kincses et al. 2013**).

Contrary to numerous DTI studies on AD, less studies used diffusion parameters to differentiate NPH patients from other types of dementia. In our analysis we have been able to compare patterns of the diffusion changes in different populations with the use of both AD and the control group of aged-matched (elderly) patients. Kanno et al. performed a voxel-based comparative study between DTI metrics in NPH, AD and Parkinson disease (PD) (Kanno et al. 2011) that also showed significantly higher MD in the periventricular WM in NPH patients as compared to either AD (in line with our results) or PD patients. Conversely, MD was found to be higher in AD and PD patients as compared to NPH in the left subcortical frontal WM. The most significant reduction of FA was noticed in the splenium of corpus callosum in NPH as compared to AD or PD patients, which is also very similar to our findings. Similarly, another tract specific ROI-based analysis showed increased FA and λ1 in the cortico-spinal tract in NPH patients (Hattori et al. 2011). This feature was shown to have a sensitivity of 94% and specificity of 80% when differentiating from AD or PD patients (Hattori et al. 2011). In another study, using tract-specific analysis Hattori implied different pathogeneses for fornix damage between NPH and AD patients, presenting significantly lower FA values in both NPH and AD, with differences concerning the length of the fornix (greater in NPH, but not altered in AD) (Hattori et al. 2012b).

A further important finding of our present research is the correlation between diffusion parameters and external and internal CSF volumes. In AD the enlargement of the ventricles is thought to be an ex vacuo process, hence the reduction of FA that correlates with the ventricular

enlargement might be seen as a signature of neurodegeneration. Contrary, the positive correlation between the periventricular FA and the size of the third ventricle points to a mechanical effect arising from the increased pressure in the ventricles. These findings might also call attention to the size of the third ventricle in the diagnosis of NPH between the various CSF volumes and indices (Yamada et al. 2015).

Earlier TBSS analyses compared NPH patients to controls (Hattori et al. 2012a) (Hattingen et al. 2010) (Scheel et al. 2012), but comparison to other diseases with similar clinical and neuroradiological features were missing (to date of the publications of the present study). We used TBSS analysis that is not compromised with the need for specific ROIs and represents a more uniform approach, convenient in the present study, in the light of a presumption of the more general effect of dilated ventricular system on the cerebral WM. Furthermore, TBSS as compared to former voxel-wise morphometric analyses, has the advantage of reducing errors arising from the possible misalignments in the WM that has a key importance in our patient population – where gross brain configuration is altered. Similar to our results, earlier TBSS studies using back-projection from the skeleton had confirmed successful registration in most of the brain. Although misalignment issues are resolved with TBSS approach to some extent, huge anatomical deformation due to ventricles enlargement are still problematic in NPH (Hattori et al. 2012a). In our study we further improved the registration by using a single image (an AD patient's image) instead of the normal standard space template and visual inspection further ensured the result of registrations. Furthermore, the regions where misregistration happened were excluded from the analysis.

Probably the biggest drawback of all types of voxel-based cross-sectional analyses (one of which is TBSS, though restricted to the core of fibre tracts) is that many steps are required, such as intersubject image registration, tissue segmentation, smoothing, and many others. Recently, parametric model fitting for the shape of a whole-brain MD histogram was developed (Ivkovic et al. 2012) and presented as a useful approach for differential diagnosis for NPH and AD, omitting the need for intersubject registration. However, this method lacks the spatial information, which looking at our results, could be a key feature of diffusion parameter alterations.

One problem with the diffusion-tensor approach is also its clinical feasibility. As seen above, DTI images require time-consuming postprocessing and statistical steps before a diagnostic or differential conclusion can be reached. This makes the clinical application challenging. Nevertheless, diffusion-tensor imaging is considered to be a very powerful approach to evaluate WM alterations on a whole-brain or tract-specific basis, and combined application of various diffusion parameters such as FA, MD, λ1 and RD is thought to enrich the information used to differentiate between various pathologies and their further description; our results seem to confirm that.

In this context, conclusion can be made with the implication of future research that should address the potential effect of VP shunt insertion in NPH patients on DTI parameters; some degree of normalisation might be assumed in shunt-responsive group. In our pre-operative study, patient group consisted only of subjects that were known to respond well, therefore the presented pattern of WM alterations in NPH as compared to AD and healthy age-matched controls may reflect the successful configuration for shunt indication.

This issue has been partially addressed in later studies (published after the present study) that showed – as expected – a significant ventricular volume reduction in VP shunt-responders, accompanied by a significant interaction between clinical improvement and decrease in ventricular size. WM regions in which FA was decreased after shunt placement included corona radiata. This finding was observed only in shunt-responsive NPH patients and might reflect the plasticity of the brain for mechanical pressure changes from the CSF system (Kanno et al. 2017).

4.3.4 Summary

In our study, TBSS analysis showed a specific patter of diffusion parameter changes that can differentiate NPH from AD and healthy aging controls. Our findings support the utility of non-invasive DTI approach in differential diagnosis of NPH and prediction of success of VP shunting. The challenge for further future research is to perform a follow up study after VP shunt insertion and to assess the diffusion characteristics against the clinical course and other diagnostic markers of NPH.

4.4. Structural and DTI patterns in TLE

The current study compares global microstructure of fibre bundles with regard to seizure-related WM alterations in both right and left TLE. The content of this chapter is a part of the following study:

- Buksakowska I, Szabó N, Martinkovič L, Faragó P, Király A, Vrána J, Kincses ZT, Meluzín J, Šulc V, Kynčl M, Roček M, Tichý M, Charvát F, Hořínek D, Marusič P *Distinctive Patterns of Seizure-Related White Matter Alterations in Right and Left TLE - submitted,* Manuscript ID: 474992

4.4.1 Methods

Subjects

Fifty-four patients with drug-resistant TLE, epilepsy surgery candidates, were enrolled into the study. All of them underwent standard preoperative examination in the Motol Epilepsy Centre. The evaluation included clinical examination, EEG and video-EEG monitoring, neuropsychological assessment, repeated MRI examinations (including fMRI with linguistic-based tasks) and, in selected cases, functional examinations like ictal SPECT or interictal PET. When it seemed necessary, the patients underwent an intracarotid sodium amobarbital procedure and/or intracranial EEG monitoring. Electroclinical diagnosis was concordant with temporal lobe epilepsy in all the patients.

The age- and sex-matched control subjects were recruited among the healthy volunteers, with no history of neurological or psychiatric disorder. The study protocol was approved by the local institutional ethics committee and informed consent was obtained from all subjects.

From the initial number of 54 TLE patients, 22 subjects were excluded: 3 patients due to extensive structural lesions (2 for astrocytoma and 1 for prior herpetic encephalitis), 6 due to uncertain lateralization or localization of epilepsy (1 with suspected bilateral TLE, 1 with differential diagnosis frontal lobe epilepsy versus TLE, 4 with temporo-parietal-occipital lesions), 8 due to the low quality of images (2 with improper acquisition, 6 with motion artefacts or incomplete examination). One patient refused subsequent examinations. Additionally, we also

excluded 4 patients that were not Czech native speakers. All patients had confirmed dominance of the left hemisphere for specialised linguistic operations as evaluated with a series of fMRI tests and/or Wada test. In the LTLE group 8 patients were diagnosed with hippocampal sclerosis - HS (53%), in the RTLE group – 10 (58%) (Table 1).

Finally, DTI data from 17 patients with RTLE (age: 40,72 ± 10,38; 10 females, 7males), 15 patients with LTLE (age: 37,33 ± 10,38; 6 females, 9 males) and 15 age-matched normal controls (age: 34,76 ± 11,16; 8 females, 7 males) were used in this study. Shapiro-Wilk tests of normality and t-tests were performed using the Statistical Package for Social Sciences (SPSS 17 for OS X, SPSS Inc., http://www.spss.com).

Data acquisition

MR imaging was carried out on a 3T GE Signa HDx MR imaging system (GE Medical Systems, Milwaukee, WI) in the Central Military Hospital, Prague. All sequences were acquired using 8-channel head coil. The MRI protocol included high resolution head imaging T1W (FSPGR), T2W (T2 CUBE) and FLAIR (FLAIR CUBE) 3D sequences. The FSPGR sequence parameters were as follows: TR/TE = 9.33/3.88, 120 slices, slice thickness 1 mm without gap, 320x256 matrix with a FOV of 24x24 cm^2. Diffusion tensor images (DTI) were obtained with a diffusion-weighted, single-shot, echo-planar imaging (b=1000s/m^2 images with 30 non-collinear diffusion directions – TR: 15000ms, TE: 89 ms, matrix: 128x128, FOV: 24x24cm, flip angle: 90 degrees, in-plane resolution: 1.8x1.8 mm^2, slice thickness: 2.4 mm and with 5 non-diffusion weighted reference volumes).

Image analysis

DTI data were corrected for eddy currents and motion artefacts by 12 degree of freedom (12DOF) affine linear registration to the first non-diffusion-weighted reference image (Jenkinson & Smith 2001), which was also used to generate a binary mask with the Brain Extraction Tool implemented in FMRIB Software Library (BET, FSLv.6.0 www.fmrib.ox.ac.uk/fsl). The extraction algorithm was optimised for each subject's data. Diffusion tensors at each voxel were fitted using the FMRIB's Diffusion Toolbox (FDT). FA, MD, and LD and RD were calculated

for the whole brain. In order to reduce possible errors arising from misalignment of the images, we used the Tract Based Spatial Statistics (TBSS) method (Smith et al. 2006).

All subjects' FA data were aligned to the FSL FMRIB58_FA template in standard Montreal Neurological Institute (MNI) space with the use of the nonlinear registration tool FNIRT (http://fsl.fmrib.ox.ac.uk/fsl/fslwiki/FNIRT), which uses a b-spline representation of the registration warp field. A mean "FA skeleton image" was computed from the mean FA image by finding the central axis of each tract, representing the centres of all tracts common to the group. Each subject's aligned FA data was then projected onto this skeleton and thresholded at 0.2 FA. In a similar fashion, the MD, LD and RD images were also warped to the thresholded mean FA skeleton image. The resulting data were fed into voxel-wise cross-subject statistics. Modelling and inference using standard general linear model (GLM) design set-up was accomplished with the use of permutation-based cluster analysis (5000 permutations) (Nichols & Holmes 2002) as implemented in FSL. The regressors of the GLM analysis coded for group membership and clinical variables in the design. The regressors, age and gender were demeaned. Correlation analysis was conducted between diffusivity parameters and seizure frequency. With the GLM design negative and positive correlations were calculated. For statistical inference Threshold-Free Cluster Enhancing (TFCE) approach was used (Smith & Nichols 2009).

Volumetric analysis of the subcortical structures

Acquired structural images were additionally processed and automatic segmentation of hippocampi and amygdalae was carried out with FMRIB's Integrated Registration Segmentation Toolkit (FIRST) (Patenaude et al. 2011). Structural data were available and complete for all the LTLE patients, 16 RTLE patients and 14 controls. Volumetric comparisons were performed using the Statistical Package for Social Sciences (SPSS 25 for Windows, SPSS Inc., http://www.spss.com). The volumes of the segmented structures of hippocampi and amygdala were compared across groups (sides included) with a nonparametric Mann-Whitney U test.

In the next step, in order to explain the variance between groups (RTLE, LTLE and controls), we examined the influence of the diagnosed HS as a covariate on the measured hippocampal volumes. For this purpose, we used Analysis of Covariance (ANCOVA), which is a combination

of an ANOVA and a regression analysis and that examines the influence of an independent variable on dependent variables, while removing the effect of the covariate factor.

4.4.2 Results

Clinical variables

The clinical and demographic variables of patients are summarized in **Table 4.3.** No significant differences were found between the age or gender distribution of the groups ($p > 0.05$). The groups didn't differ in handedness ($p > 0.05$). In regard to disease duration and seizure frequency (seizure/month) the patients' groups didn't show difference ($p > 0.05$).

Table 4.3. Characteristics of patient groups.

		age	gender	handed-ness	disease duration (years)	seizure frequency/ month	MRI diagnosis			age	gender	handed-ness	disease duration (years)	seizure frequency/ month	MRI diagnosis
RTLE	1	27	M	right	20	1	amygdala hamartoma	LTLE	1	21	M	mixed	6	12	temporal encephalocele
	2	34	M	right	31	3	HS		2	36	F	right	26	2	HS
	3	38	F	right	11	9	HS		3	34	F	right	4	3	HS
	4	31	F	left	16	3	non-lesional		4	29	F	right	24	3	HS
	5	43	M	right	25	5	FCD1 T pole +amygdala		5	42	F	right	36	16	HS
	6	26	F	right	16	2	HS		6	48	M	right	9	2	hippocampal cavernoma
	7	60	M	mixed	18	3	T pole cavernoma		7	55	M	right	22	2	HS
	8	35	F	right	11	3	HS		8	30	M	right	15	6	FCD1 T pole
	9	29	M	right	5	12	amygdala hamartoma		9	29	M	right	13	15	non-lesional
	10	54	F	right	9	13	HS		10	37	M	right	12	8	HS
	11	39	F	right	9	4	non-lesional		11	54	M	right	6	24	T pole cavernoma
	12	41	F	left	30	1	HS		12	39	M	right	31	20	HS
	13	48	F	right	37	6	HS		13	37	M	right	19	8	non-lesional
	14	49	F	right	48	4	HS		14	45	F	right	4	2	amygdala hamartoma
	15	40	F	right	30	10	HS		15	25	F	left	21	5	HS
	16	57	M	right	41	4	HS								
	17	37	F	right	6	6	T pole cavernoma								

HS – hippocampal sclerosis, RTLE – right temporal lobe epilepsy, LTLE – left temporal lobe epilepsy, FCD1 – focal cortical dysplasia type 1

Hippocampal and amygdalar volumetry

The size of hippocampi and amygdala were compared between groups. A total of 18 tests were conducted. Because the Kolgomorow-Smirnof test indicated that the normality assumption was violated, a nonparametric Mann-Whitney U test was performed.

The RTLE group of patients showed a significantly smaller size of the right hippocampi (unilateral side) compared to the left side ($p<0.024$). The size of unilateral amygdala was also smaller, but the difference was not significant ($p<0.193$).

It was also shown that the right hippocampi were significantly smaller when the RTLE group was compared with the LTLE. Unilateral hippocampal and amygdalar volumes were also smaller for the LTLE group, although with no significant difference ($p<0.290$ and $p<0.130$).

When compared with the controls, the only statistically significant result was shown for amygdalar volumes in LTLE ($p<0.023$).

These results were further confirmed with the analysis of covariance. While the data were adjusted for the effect of HS (roughly more than half of subjects in patient's groups), the difference between the LTLE and RTLE groups for the right hippocampal volume remained the only statistically significant finding ($p < 0.014$) (**Fig. 4.12**).

No significant differences were found between the patients and controls.

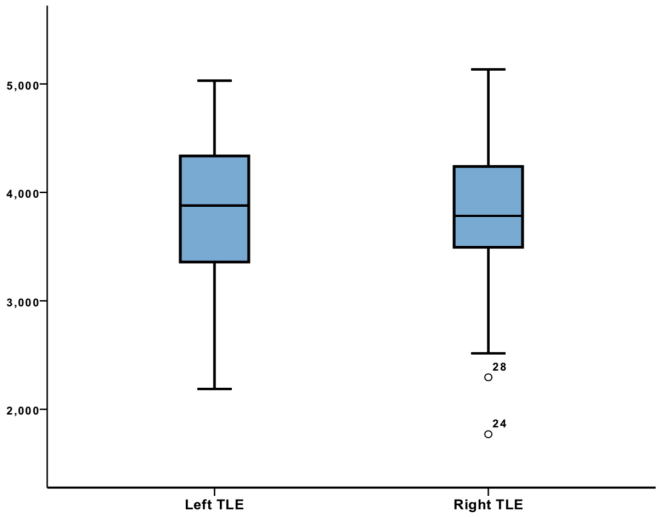

Fig.4.12. Right hippocampal volume comparison between left TLE and right TLE adjusted for HS with ANCOVA

WM microstructure alterations in patients with RTLE compared to controls

Significantly reduced FA ($p< 0.01$) was found bilaterally over widespread brain regions in right TLE patients when compared to controls **(Fig. 4.13)**, including the genu and body of corpus callosum (but not splenium), fornix and posterior limb of internal (and external) capsule. Reduced FA values were more widely distributed in the ipsilateral hemisphere in the inferior fronto-occipital fasciculus, uncinate fasciculus, inferior longitudinal fasciculus and caudal part of forceps minor; the largest changes were seen in the WM of the right temporal pole and the WM close to the temporal and occipital fusiform cortex and parahippocampal gyrus. Additionally, reduced FA values were present in the contralateral superior longitudinal fasciculus, superior and posterior part of the corona radiata and cranial parts of the forceps minor.

Increased MD ($p< 0.02$) was widespread in the RTLE patients, highly overlapping with the FA changes. Again, an increase of MD was predominantly seen in the ipsilateral hemisphere: in the inferior fronto-occipital fasciculus, uncinate fasciculus and inferior longitudinal fasciculus. Moreover, higher MD values in the superior longitudinal fasciculus, superior and posterior parts of the corona radiata and the forceps minor were also essentially ipsilateral. Only some fibre bundles (the forceps major and the posterior part of the inferior fronto-occipital fasciculus) showed a predominantly contralateral MD increase (**Fig. 4.13**).

RD was also higher ($p<0.01$) in the RTLE patients as compared to the controls over the widespread WM fibre bundles, mostly ipsilaterally (**Fig.4.13**). Regions with significantly higher RD included WM fibres arising from the frontal and parietal cortex passing through the posterior limb of the internal capsule, superior longitudinal fasciculus, inferior longitudinal fasciculus, inferior fronto-occipital fasciculus (mostly the anterior part), uncinate fasciculus and forceps minor. Whereas generally diffuse, these changes were mostly presented in the right hemisphere.

Again, solitary clusters in the posterior part of the left inferior fronto-occipital fasciculus/forceps major were more noticeable contralaterally. Whereas there were higher values in the bilateral body and genu of the CC (less in the splenium), no RD changes were shown in fornix.

Finally, higher values of LD ($p < 0.02$) were found exclusively (or almost exclusively) in the ipsilateral inferior longitudinal fasciculus, uncinate fasciculus, superior longitudinal fasciculus and posterior limb of internal capsule; minor changes in the genu and body of the CC were seen bilaterally (**Fig.4.13**).

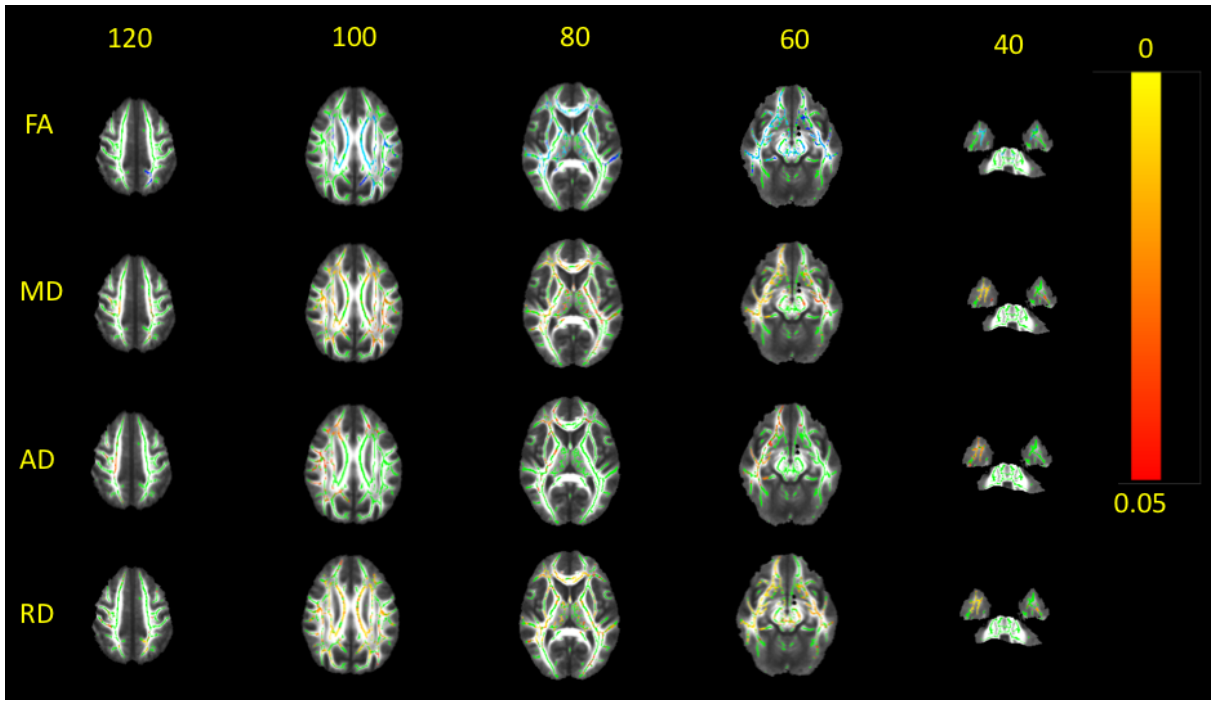

Fig. 4.13. White matter alterations in RTLE as compared to normal controls. Blue clusters indicate reduced FA in patients, while yellow-red regions indicate an increase in diffusion parameters: mean diffusivity (MD), AD (axial/longitudinal diffusivity) and RD (radial/perpendicular diffusivity). Images are overlaid on the mean FA image; the WM skeleton thresholded at 0.2 is shown in green. Images are thresholded at $p<0.05$, corrected for multiple comparisons.

WM microstructure alterations in patients with LTLE compared to controls

FA was reduced in the patients with LTLE compared to the controls over the WM fibre bundles in the ipsilateral hemisphere, most prominently in the left uncinate fasciculus and inferior fronto-occipital fasciculus ($p < 0.01$) **(Fig. 4.14)**. Additional WM regions with significantly lower FA ($p < 0.02$) were also found in the ipsilateral inferior longitudinal fasciculus, superior longitudinal fasciculus, forceps minor and forceps major body and genu of the corpus callosum.

Furthermore, some smaller clusters also appeared in the contralateral inferior fronto-occipital fasciculus and uncinate fasciculus.

Increased MD and RD values ($p< 0.02$) were observed in widespread WM fibre bundles ipsilaterally, largely overlapping with regions where FA was lower (inferior longitudinal fasciculus, uncinate fasciculus, inferior fronto-occipital fasciculus and superior longitudinal fasciculus). Moreover, MD was higher in ipsilateral corona radiata; small clusters of higher MD were also found in the genu and body of the corpus callosum. No higher MD values were seen contralaterally, and only some clusters of higher perpendicular diffusivity were shown in the right superior and inferior longitudinal fasciculus, when the threshold was lower ($p<0.05$)

No LD increase was observed in the patients with LTLE compared to the controls (**4.14**).

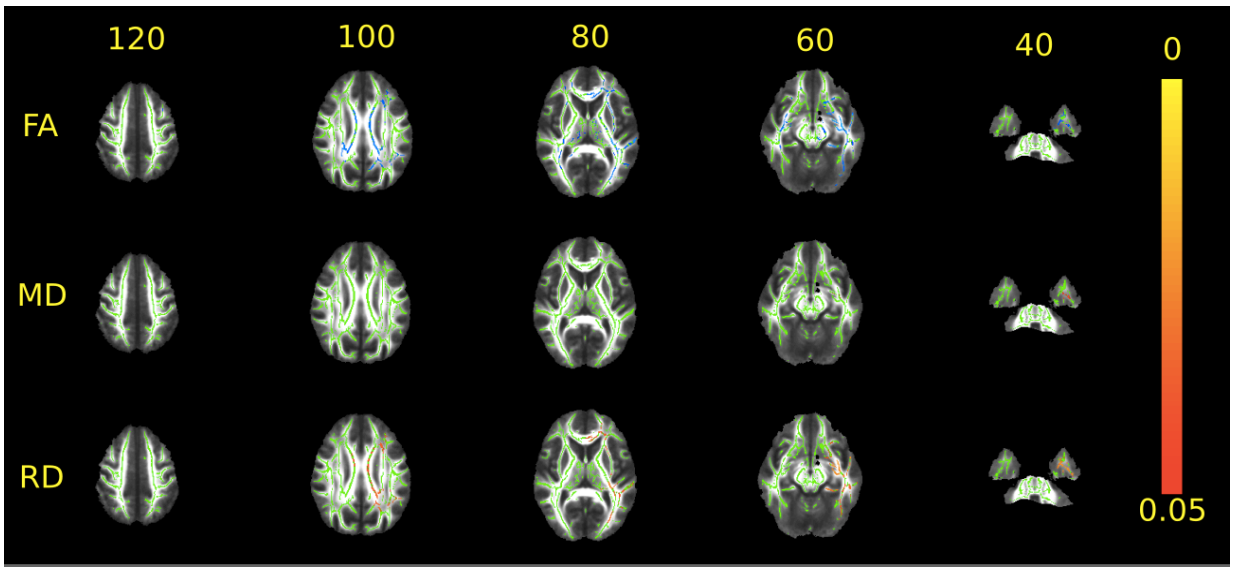

Fig. 4.14. White matter alterations in LTLE as compared to normal controls. Blue clusters indicate reduced FA in patients, while yellow-red regions indicate an increase in diffusion parameters: mean diffusivity (MD) and RD (radial/perpendicular diffusivity). Images are overlaid on the mean FA image; the WM skeleton thresholded at 0.2 is shown in green. Images are thresholded at $p<0.05$, corrected for multiple comparisons.

WM microstructure alterations in patients with LTLE compared to RTLE

No difference was found between the left and right TLE groups.

4.4.3 Discussion

Group-level analyses of multiple diffusion parameters in the core of WM fibre bundles showed different patterns of WM changes in the RTLE and LTLE as compared to the controls. Whereas LTLE-related WM alterations were predominately or exclusively ipsilateral, temporal and extra-temporal WM abnormalities in the RTLE appeared to be more widespread and bilateral, (although also predominantly ipsilateral).

As expected, widespread WM changes were most pronounced in pathways terminating in the temporal lobe (including the inferior longitudinal fasciculus, uncinate fasciculus and superior longitudinal fasciculus). Our findings are consistent with previous DTI studies that showed TLE-related WM abnormalities which are not only confined to the temporal lobe but associated with a larger epileptogenic network (Bao et al. 2018) (Gross 2011) (Riley et al. 2010) (Focke et al. 2008) (Schoene-Bake et al. 2009) (Lemkaddem et al. 2014).

Some previous TBSS studies either combined the image data from both left and right TLE (Tsuda et al. 2018) (Bao et al. 2018) (Liu et al. 2014) (Scanlon et al. 2013) (Afzali et al. 2011) or mirrored RTLE images across the midline (Scanlon et al. 2013) (Riley et al. 2010), thus adding more anatomical variances and making group differences more difficult to detect (Riley et al. 2010). We solved these issues by keeping left and right TLE data distinct and comparing them separately with age and sex-matched controls in order to further differentiate WM abnormalities depending on the hemisphere of the seizure onset.

Most of the previous TBSS studies demonstrated TLE-related WM aberrations as illustrated solely by either FA reduction (Schoene-Bake et al. 2009) (Scanlon et al. 2013) or FA reduction followed by MD increase (Nguyen et al. 2011) (Liu et al. 2014). In our study, we used multiple DTI metrics to provide complementary information about the underlying WM seizure-related WM damage and to strengthen the comprehensibility of the results.

In general, high MD values indicate reduced axonal fibre calibre and increased extracellular space. Whereas FA values reflect the underlying integrity of WM tracts, MD values can also indicate the structural changes in grey matter neurons (Bao et al. 2018). The increased

longitudinal diffusivity can be explained by increased extra-axonal space due to reduced axonal density and greater diffusion parallel to axons (Sun et al. 2008) as a result of axonal damage and degeneration (secondary to Wallerian degeneration), whereas diffusivity perpendicular to the principal diffusion direction reflect mainly the degree of demyelination (Budde et al. 2007) (Della Nave et al. 2010).

The pattern that we observed in LTLE with ipsilaterally decreased FA and increased perpendicular diffusivity, accompanied by non-significant change in longitudinal diffusivity, may be suggestive of earlier or less severe stages of degeneration (Weaver et al. 2009) (Cosottini et al. 2005).

Conversely, severe and extensive WM microstructural alterations in RTLE represented by reduced FA and higher values of MD, LD and RD in temporal and extratemporal WM bundles suggest an underlying combination of axon and myelin loss, and indicate more severe tract damage related to advanced stages of Wallerian degeneration, likely as a result of cortical and subcortical grey matter pathology. Hippocampal volumetric measures confirmed these results, suggesting that damage of both white and grey matter was more severe in the RTLE group, as addressed later in discussion.

Previous studies have confirmed that WM structural integrity in TLE is thought to be disturbed more severely in the ipsilateral rather than contralateral hemisphere, as revealed by FA and MD changes (Deleo et al. 2018) (Bao et al. 2018) (Otte et al. 2012) (Oguz et al. 2013). Usually, fibre bundles connected with the affected temporal lobe are the ones most severely altered (Otte et al. 2012) and showing a centrifugal pattern of changes. Similarly, asymmetry of WM integrity (explored in terms of lower FA values) was found to be associated with a leftward or rightward tendency, depending on the affected hemisphere (Li et al. 2014). Interestingly, some studies indicated that TLE patients with left hemispheric onset exhibit more alterations in ipsilateral and contralateral regions than those with RTLE, manifested as FA reduction and/or MD increase in temporal and extra-temporal fibre bundles (Focke et al. 2008) (Ahmadi et al. 2009) (Lu et al. 2013); these findings were also confirmed postoperatively (Schoene-Bake et al. 2009). Other studies on the effect of hemispheric laterality on diffusion parameters revealed more widespread WM abnormalities in RTLE patients than in those with LTLE (Bonilha et al. 2010) (Lemkaddem

et al. 2014). It can be concluded that the diverse distribution of WM alterations suggests that the localization of epileptic networks may play a role in the WM burden, regardless of which initial side is studied (Campos et al. 2015).

Several possible explanations have been proposed to resolve the hemispheric predominance of WM changes. It has been suggested that neuronal connections in either the left or right hemisphere, respectively, may be more likely to support seizure propagation to the contralateral hemisphere (Ahmadi et al. 2009) (Lu et al. 2013). In particular, it is possible that seizures cause more excitotoxic damage while originating in the dominant hemisphere, whereas the brain tissue in the dominant hemisphere may be more susceptible to pathological impact (Lu et al. 2013). In addition, the role of different maturation speed between both hemispheres has been proposed as another potential explanation for these asymmetries, implying that neurodevelopmental factors may play an important role in the epileptogenic process of TLE (Voets et al. 2011).

Importantly, many discrepancies between laterality of findings may be explained by the heterogeneity in the studied populations, followed by differences in analytical approaches. Overall, a growing corpus of research demonstrates the strong effect of etiologically distinct and pathologically different syndromes underlying TLE, while mesiotemporal – hippocampal sclerosis (HS) is considered to be a distinct clinico-pathologic entity from a non-HS group that appears to be highly heterogeneous (Mueller et al. 2006).

Our results, suggesting that the epileptogenic network appears to be larger in RTLE, are partially consistent with findings presented by (Bonilha et al. 2010) that identified additional MD changes expressed in RTLE (additionally to diffuse pattern of FA changes in both LTLE and RTLE) and with findings described by (Oguz et al. 2013) that showed more extensive MD changes in RTLE in groups of both female and male patients. Also, the results described by Lemkaddem et al. are broadly consistent with the evidence that bilateral neocortical networks are severely affected in RTLE; the extensive pattern of alterations affecting temporal and extratemporal structures has been shown with a more complex combination of microstructural changes (Lemkaddem et al. 2014).

Our study confirmed more restricted WM abnormalities in LTLE than in RTLE as compared to controls; the diffusion-related asymmetry was thus more obvious in the LTLE group, with WM alterations found predominantly or almost exclusively ipsilaterally. The number of significant voxels was considerably larger in the contralateral hemisphere in RTLE subjects. Also, hippocampal volumes were significantly smaller ipsilaterally in the RTLE group, although significant analogous results were not confirmed in the LTLE group.

As already implied, several factors may influence the degree and extent of diffusion alterations in TLE, including the severity of mesiotemporal lobe sclerosis (neuronal loss and gliosis) (Deleo et al. 2018) (Scanlon et al. 2013). Our results seem to partially confirm that: widespread and severe diffusion abnormalities were more apparent in the group with significant ipsilateral hippocampal volume reduction. Contrary to studies that did not detail the repartition of HS versus non-HS findings on MRI, we examined the influence of HS on the measured volumes, given the fact that more than half of the patients in each group demonstrated HS with a similar rate. Our analyses confirmed the diagnostic role of HS as a covariate when explaining the variance between RTLE and LTLE, but no volume differences were found in comparison to the controls. Our primary objective was to assess the degree of severity of hippocampal atrophic rates in both right and left TLE, and the diagnostic partition appeared to be consistent with these results. Our results might therefore be dominated to some extent by the finding of more prominent hippocampal atrophy in the RTLE group; however, these findings may not necessarily imply a causal relationship.

Whereas a growing number of studies imply that the degree of WM alterations appears to be heavily influenced by the side of seizure onset and macroscopic structural changes, converse evidence from animal models and human studies suggests that hippocampal neural loss can occur following severe or prolonged seizure activity (Cavazos et al. 1994). Some authors suggest that patients who experience secondary generalised seizures are more prone to contralateral hippocampal volume loss (Alhusaini et al. 2012). Others, on the other hand, argue against the hypothesis that epileptiform activity per se contributes to focal brain injury in previously undamaged cortical regions (Noè et al. 2019) and imply that structural brain damage is not an inevitable consequence of epileptic seizures (Liu et al. 2005).

Likewise, early presentation of diffusion abnormalities despite the lack of volumetric changes (Hutchinson et al. 2010), would be indicative of contributing factors of neurodevelopmental nature. It is also possible that the microstructural architecture of WM can be at least partially altered by the presence of developmental neuronal remnants (interstitial neurons) that have been more recently reported in epilepsy (Deleo et al. 2018). These findings may be interpreted as arrested neuronal migration and/or increased WM neurogenesis from progenitor cells (Richter et al. 2016) (Lojewski et al. 2014).

One important limitation of our study is that the time between the last seizure and MR scan was unknown and thus interictal heterogeneity within the patient groups was possible. There is growing evidence of postictal changes that may persist for longer periods of time in some patients, and which are reflected as a decrease in diffusivity (Diehl et al. 2005). Specifically, these changes likely indicate cellular swelling in the area of seizure onset and possibly areas of seizure spread. Further systematic studies may therefore shed more light on complex and dynamic changes that reflect the timing of seizure and imaging. Special focus on the correlation of these changes with outcome after epileptic surgery may be the key component to determining the role of postictal diffusion measures in the presurgical evaluation of epilepsy patients.

Moreover, due to recent findings suggesting that WM architectural changes may be reversible in the contralateral hemisphere after a successful surgery in TLE (Li et al. 2019), it would also be interesting to perform analyses on pre- and post-postoperative data, as it may help differentiate the impairment attributed either to the outcome of resection or to underlying seizure disorder. Also, further correlations of diffusion-derived metrics with quantified neuropsychological and functional imaging findings may provide complementary information about the underlying seizure-related WM abnormalities with regard to functional hemispheric specialization.

4.4.4 Summary

Overall, our results are broadly consistent with studies confirming that patients with TLE suffer from dysfunctions affecting large-scale brain networks rather than a single focal region. Our

study implies that right and left TLE have different distinctive spatial patterns of WM microstructural abnormalities that can be differentiated and interpreted with the use of multiple diffusion metrics. It appears that patients with RTLE exhibit a more widespread pattern of WM alterations that extends far beyond the temporal lobe in both the ipsilateral and contralateral hemisphere; furthermore, these changes seem to reflect more severe damage related to chronic degeneration. On the other hand, diffusion changes in LTLE may suggest a pattern of less severe axonal damage, more restricted to ipsilateral hemisphere. Partially comprehensive finding of more prominent hippocampal atrophy in the RTLE raises an interesting issue of seizure-induced implications on grey and white matter microstructure that may not necessarily mean a straightforward causal relationship. Additional correlations of diffusion-derived metrics with neuropsychological and functional imaging measures may provide complementary information about underlying seizure-related WM abnormalities with regard to functional hemispheric specialization; and correlations with outcome after epileptic surgery may determine the role of postictal diffusion measures in the presurgical evaluation of TLE patients. An interesting issue to address further would be whether these abnormalities might be reversible with good seizure control or surgery.

5 Conclusions

Structural and diffusion imaging patterns seen as dementia-related changes in the brain were the central theme of the proposed thesis. As pointed out in consecutive chapters of the presented work, MRI is in fact an excellent tool that may be used for this purpose. With this intention, the clinical and scientific implications of MRI patterns seen in AD and other conditions related with cognitive deterioration were first emphasized in the theoretical part of this work (**subchapters 3.1-3.3**).

On this basis, the utility of several structural and diffusion MRI approaches was further demonstrated in the experimental part. As assumed, it was possible to identify the specific motifs of grey and white matter alterations in AD (**subchapters 4.1, 4.2, 4.3**), NPH (**subchapter 4.3**) and TLE (**subchapter 4.4**). The results from each of the four studies included in the thesis allowed the following conclusions to be drawn:

1) Structural patterns in AD

The broad implication of this study (**subchapter 4.1**) emphasises the advantage of the integrative approach in assessment of brain atrophy in AD. As assumed, the use of several distinctive morphometric methods resulted in obtainment of complementary information about AD-related atrophy patterns:

- In addition to the *whole-brain atrophy* (including GM and WM loss) that distinguished AD patients from elderly age-matched controls, we confirmed that it is the *regional pattern* of grey matter atrophy that appears to be more specific and of discriminative value (the most substantial volume reduction was shown in the bilateral temporal regions extending to the parietal area – predominantly on the left side).
- Likewise, the atrophy of bilateral thalami and hippocampi was identified and shown to be regionally specific (focal atrophy in the antero-ventromedial and antero-medio-dorsal regions of the thalami and medial aspects of the left hippocampus).

- Moreover, of more significance than the atrophy rates of individual structures, was the finding that the volumes of the subcortical structures were correlated in AD patients, but not in healthy controls.

One important conclusion that can be drawn from our results is that a similar rate of atrophy in the hippocampi and the thalami, coupled with their specific focal structural changes, may suggest a non-independent sequence of the neurodegenerative processes that resulted in the described atrophic pattern. It should be noted, however, that our findings do not necessarily imply a causal relationship. Further, longitudinal studies on structural and functional connectivity should bring more insight to our understanding of the dynamics of brain atrophy; in particular, they may clarify the relation between its different components.

Overall, our results add to a growing corpus of research that puts focus on obtainment of specific information on the shape of individual subcortical structures rather than sole measurement of their overall volume. Likewise, morphometric features specified regionally are believed to be more disease-specific and correlated cross-sectionally than global atrophy rates, and our results confirm this. Despite the limiting factor of a small study group, our integrative evaluation appears to be fairly conclusive and contributive in terms of the interpretation of AD-related patterns of atrophy on both cortical and subcortical levels.

2) Diffusion patterns in AD

Having obtained the complementary multi-level information on structural MRI patterns in AD, we further used DTI data from the same population of patients and age-matched elderly controls (extended by additional subjects). In this study (**subchapter 4.2**), we intended to gain more insight into the WM microstructural disintegration underpinning AD pathological processes.

We achieved this aim using a model-free approach of linked independent component analysis that identified a motif of diffusion parameter alterations exemplifying AD:

- Analysis revealed six independent components, two of which demonstrated differences between AD patients and controls. One of the most crucial findings of this analysis was

that diffusion alterations in AD are dominated by *increased axial diffusivity,* paralleled by increased mean and perpendicular diffusivity (found in the intersection of major WM fibre bundles such as forceps major and minor, corona radiata and superior longitudinal fasciculus). Similar changes were found in the medio-temporal structures. Importantly, the alterations spared the internal capsulae.

The major contribution of this work consists in the finding of apparent pathological relevance of diffusion alterations in AD. In the first place, predominant influence of the axial diffusivity may imply that axonal loss is the key pathological process in WM disintegrated fibres. On this basis we further conclude that the revealed pattern of WM microstructural alterations may correspond to the coexistence of two models of WM disintegration: that of the late myelinating associating fibres, and that related to Wallerian degeneration – in accordance with the retrogenesis and Wallerian hypothesis, respectively. Alterations found in the association fibres as well as in the parahippocampal WM may indicate that these two processes can occur in parallel.

Nevertheless, apart from axial diffusivity, the influence of other diffusion metrics in independent components also contributed to our results, with possible implications of their suggested pathological relevance. Further work could disentangle these complexities and successfully explore this issue further, possibly in a longitudinal framework. If our findings can be confirmed and extended using a larger sample, it would accordingly emphasize the role of DTI as a potential biomarker in studies testing putative neuroprotective treatments.

3) Diffusion patterns in AD and NPH

In our subsequent DTI study (**subchapter 4.3**), we expanded the evaluated sample to normal pressure hydrocephalus (NPH) and compared the whole brain WM integrity in AD, NPH and normal aging. Structural imaging patterns in these conditions can sometimes be challenging to interpret and distinguish in the context of widespread atrophy. With this in mind, we hypothesised that comparison of disproportionate ventricular enlargement in NPH to the prominent ex-vacuo pattern in AD would possibly bring more information on periventricular

WM integrity than solitary comparison to a normal aging pattern, which would presumably bring more obvious results.

On the other hand, it should be mentioned that ventricular disproportionate enlargement in NPH, along with group heterogeneity, may be seen as a certain drawback compromising further analyses in between groups. To verify the reliability of these comparisons, we checked the results for possible misregistrations and excluded problematic areas (found focally in NPH – extending to internal capsule) from further analysis and interpretation.

As assumed, the whole-brain analysis restricted to the core of WM fibre tracts revealed a specific pattern of diffusion metrics changes in NPH that differentiated it from AD and healthy aging controls:

- The most characteristic findings in NPH were increased FA in the cortico-fugal tracts adjacent to the lateral ventricles, along with increased MD and axial diffusivity when compared to AD and normal aging. In contrast, posterior callosal WM and optic radiation pathways had reduced FA in parallel to increased RD in NPH patients.
- While no significant FA differences were found between AD patients and normal controls, we reported an increase in axial diffusivity, accompanied by an increase in MD – in the temporal, parietal and frontal lobes in AD patients, in correspondence with our previous findings (described in **subchapter 4.2**). The pattern of these changes was different from the one found in NPH; AD patients additionally showed higher axial diffusivity in posterior callosal WM and optic radiation when compared to NPH.
- Finally, increased lateral ventricular volume negatively correlated with the FA of the frontal white matter in AD, and the third ventricular volume positively correlated with the FA of the frontal and parietal periventricular WM in NPH.

Broadly translated, our results indicate the utility of the TBSS method in evaluation of WM microstructural alterations in the differential diagnosis of AD, NPH and normal aging. Employment of a combination of diffusion metrics appeared to facilitate the interpretation of complex underlying changes caused by different conditions:

- Parts of the experiment were broadly consistent with our previous research. With different methodology (TBSS approach versus model free approach), we confirmed the predominant role of axial diffusivity in the AD-related pattern of WM changes, which implies an increased extra-axonal space due to reduced axonal density and faster diffusion parallel to axons. As previously reviewed, the location of alterations (association fibres of the temporal, parietal and frontal lobes when compared to controls, and also optic radiation and callosal WM when compared to NPH) most probably imply a combination of axonal damage occurring secondarily to Wallerian degeneration and disintegration of late myelinating fibres in accordance with retrogenesis theory.
- We proposed two alternative explanations for the widespread changes in diffusion parameters seen in the periventricular cortico-fugal fibres in NPH. One possibility is that the increased mechanical pressure arising from reduced CSF turnover may stretch the ventricles and compress the WM fibres, which in turn will reduce the winding of the fibres within a voxel, resulting in increased water diffusivity in the main direction parallel to fibres. Alternatively, the degeneration of crossing fibres that are running through the corpus callosum (the region where reduced FA was found) may reduce perpendicular diffusivity. However, since no reduction of perpendicular diffusivity was measured here, this second hypothesis seems less likely.
- Changes in the corpus callosum and posterior periventricular WM fibres in NPH can possibly be explained by mechanical pressure on the callosal and periventricular fibres caused by the ventricular enlargement to an extent that may involve axonal degeneration (widespread increase in RD). Further implications would be strictly of a mechanical nature (stretching perpendicular to the main fibre direction) or related to CSF effusion.

A further important finding of this study was the correlation between diffusion parameters and external and internal CSF volumes. While the enlargement of the ventricles in AD is generally thought to be an ex vacuo process, our results, which show reduction of FA in frontal WM that correlates with ventricular enlargement, might also be interpreted as a sign of neurodegeneration. In contrast, the positive correlation between the periventricular FA and the size of the third ventricle points to a mechanical effect arising from increased pressure in the ventricles. These

findings might also call attention to the size of the third ventricle in diagnosis of NPH between the various CSF volumes and indices.

In this context, our conclusions could be supplemented with further research that should address the potential effect of VP shunt insertion in NPH patients on DTI parameters; some degree of normalisation might be assumed in the shunt-responsive group. Nevertheless, because our pre-operative study patient group consisted exclusively of shunt-responders (non-responders were excluded), the identified pattern of WM alterations in NPH as compared to AD and healthy age-matched controls may reflect the successful configuration for shunt indication.

Our findings therefore support the utility of diffusion imaging in differential diagnosis of NPH with the potential prediction of benefit from VP shunting. Whereas the latter assumption has already been partially addressed in later studies, further longitudinal research that would include a combination of diffusion metrics in order to assess the diffusion characteristics against the clinical course and other diagnostic markers of NPH might still prove important.

4) **Diffusion patterns in TLE**

As has been shown previously, diffusion-tensor imaging can be a very powerful approach to evaluating WM alterations on a whole-brain and tract-specific basis, and combined application of various diffusion parameters is thought to enrich the information used to differentiate between underlying conditions and describe them further; our results on AD and NPH groups seem to confirm that.

Likewise, in our further study using the TBSS approach (**subchapter 4.4**), we showed that right and left TLE have distinctive spatial patterns of WM microstructural abnormalities that can be differentiated and interpreted with the use of multiple diffusion metrics:

- Significantly reduced FA, increased MD, LD and RD were found bilaterally over widespread brain regions in RTLE as compared to the controls. An increase in MD and RD values were observed in widespread WM fibre bundles ipsilaterally in LTLE, largely

overlapping with regions where FA was lower; while no increase in LD was observed. It therefore appears that patients with RTLE exhibit a more widespread pattern of WM alterations that extend far beyond the temporal lobe in both ipsilateral and contralateral hemisphere; furthermore, these changes seem to reflect more severe damage related to chronic degeneration. Conversely, more restrained changes in the LTLE may imply a pattern of less severe axonal damage, more restricted to ipsilateral hemisphere.

- We also found a difference between the LTLE and RTLE groups for the right hippocampal volume (with and without adjustment for hippocampal sclerosis), whereas no significant volume differences were found between patients and controls. Partially comprehensive finding of more prominent hippocampal atrophy in the RTLE therefore raises an interesting issue of seizure-induced implications on grey and white matter microstructure that may not necessarily mean a straightforward causal relationship.

Several factors may influence the degree and extent of diffusion alterations in TLE, including the group heterogeneity and the severity of mesiotemporal lobe sclerosis; our results seem to partially confirm that, with the finding of widespread and severe diffusion abnormalities more apparent in the group with significant ipsilateral hippocampal volume reduction (with and without adjustment for HS). Several additional explanations have been proposed to further resolve the issue of hemispheric predominance of WM changes.

Overall, our results are broadly consistent with studies confirming that patients with TLE suffer from dysfunctions affecting large-scale brain networks rather than a single focal region. An interesting issue to address further would be to examine whether these abnormalities might be reversible with good seizure control or surgery. Additional correlations of diffusion-derived metrics with neuropsychological and functional imaging measures may provide complementary information about underlying seizure-related WM abnormalities with regard to functional hemispheric specialization; and correlations with outcome after epileptic surgery may determine the role of postictal diffusion measures in the presurgical evaluation of TLE patients.

***

The most important conclusion than can be drawn from our studies is that structural and diffusion imaging proved to be useful in identifying regionally specific and disproportionate loss of brain volume and microstructure in several pathological processes underlying cognitive deterioration. The use of several distinctive morphometric methods resulted in obtainment of complementary information on AD-related atrophy patterns, and further employment of a combination of diffusion metrics appeared to facilitate the interpretation of complex underlying pathological changes in AD, NPH and TLE. While these MRI approaches can be seen as useful diagnostic and differential support, further longitudinal studies should verify the prognostic value of distinctive measures in disease progression (AD) and in the identification of patients that would benefit from a surgical approach (NPH, TLE).

6 Lists of publications

6.1 Publications related to the thesis

(1) **Stěpán-Buksakowska I**, Keller J, Laczó J, Rulseh A, Hort J, Lisý J, Charvát F, Roček M, Hořínek D. Diffusion tensor imaging in Alzheimer disease and mild cognitive impairment. *Neurol Neurochir Pol. 2012* Sep-Oct;46(5):462-71. Review. IF: 0.486 (2012), IF: 0.817 (2017/2018)

(2) Hořínek D, **Štěpán-Buksakowska I**, Szabó N, Erickson BJ, Tóth E, Šulc V, Beneš V, Vrána J, Hort J, Nimsky C, Mohapl M, Roček M, Vécsei L, Kincses ZT. Difference in white matter microstructure in differential diagnosis of normal pressure hydrocephalus and Alzheimer's disease. *Clin Neurol Neurosurg. 2016* Jan; 140:52-9. IF: 1.381 (2016), IF: 1.736 (2017/2018)

(3) **Štěpán-Buksakowska I**, Szabó N, Hořínek D, Tóth E, Hort J, Warner J, Charvát F, Vécsei L, Roček M, Kincses ZT. Cortical and subcortical atrophy in Alzheimer disease: parallel atrophy of thalamus and hippocampus. *Alzheimer Dis Assoc Disord. 2014* Jan-Mar;28(1):65-72. IF: 2.44 (2014), IF: 1.94 (2017/2018)

(4) Kincses ZT, Hořínek D, Szabó N, Tóth E, Csete G, **Stěpán-Buksakowska I**, Hort J, Vécsei L. The pattern of diffusion parameter changes in Alzheimer's disease, identified by means of linked independent component analysis. *J Alzheimers Dis. 2013*;36(1):119-28. IF: 3.612 (2013), IF: 3.476 (2017/2018)

(5) **Buksakowska I,** Szabó N, Martinkovič L, Faragó P, Király A, Vrána J, Kincses ZT, Meluzín J, Šulc V, Kynčl M, Roček M, Tichý M, Charvát F, Hořínek D, Marusič P Distinctive Patterns of Seizure-Related White Matter Alterations in Right and Left Temporal Lobe Epilepsy – *submitted* Manuscript ID: 474992

6.2 Other publications

(1) **Štepán-Buksakowska IL**, Accurso JM, Diehn FE, Huston J, Kaufmann TJ, Luetmer PH, Wood CP, Yang X, Blezek DJ, Carter R, Hagen C, Hořínek D, Hejčl A, Roček M, Erickson BJ. Computer-aided diagnosis improves detection of small intracranial aneurysms on MRA in a clinical setting. *AJNR Am J Neuroradiol. 2014* Oct;35(10):1897-902. IF: 3.675 (2014), IF: 3.653 (2017/2018)

(2) Peter R, Korfiatis P, Blezek D, Oscar Beitia A, **Stepan-Buksakowska I**, Horinek D, Flemming KD, Erickson BJ. A quantitative symmetry-based analysis of hyperacute ischemic stroke lesions in noncontrast computed tomography. *Med Phys. 2017* Jan;44(1):192-199. IF: 2.884

7 References

Aboitiz, F., Scheibel, A.B., Fisher, R.S. & Zaidel, E. (1992) Fiber composition of the human corpus callosum. *Brain Research* 598: 143–153.

ADAMS, R.D., FISHER, C.M., HAKIM, S., OJEMANN, R.G. & SWEET, W.H. (1965) SYMPTOMATIC OCCULT HYDROCEPHALUS WITH "NORMAL" CEREBROSPINAL-FLUID PRESSURE.A TREATABLE SYNDROME. *The New England journal of medicine* 273: 117–126.

Afzali, M., Soltanian-Zadeh, H. & Elisevich, K.V. (2011) Tract based spatial statistical analysis and voxel based morphometry of diffusion indices in temporal lobe epilepsy. *Computers in Biology and Medicine* 41: 1082–1091.

Ahmadi, M.E., Hagler, D.J., McDonald, C.R., Tecoma, E.S., Iragui, V.J., Dale, A.M. & Halgren, E. (2009) Side matters: diffusion tensor imaging tractography in left and right temporal lobe epilepsy. *AJNR. American journal of neuroradiology* 30: 1740–1747.

Aizenstein, H.J., Nebes, R.D., Saxton, J.A., Price, J.C., Mathis, C.A., Tsopelas, N.D., Ziolko, S.K., James, J.A., Snitz, B.E., Houck, P.R., Bi, W., Cohen, A.D., Lopresti, B.J., DeKosky, S.T., Halligan, E.M. & Klunk, W.E. (2008) Frequent amyloid deposition without significant cognitive impairment among the elderly. *Archives of Neurology* 65: 1509–1517.

Albert, M.S., DeKosky, S.T., Dickson, D., Dubois, B., Feldman, H.H., Fox, N.C., Gamst, A., Holtzman, D.M., Jagust, W.J., Petersen, R.C., Snyder, P.J., Carrillo, M.C., Thies, B. & Phelps, C.H. (2011) The diagnosis of mild cognitive impairment due to Alzheimer's disease: recommendations from the National Institute on Aging-Alzheimer's Association workgroups on diagnostic guidelines for Alzheimer's disease. *Alzheimer's & Dementia: The Journal of the Alzheimer's Association* 7: 270–279.

Alexander, G.E., Chen, K., Pietrini, P., Rapoport, S.I. & Reiman, E.M. (2002) Longitudinal PET Evaluation of Cerebral Metabolic Decline in Dementia: A Potential Outcome Measure in Alzheimer's Disease Treatment Studies. *The American Journal of Psychiatry* 159: 738–745.

Alhusaini, S., Doherty, C.P., Scanlon, C., Ronan, L., Maguire, S., Borgulya, G., Brennan, P., Delanty, N., Fitzsimons, M. & Cavalleri, G.L. (2012) A cross-sectional MRI study of brain regional atrophy and clinical characteristics of temporal lobe epilepsy with hippocampal sclerosis. *Epilepsy Research* 99: 156–166.

Alzheimer's Association. 2019 Alzheimers's Disease Facts and Figures. (2019).

Anchisi, D., Borroni, B., Franceschi, M., Kerrouche, N., Kalbe, E., Beuthien-Beumann, B., Cappa, S., Lenz, O., Ludecke, S., Marcone, A., Mielke, R., Ortelli, P., Padovani, A., Pelati, O., Pupi, A., Scarpini, E., Weisenbach, S., Herholz, K., Salmon, E., Holthoff, V., Sorbi, S., Fazio, F. & Perani, D. (2005) Heterogeneity of brain glucose metabolism in mild cognitive impairment and clinical progression to Alzheimer disease. *Archives of Neurology* 62: 1728–1733.

Andersson, JLR, Jenkinson, M & Smith, S (2007) FMRIB Analysis Group Technical Reports TR07JA1 : Non-linear optimisation.

Apostolova, L.G. & Thompson, P.M. (2008) Mapping Progressive Brain Structural Changes in Early Alzheimer's Disease and Mild Cognitive Impairment. *Neuropsychologia* 46: 1597–1612.

Ashburner, J. (2007) A fast diffeomorphic image registration algorithm. *NeuroImage* 38: 95–113.

Ashburner, J. & Friston, K.J. (2000) Voxel-based morphometry--the methods. *NeuroImage* 11: 805–821.

Ashburner, J. & Friston, K.J. (2001) Why voxel-based morphometry should be used. *NeuroImage* 14: 1238–1243.

Ashburner, J., Hutton, C., Frackowiak, R., Johnsrude, I., Price, C. & Friston, K. (1998) Identifying global anatomical differences: deformation-based morphometry. *Human Brain Mapping* 6: 348–357.

Assaf, Y., Ben-Sira, L., Constantini, S., Chang, L.C. & Beni-Adani, L. (2006) Diffusion tensor imaging in hydrocephalus: initial experience. *AJNR. American journal of neuroradiology* 27: 1717–1724.

Asselin, A., Potvin, O., Bouchard, L.-O., Brisson, M. & Duchesne, S. (2019) Validation of an Magnetic Resonance Imaging Acquisition and Review Protocol for Alzheimer's Disease and Related Disorders. *Canadian Association of Radiologists Journal = Journal l'Association Canadienne Des Radiologistes*.

Aygok, G., Marmarou, A. & Young, H.F. (2005) Three-year outcome of shunted idiopathic NPH patients. *Acta neurochirurgica. Supplement* 95: 241–245.

Bao, Y., He, R., Zeng, Q., Zhu, P., Zheng, R. & Xu, H. (2018) Investigation of microstructural abnormalities in white and gray matter around hippocampus with diffusion tensor imaging (DTI) in temporal lobe epilepsy (TLE). *Epilepsy & Behavior: E&B* 83: 44–49.

Baron, J.C., Chételat, G., Desgranges, B., Perchey, G., Landeau, B., de la Sayette, V. & Eustache, F. (2001) In vivo mapping of gray matter loss with voxel-based morphometry in mild Alzheimer's disease. *NeuroImage* 14: 298–309.

Bartzokis, G. (2004) Age-related myelin breakdown: a developmental model of cognitive decline and Alzheimer's disease. *Neurobiology of Aging* 25: 5–18; author reply 49-62.

Basser, P.J. & Jones, D.K. (2002) Diffusion-tensor MRI: theory, experimental design and data analysis – a technical review. *NMR in Biomedicine* 15: 456–467.

Basser, P.J. & Pierpaoli, C. (1996) Microstructural and physiological features of tissues elucidated by quantitative-diffusion-tensor MRI. *Journal of Magnetic Resonance. Series B* 111: 209–219.

Bateman, G.A. & Loiselle, A.M. (2007) Can MR measurement of intracranial hydrodynamics and compliance differentiate which patient with idiopathic normal pressure hydrocephalus will improve following shunt insertion? *Acta Neurochirurgica* 149: 455–462; discussion 462.

Beaulieu, C. (2002) The basis of anisotropic water diffusion in the nervous system - a technical review. *NMR in biomedicine* 15: 435–455.

Bech-Azeddine, R., Høgh, P., Juhler, M., Gjerris, F. & Waldemar, G. (2007) Idiopathic normal-pressure hydrocephalus: clinical comorbidity correlated with cerebral biopsy findings and outcome of cerebrospinal fluid shunting. *Journal of neurology, neurosurgery, and psychiatry* 78: 157–161.

Bennett, D.A., Schneider, J.A., Wilson, R.S., Bienias, J.L. & Arnold, S.E. (2004) Neurofibrillary tangles mediate the association of amyloid load with clinical Alzheimer disease and level of cognitive function. *Archives of Neurology* 61: 378–384.

Blennow, K. & Hampel, H. (2003) CSF markers for incipient Alzheimer's disease. *The Lancet. Neurology* 2: 605–613.

Blümcke, I., Thom, M., Aronica, E., Armstrong, D.D., Bartolomei, F., Bernasconi, A., Bernasconi, N., Bien, C.G., Cendes, F., Coras, R., Cross, J.H., Jacques, T.S., Kahane, P., Mathern, G.W., Miyata, H., Moshé, S.L., Oz, B., Özkara, Ç., Perucca, E., Sisodiya, S., Wiebe, S. & Spreafico, R. (2013) International consensus classification of hippocampal sclerosis in temporal lobe epilepsy: a Task Force report from the ILAE Commission on Diagnostic Methods. *Epilepsia* 54: 1315–1329.

Bonilha, L., Edwards, J.C., Kinsman, S.L., Morgan, P.S., Fridriksson, J., Rorden, C., Rumboldt, Z., Roberts, D.R., Eckert, M.A. & Halford, J.J. (2010) Extrahippocampal gray matter loss and hippocampal deafferentation in patients with temporal lobe epilepsy. *Epilepsia* 51: 519–528.

Bosch, B., Arenaza-Urquijo, E.M., Rami, L., Sala-Llonch, R., Junqué, C., Solé-Padullés, C., Peña-Gómez, C., Bargalló, N., Molinuevo, J.L. & Bartrés-Faz, D. (2012) Multiple DTI index

analysis in normal aging, amnestic MCI and AD. Relationship with neuropsychological performance. *Neurobiology of Aging* 33: 61–74.

Bozzali, M., Falini, A., Franceschi, M., Cercignani, M., Zuffi, M., Scotti, G., Comi, G. & Filippi, M. (2002) White matter damage in Alzheimer's disease assessed in vivo using diffusion tensor magnetic resonance imaging. *Journal of Neurology, Neurosurgery, and Psychiatry* 72: 742–746.

Braak, H. & Braak, E. (1997) Frequency of stages of Alzheimer-related lesions in different age categories. *Neurobiology of aging* 18: 351–357.

Braak, H., Braak, E. & Bohl, J. (1993) Staging of Alzheimer-related cortical destruction. *European Neurology* 33: 403–408.

Braak, H. & Del Tredici, K. (2011) The pathological process underlying Alzheimer's disease in individuals under thirty. *Acta Neuropathologica* 121: 171–181.

Brenowitz, W.D., Hubbard, R.A., Keene, C.D., Hawes, S.E., Longstreth, W.T., Woltjer, R.L. & Kukull, W.A. (2017) Mixed neuropathologies and estimated rates of clinical progression in a large autopsy sample. *Alzheimer's & Dementia: The Journal of the Alzheimer's Association* 13: 654–662.

Brickman, A.M., Muraskin, J. & Zimmerman, M.E. (2009) Structural neuroimaging in Altheimer's disease: do white matter hyperintensities matter? *Dialogues in Clinical Neuroscience* 11: 181–190.

Brun, A. & Englund, E. (1986) A white matter disorder in dementia of the Alzheimer type: a pathoanatomical study. *Annals of Neurology* 19: 253–262.

Budde, M.D., Kim, J.H., Liang, H.-F., Russell, J.H., Cross, A.H. & Song, S.-K. (2008) Axonal injury detected by in vivo diffusion tensor imaging correlates with neurological disability in a mouse model of multiple sclerosis. *NMR in biomedicine* 21: 589–597.

Budde, M.D., Kim, J.H., Liang, H.-F., Schmidt, R.E., Russell, J.H., Cross, A.H. & Song, S.-K. (2007) Toward accurate diagnosis of white matter pathology using diffusion tensor imaging. *Magnetic Resonance in Medicine: Official Journal of the Society of Magnetic Resonance in Medicine / Society of Magnetic Resonance in Medicine* 57: 688–695.

Campos, B.M., Coan, A.C., Beltramini, G.C., Liu, M., Yassuda, C.L., Ghizoni, E., Beaulieu, C., Gross, D.W. & Cendes, F. (2015) White matter abnormalities associate with type and localization of focal epileptogenic lesions. *Epilepsia* 56: 125–132.

Cavazos, J.E., Das, I. & Sutula, T.P. (1994) Neuronal loss induced in limbic pathways by kindling: evidence for induction of hippocampal sclerosis by repeated brief seizures. *The Journal of Neuroscience: The Official Journal of the Society for Neuroscience* 14: 3106–3121.

Ceritoglu, C., Tang, X., Chow, M., Hadjiabadi, D., Shah, D., Brown, T., Burhanullah, M.H., Trinh, H., Hsu, J., Ament, K.A., Crocetti, D., Mori, S., Mostofsky, S.H., Yantis, S., Miller, M.I. & Ratnanather, J.T. (2013) Computational analysis of LDDMM for brain mapping. *Frontiers in Neuroscience* 7:.

Chen, T.-F., Lin, C.-C., Chen, Y.-F., Liu, H.-M., Hua, M.-S., Huang, Y.-C. & Chiu, M.-J. (2009) Diffusion tensor changes in patients with amnesic mild cognitive impairment and various dementias. *Psychiatry Research* 173: 15–21.

Cherubini, A., Péran, P., Spoletini, I., Di Paola, M., Di Iulio, F., Hagberg, G.E., Sancesario, G., Gianni, W., Bossù, P., Caltagirone, C., Sabatini, U. & Spalletta, G. (2010) Combined volumetry and DTI in subcortical structures of mild cognitive impairment and Alzheimer's disease patients. *Journal of Alzheimer's disease: JAD* 19: 1273–1282.

Cho, H., Yang, D.W., Shon, Y.M., Kim, B.S., Kim, Y.I., Choi, Y.B., Lee, K.S., Shim, Y.S., Yoon, B., Kim, W. & Ahn, K.J. (2008) Abnormal integrity of corticocortical tracts in mild cognitive impairment: a diffusion tensor imaging study. *Journal of Korean Medical Science* 23: 477–483.

Cho, Y., Seong, J.-K., Jeong, Y., Shin, S.Y. & Alzheimer's Disease Neuroimaging Initiative (2012) Individual subject classification for Alzheimer's disease based on incremental learning using a spatial frequency representation of cortical thickness data. *NeuroImage* 59: 2217–2230.

Choi, S.J., Lim, K.O., Monteiro, I. & Reisberg, B. (2005) Diffusion tensor imaging of frontal white matter microstructure in early Alzheimer's disease: a preliminary study. *Journal of Geriatric Psychiatry and Neurology* 18: 12–19.

Christensen, G.E., Rabbitt, R.D. & Miller, M.I. (1996) Deformable templates using large deformation kinematics. *IEEE transactions on image processing: a publication of the IEEE Signal Processing Society* 5: 1435–1447.

Chupin, M., Gérardin, E., Cuingnet, R., Boutet, C., Lemieux, L., Lehéricy, S., Benali, H., Garnero, L., Colliot, O. & Alzheimer's Disease Neuroimaging Initiative (2009) Fully automatic hippocampus segmentation and classification in Alzheimer's disease and mild cognitive impairment applied on data from ADNI. *Hippocampus* 19: 579–587.

Coleman, M. (2005) Axon degeneration mechanisms: commonality amid diversity. *Nature Reviews. Neuroscience* 6: 889–898.

Colnat-Coulbois, S., Mok, K., Klein, D., Pénicaud, S., Tanriverdi, T. & Olivier, A. (2010) Tractography of the amygdala and hippocampus: anatomical study and application to selective amygdalohippocampectomy. *Journal of Neurosurgery* 113: 1135–1143.

Cosottini, M., Giannelli, M., Siciliano, G., Lazzarotti, G., Michelassi, M.C., Del Corona, A., Bartolozzi, C. & Murri, L. (2005) Diffusion-tensor MR imaging of corticospinal tract in amyotrophic lateral sclerosis and progressive muscular atrophy. *Radiology* 237: 258–264.

Csernansky, J.G., Wang, L., Swank, J., Miller, J.P., Gado, M., McKeel, D., Miller, M.I. & Morris, J.C. (2005) Preclinical detection of Alzheimer's disease: hippocampal shape and volume predict dementia onset in the elderly. *NeuroImage* 25: 783–792.

Cuingnet, R., Glaunes, J.A., Chupin, M., Benali, H. & Colliot, O. (2013a) Spatial and Anatomical Regularization of SVM: A General Framework for Neuroimaging Data. *IEEE Transactions on Pattern Analysis and Machine Intelligence* 35: 682–696.

Dale, B.D., Brown, M.A. & Semelka, R.C. (2015) *MRI: basic principles and applications*.

Damasceno, B.P. (2015) Neuroimaging in normal pressure hydrocephalus. *Dementia & Neuropsychologia* 9: 350–355.

Damoiseaux, J.S., Smith, S.M., Witter, M.P., Sanz-Arigita, E.J., Barkhof, F., Scheltens, P., Stam, C.J., Zarei, M. & Rombouts, S.A.R.B. (2009) White matter tract integrity in aging and Alzheimer's disease. *Human brain mapping* 30: 1051–1059.

Dang, C., Harrington, K.D., Lim, Y.Y., Ames, D., Hassenstab, J., Laws, S.M., Yassi, N., Hickey, M., Rainey-Smith, S., Robertson, J., Sohrabi, H.R., Salvado, O., Weinborn, M., Villemagne, V.L., Rowe, C.C., Masters, C.L., Maruff, P. & AIBL Research Group (2018) Relationship Between Amyloid-β Positivity and Progression to Mild Cognitive Impairment or Dementia over 8 Years in Cognitively Normal Older Adults. *Journal of Alzheimer's disease: JAD* 65: 1313–1325.

Dartigues, J.F. (2009) Alzheimer's disease: a global challenge for the 21st century. *The Lancet. Neurology* 8: 1082–1083.

Davatzikos, C., Resnick, S.M., Wu, X., Parmpi, P. & Clark, C.M. (2008) Individual patient diagnosis of AD and FTD via high-dimensional pattern classification of MRI. *NeuroImage* 41: 1220–1227.

Davies, R.R., Kipps, C.M., Mitchell, J., Kril, J.J., Halliday, G.M. & Hodges, J.R. (2006) Progression in frontotemporal dementia: identifying a benign behavioral variant by magnetic resonance imaging. *Archives of Neurology* 63: 1627–1631.

Davies, R.R., Scahill, V.L., Graham, A., Williams, G.B., Graham, K.S. & Hodges, J.R. (2009) Development of an MRI rating scale for multiple brain regions: comparison with volumetrics and with voxel-based morphometry. *Neuroradiology* 51: 491–503.

De Leon, M.J., George, A.E., Golomb, J., Tarshish, C., Convit, A., Kluger, A., De Santi, S., McRae, T., Ferris, S.H., Reisberg, B., Ince, C., Rusinek, H., Bobinski, M., Quinn, B., Miller, D.C. & Wisniewski, H.M. (1997) Frequency of hippocampal formation atrophy in normal aging and Alzheimer's disease. *Neurobiology of Aging* 18: 1–11.

De Reuck, J., Maurage, C.-A., Deramecourt, V., Pasquier, F., Cordonnier, C., Leys, D. & Bordet, R. (2018) Aging and cerebrovascular lesions in pure and in mixed neurodegenerative and vascular dementia brains: a neuropathological study. *Folia Neuropathologica* 56: 81–87.

Del Bigio, M.R., Wilson, M.J. & Enno, T. (2003) Chronic hydrocephalus in rats and humans: white matter loss and behavior changes. *Annals of neurology* 53: 337–346.

Delbeuck, X., Van der Linden, M. & Collette, F. (2003) Alzheimer's disease as a disconnection syndrome? *Neuropsychology Review* 13: 79–92.

Deleo, F., Thom, M., Concha, L., Bernasconi, A., Bernhardt, B.C. & Bernasconi, N. (2018) Histological and MRI markers of white matter damage in focal epilepsy. *Epilepsy Research* 140: 29–38.

Della Nave, R., Ginestroni, A., Tessa, C., Giannelli, M., Piacentini, S., Filippi, M. & Mascalchi, M. (2010) Regional distribution and clinical correlates of white matter structural damage in Huntington disease: a tract-based spatial statistics study. *AJNR. American journal of neuroradiology* 31: 1675–1681.

Deng, W., Wang, H., Rosenberg, P.A., Volpe, J.J. & Jensen, F.E. (2004) Role of metabotropic glutamate receptors in oligodendrocyte excitotoxicity and oxidative stress. *Proceedings of the National Academy of Sciences of the United States of America* 101: 7751–7756.

Desai, M.K., Sudol, K.L., Janelsins, M.C., Mastrangelo, M.A., Frazer, M.E. & Bowers, W.J. (2009) Triple-transgenic Alzheimer's disease mice exhibit region-specific abnormalities in brain myelination patterns prior to appearance of amyloid and tau pathology. *Glia* 57: 54–65.

Di Paola, M., Luders, E., Di Iulio, F., Cherubini, A., Passafiume, D., Thompson, P.M., Caltagirone, C., Toga, A.W. & Spalletta, G. (2010) Callosal atrophy in mild cognitive impairment and Alzheimer's disease: different effects in different stages. *NeuroImage* 49: 141–149.

Dick, A.S. & Tremblay, P. (2012) Beyond the arcuate fasciculus: consensus and controversy in the connectional anatomy of language. *Brain: A Journal of Neurology* 135: 3529–3550.

Dicks, E., Vermunt, L., van der Flier, W.M., Visser, P.J., Barkhof, F., Scheltens, P., Tijms, B.M. & Alzheimer's Disease Neuroimaging Initiative (2019) Modeling grey matter atrophy as a function of time, aging or cognitive decline show different anatomical patterns in Alzheimer's disease. *NeuroImage. Clinical* 22: 101786.

Diehl, B., Symms, M.R., Boulby, P.A., Salmenpera, T., Wheeler-Kingshott, C.A.M., Barker, G.J. & Duncan, J.S. (2005) Postictal diffusion tensor imaging. *Epilepsy Research* 65: 137–146.

Ding, Y., McAllister, J.P., 2nd, Yao, B., Yan, N. & Canady, A.I. (2001) Axonal damage associated with enlargement of ventricles during hydrocephalus: a silver impregnation study. *Neurological research* 23: 581–587.

Douaud, G., Jbabdi, S., Behrens, T.E.J., Menke, R.A., Gass, A., Monsch, A.U., Rao, A., Whitcher, B., Kindlmann, G., Matthews, P.M. & Smith, S. (2011) DTI measures in crossing-fibre areas: increased diffusion anisotropy reveals early white matter alteration in MCI and mild Alzheimer's disease. *NeuroImage* 55: 880–890.

Douaud, G., Smith, S., Jenkinson, M., Behrens, T., Johansen-Berg, H., Vickers, J., James, S., Voets, N., Watkins, K., Matthews, P.M. & James, A. (2007) Anatomically related grey and white matter abnormalities in adolescent-onset schizophrenia. *Brain: A Journal of Neurology* 130: 2375–2386.

Douet, V. & Chang, L. (2015) Fornix as an imaging marker for episodic memory deficits in healthy aging and in various neurological disorders. *Frontiers in Aging Neuroscience* 6:.

Duan, J.-H., Wang, H.-Q., Xu, J., Lin, X., Chen, S.-Q., Kang, Z. & Yao, Z.-B. (2006) White matter damage of patients with Alzheimer's disease correlated with the decreased cognitive function. *Surgical and radiologic anatomy: SRA* 28: 150–156.

Dubois, B., Feldman, H.H., Jacova, C., Dekosky, S.T., Barberger-Gateau, P., Cummings, J., Delacourte, A., Galasko, D., Gauthier, S., Jicha, G., Meguro, K., O'brien, J., Pasquier, F., Robert, P., Rossor, M., Salloway, S., Stern, Y., Visser, P.J. & Scheltens, P. (2007) Research criteria for the diagnosis of Alzheimer's disease: revising the NINCDS-ADRDA criteria. *The Lancet. Neurology* 6: 734–746.

Espay, A.J., Da Prat, G.A., Dwivedi, A.K., Rodriguez-Porcel, F., Vaughan, J.E., Rosso, M., Devoto, J.L., Duker, A.P., Masellis, M., Smith, C.D., Mandybur, G.T., Merola, A. & Lang, A.E. (2017) Deconstructing normal pressure hydrocephalus: Ventriculomegaly as early sign of neurodegeneration. *Annals of Neurology* 82: 503–513.

Fazekas, F., Chawluk, J.B., Alavi, A., Hurtig, H.I. & Zimmerman, R.A. (1987) MR signal abnormalities at 1.5 T in Alzheimer's dementia and normal aging. *AJR. American journal of roentgenology* 149: 351–356.

Fein, G., Di Sclafani, V., Taylor, C., Moon, K., Barakos, J., Tran, H., Landman, B. & Shumway, R. (2004) Controlling for premorbid brain size in imaging studies: T1-derived cranium scaling factor vs. T2-derived intracranial vault volume. *Psychiatry Research* 131: 169–176.

Fellgiebel, A., Schermuly, I., Gerhard, A., Keller, I., Albrecht, J., Weibrich, C., Müller, M.J. & Stoeter, P. (2008) Functional relevant loss of long association fibre tracts integrity in early Alzheimer's disease. *Neuropsychologia* 46: 1698–1706.

Fellgiebel, A., Scheurich, A., Bartenstein, P. & Müller, M.J. (2007) FDG-PET and CSF phospho-tau for prediction of cognitive decline in mild cognitive impairment. *Psychiatry Research* 155: 167–171.

Fischl, B. (2012) FreeSurfer. *NeuroImage* 62: 774–781.

Fischl, B., Liu, A. & Dale, A.M. (2001) Automated manifold surgery: constructing geometrically accurate and topologically correct models of the human cerebral cortex. *IEEE transactions on medical imaging* 20: 70–80.

Fletcher, E., Raman, M., Huebner, P., Liu, A., Mungas, D., Carmichael, O. & DeCarli, C. (2013) Loss of fornix white matter volume as a predictor of cognitive impairment in cognitively normal elderly individuals. *JAMA neurology* 70: 1389–1395.

Focke, N.K., Yogarajah, M., Bonelli, S.B., Bartlett, P.A., Symms, M.R. & Duncan, J.S. (2008) Voxel-based diffusion tensor imaging in patients with mesial temporal lobe epilepsy and hippocampal sclerosis. *NeuroImage* 40: 728–737.

Foster, N.L., Heidebrink, J.L., Clark, C.M., Jagust, W.J., Arnold, S.E., Barbas, N.R., DeCarli, C.S., Turner, R.S., Koeppe, R.A., Higdon, R. & Minoshima, S. (2007) FDG-PET improves accuracy in distinguishing frontotemporal dementia and Alzheimer's disease. *Brain: A Journal of Neurology* 130: 2616–2635.

Friman, O., Farnebäck, G. & Westin, C.-F. (2006) A Bayesian approach for stochastic white matter tractography. *IEEE transactions on medical imaging* 25: 965–978.

Frisoni, G.B., Fox, N.C., Jack, C.R., Scheltens, P. & Thompson, P.M. (2010) The clinical use of structural MRI in Alzheimer disease. *Nature reviews. Neurology* 6: 67–77.

Frisoni, G.B., Ganzola, R., Canu, E., Rüb, U., Pizzini, F.B., Alessandrini, F., Zoccatelli, G., Beltramello, A., Caltagirone, C. & Thompson, P.M. (2008) Mapping local hippocampal changes in Alzheimer's disease and normal ageing with MRI at 3 Tesla. *Brain: A Journal of Neurology* 131: 3266–3276.

Galton, C.J., Gomez-Anson, B., Antoun, N., Scheltens, P., Patterson, K., Graves, M., Sahakian, B.J. & Hodges, J.R. (2001) Temporal lobe rating scale: application to Alzheimer's disease and frontotemporal dementia. *Journal of Neurology, Neurosurgery, and Psychiatry* 70: 165–173.

Golomb, J., Wisoff, J., Miller, D.C., Boksay, I., Kluger, A., Weiner, H., Salton, J. & Graves, W. (2000) Alzheimer's disease comorbidity in normal pressure hydrocephalus: prevalence and shunt response. *Journal of neurology, neurosurgery, and psychiatry* 68: 778–781.

Gómez-Isla, T., Hollister, R., West, H., Mui, S., Growdon, J.H., Petersen, R.C., Parisi, J.E. & Hyman, B.T. (1997) Neuronal loss correlates with but exceeds neurofibrillary tangles in Alzheimer's disease. *Annals of Neurology* 41: 17–24.

Good, C.D., Johnsrude, I.S., Ashburner, J., Henson, R.N., Friston, K.J. & Frackowiak, R.S. (2001) A voxel-based morphometric study of ageing in 465 normal adult human brains. *NeuroImage* 14: 21–36.

Gorelick, P.B., Scuteri, A., Black, S.E., Decarli, C., Greenberg, S.M., Iadecola, C., Launer, L.J., Laurent, S., Lopez, O.L., Nyenhuis, D., Petersen, R.C., Schneider, J.A., Tzourio, C., Arnett, D.K., Bennett, D.A., Chui, H.C., Higashida, R.T., Lindquist, R., Nilsson, P.M., Roman, G.C., Sellke, F.W., Seshadri, S. & American Heart Association Stroke Council, Council on Epidemiology and Prevention, Council on Cardiovascular Nursing, Council on Cardiovascular Radiology and Intervention, and Council on Cardiovascular Surgery and Anesthesia (2011) Vascular contributions to cognitive impairment and dementia: a statement for healthcare professionals from the american heart association/american stroke association. *Stroke* 42: 2672–2713.

Gorno-Tempini, M.L., Hillis, A.E., Weintraub, S., Kertesz, A., Mendez, M., Cappa, S.F., Ogar, J.M., Rohrer, J.D., Black, S., Boeve, B.F., Manes, F., Dronkers, N.F., Vandenberghe, R., Rascovsky, K., Patterson, K., Miller, B.L., Knopman, D.S., Hodges, J.R., Mesulam, M.M. & Grossman, M. (2011) Classification of primary progressive aphasia and its variants. *Neurology* 76: 1006–1014.

Greicius, M.D., Srivastava, G., Reiss, A.L. & Menon, V. (2004) Default-mode network activity distinguishes Alzheimer's disease from healthy aging: evidence from functional MRI. *Proceedings of the National Academy of Sciences of the United States of America* 101: 4637–4642.

Gross, D.W. (2011) Diffusion tensor imaging in temporal lobe epilepsy. *Epilepsia* 52 Suppl 4: 32–34.

Groves, A.R., Beckmann, C.F., Smith, S.M. & Woolrich, M.W. (2011) Linked independent component analysis for multimodal data fusion. *NeuroImage* 54: 2198–2217.

Gunning-Dixon, F.M. & Raz, N. (2000) The cognitive correlates of white matter abnormalities in normal aging: a quantitative review. *Neuropsychology* 14: 224–232.

Hamilton, R., Patel, S., Lee, E.B., Jackson, E.M., Lopinto, J., Arnold, S.E., Clark, C.M., Basil, A., Shaw, L.M., Xie, S.X., Grady, M.S. & Trojanowski, J.Q. (2010) Lack of shunt response in suspected idiopathic normal pressure hydrocephalus with Alzheimer disease pathology. *Annals of neurology* 68: 535–540.

Hampel, H., Frank, R., Broich, K., Teipel, S.J., Katz, R.G., Hardy, J., Herholz, K., Bokde, A.L.W., Jessen, F., Hoessler, Y.C., Sanhai, W.R., Zetterberg, H., Woodcock, J. & Blennow, K. (2010) Biomarkers for Alzheimer's disease: academic, industry and regulatory perspectives. *Nature Reviews. Drug Discovery* 9: 560–574.

Hanamiya, M., Korogi, Y., Kakeda, S., Ohnari, N., Kamada, K., Moriya, J., Sato, T., Kitajima, M., Akamatsu, N. & Tsuji, S. (2009) Partial loss of hippocampal striation in medial temporal lobe epilepsy: pilot evaluation with high-spatial-resolution T2-weighted MR imaging at 3.0 T. *Radiology* 251: 873–881.

Harper, L., Barkhof, F., Fox, N.C. & Schott, J.M. (2015) Using visual rating to diagnose dementia: a critical evaluation of MRI atrophy scales. *Journal of Neurology, Neurosurgery, and Psychiatry* 86: 1225–1233.

Harper, L., Barkhof, F., Scheltens, P., Schott, J.M. & Fox, N.C. (2014) An algorithmic approach to structural imaging in dementia. *J Neurol Neurosurg Psychiatry* 85: 692–698.

Harper, L., Fumagalli, G.G., Barkhof, F., Scheltens, P., O'Brien, J.T., Bouwman, F., Burton, E.J., Rohrer, J.D., Fox, N.C., Ridgway, G.R. & Schott, J.M. (2016) MRI visual rating scales in the diagnosis of dementia: evaluation in 184 post-mortem confirmed cases. *Brain: A Journal of Neurology* 139: 1211–1225.

Hashimoto, M., Ishikawa, M., Mori, E., Kuwana, N. & Study of INPH on neurological improvement (SINPHONI) (2010) Diagnosis of idiopathic normal pressure hydrocephalus is supported by MRI-based scheme: a prospective cohort study. *Cerebrospinal Fluid Research* 7: 18.

Hattingen, E., Jurcoane, A., Melber, J., Blasel, S., Zanella, F.E., Neumann-Haefelin, T. & Singer, O.C. (2010) Diffusion tensor imaging in patients with adult chronic idiopathic hydrocephalus. *Neurosurgery* 66: 917–924.

Hattori, T., Ito, K., Aoki, S., Yuasa, T., Sato, R., Ishikawa, M., Sawaura, H., Hori, M. & Mizusawa, H. (2012a) White matter alteration in idiopathic normal pressure hydrocephalus: tract-based spatial statistics study. *AJNR. American journal of neuroradiology* 33: 97–103.

Hattori, T., Sato, R., Aoki, S., Yuasa, T. & Mizusawa, H. (2012b) Different patterns of fornix damage in idiopathic normal pressure hydrocephalus and Alzheimer disease. *AJNR. American journal of neuroradiology* 33: 274–279.

Hattori, T., Yuasa, T., Aoki, S., Sato, R., Sawaura, H., Mori, T. & Mizusawa, H. (2011) Altered microstructure in corticospinal tract in idiopathic normal pressure hydrocephalus: comparison with Alzheimer disease and Parkinson disease with dementia. *AJNR. American journal of neuroradiology* 32: 1681–1687.

He, W., Goodkind, D. & Kowal, P. (2015) International Population Reports. 175.

Hebert, L.E., Scherr, P.A., Bienias, J.L., Bennett, D.A. & Evans, D.A. (2003) Alzheimer disease in the US population: prevalence estimates using the 2000 census. *Archives of Neurology* 60: 1119–1122.

Hebert, L.E., Weuve, J., Scherr, P.A. & Evans, D.A. (2013) Alzheimer disease in the United States (2010-2050) estimated using the 2010 census. *Neurology* 80: 1778–1783.

Heimann, T. & Meinzer, H.-P. (2009) Statistical shape models for 3D medical image segmentation: A review. *Medical Image Analysis* 13: 543–563.

Hoffman, J.M., Welsh-Bohmer, K.A., Hanson, M., Crain, B., Hulette, C., Earl, N. & Coleman, R.E. (2000) FDG PET imaging in patients with pathologically verified dementia. *Journal of Nuclear Medicine: Official Publication, Society of Nuclear Medicine* 41: 1920–1928.

Hong, Y.J., Yoon, B., Shim, Y.S., Cho, A.H., Lim, S.C., Ahn, K.J. & Yang, D.W. (2010) Differences in microstructural alterations of the hippocampus in Alzheimer disease and idiopathic normal pressure hydrocephalus: a diffusion tensor imaging study. *AJNR. American journal of neuroradiology* 31: 1867–1872.

Horínek, D., Varjassyová, A. & Hort, J. (2007) Magnetic resonance analysis of amygdalar volume in Alzheimer's disease. *Current Opinion in Psychiatry* 20: 273–277.

Horiuchi, M., Maezawa, I., Itoh, A., Wakayama, K., Jin, L.-W., Itoh, T. & Decarli, C. (2012) Amyloid β1-42 oligomer inhibits myelin sheet formation in vitro. *Neurobiology of Aging* 33: 499–509.

Hornberger, M., Savage, S., Hsieh, S., Mioshi, E., Piguet, O. & Hodges, J.R. (2010) Orbitofrontal dysfunction discriminates behavioral variant frontotemporal dementia from Alzheimer's disease. *Dementia and Geriatric Cognitive Disorders* 30: 547–552.

Hort, J., O'Brien, J.T., Gainotti, G., Pirttila, T., Popescu, B.O., Rektorova, I., Sorbi, S., Scheltens, P. & EFNS Scientist Panel on Dementia (2010) EFNS guidelines for the diagnosis and management of Alzheimer's disease. *European Journal of Neurology* 17: 1236–1248.

Hua, X., Leow, A.D., Lee, S., Klunder, A.D., Toga, A.W., Lepore, N., Chou, Y.-Y., Brun, C., Chiang, M.-C., Barysheva, M., Jack, C.R., Bernstein, M.A., Britson, P.J., Ward, C.P., Whitwell, J.L., Borowski, B., Fleisher, A.S., Fox, N.C., Boyes, R.G., Barnes, J., Harvey, D., Kornak, J., Schuff, N., Boreta, L., Alexander, G.E., Weiner, M.W., Thompson, P.M. & Alzheimer's Disease Neuroimaging Initiative (2008) 3D characterization of brain atrophy in Alzheimer's disease and mild cognitive impairment using tensor-based morphometry. *NeuroImage* 41: 19–34.

Huang, J. & Auchus, A.P. (2007) Diffusion tensor imaging of normal appearing white matter and its correlation with cognitive functioning in mild cognitive impairment and Alzheimer's disease. *Annals of the New York Academy of Sciences* 1097: 259–264.

Hutchinson, E., Pulsipher, D., Dabbs, K., Myers y Gutierrez, A., Sheth, R., Jones, J., Seidenberg, M., Meyerand, E. & Hermann, B. (2010) Children with new-onset epilepsy exhibit diffusion abnormalities in cerebral white matter in the absence of volumetric differences. *Epilepsy Research* 88: 208–214.

Hyman, B.T. (1997) The neuropathological diagnosis of Alzheimer's disease: clinical-pathological studies. *Neurobiology of Aging* 18: S27-32.

Ingelsson, M., Fukumoto, H., Newell, K.L., Growdon, J.H., Hedley-Whyte, E.T., Frosch, M.P., Albert, M.S., Hyman, B.T. & Irizarry, M.C. (2004) Early Abeta accumulation and progressive synaptic loss, gliosis, and tangle formation in AD brain. *Neurology* 62: 925–931.

Ivkovic, M., Liu, B., Ahmed, F., Moore, D., Huang, C., Raj, A., Kovanlikaya, I., Heier, L. & Relkin, N. (2012) Differential Diagnosis of Normal Pressure Hydrocephalus by MRI Mean Diffusivity Histogram Analysis. *AJNR. American journal of neuroradiology*.

Jack, C.R., Albert, M.S., Knopman, D.S., McKhann, G.M., Sperling, R.A., Carrillo, M.C., Thies, B. & Phelps, C.H. (2011) Introduction to the recommendations from the National Institute on Aging-Alzheimer's Association workgroups on diagnostic guidelines for Alzheimer's disease. *Alzheimer's & Dementia: The Journal of the Alzheimer's Association* 7: 257–262.

Jack, C.R., Bernstein, M.A., Fox, N.C., Thompson, P., Alexander, G., Harvey, D., Borowski, B., Britson, P.J., Whitwell, J.L., Ward, C., Dale, A.M., Felmlee, J.P., Gunter, J.L., Hill, D.L.G., Killiany, R., Schuff, N., Fox-Bosetti, S., Lin, C., Studholme, C., DeCarli, C.S., Krueger, G., Ward, H.A., Metzger, G.J., Scott, K.T., Mallozzi, R., Blezek, D., Levy, J., Debbins, J.P., Fleisher, A.S., Albert, M., Green, R., Bartzokis, G., Glover, G., Mugler, J. & Weiner, M.W. (2008a) The Alzheimer's Disease Neuroimaging Initiative (ADNI): MRI Methods. *Journal of magnetic resonance imaging : JMRI* 27: 685–691.

Jack, C.R., Jr, Petersen, R.C., Xu, Y.C., O'Brien, P.C., Smith, G.E., Ivnik, R.J., Boeve, B.F., Waring, S.C., Tangalos, E.G. & Kokmen, E. (1999) Prediction of AD with MRI-based hippocampal volume in mild cognitive impairment. *Neurology* 52: 1397–1403.

Jack, C.R., Lowe, V.J., Senjem, M.L., Weigand, S.D., Kemp, B.J., Shiung, M.M., Knopman, D.S., Boeve, B.F., Klunk, W.E., Mathis, C.A. & Petersen, R.C. (2008b) 11C PiB and structural MRI provide complementary information in imaging of Alzheimer's disease and amnestic mild cognitive impairment. *Brain: A Journal of Neurology* 131: 665–680.

Jack, C.R., Lowe, V.J., Weigand, S.D., Wiste, H.J., Senjem, M.L., Knopman, D.S., Shiung, M.M., Gunter, J.L., Boeve, B.F., Kemp, B.J., Weiner, M., Petersen, R.C. & Alzheimer's Disease Neuroimaging Initiative (2009) Serial PIB and MRI in normal, mild cognitive impairment and Alzheimer's disease: implications for sequence of pathological events in Alzheimer's disease. *Brain: A Journal of Neurology* 132: 1355–1365.

Jack, C.R., Weigand, S.D., Shiung, M.M., Przybelski, S.A., O'Brien, P.C., Gunter, J.L., Knopman, D.S., Boeve, B.F., Smith, G.E. & Petersen, R.C. (2008c) Atrophy rates accelerate in amnestic mild cognitive impairment. *Neurology* 70: 1740–1752.

Jack, C.R., Wiste, H.J., Vemuri, P., Weigand, S.D., Senjem, M.L., Zeng, G., Bernstein, M.A., Gunter, J.L., Pankratz, V.S., Aisen, P.S., Weiner, M.W., Petersen, R.C., Shaw, L.M., Trojanowski, J.Q., Knopman, D.S. & Alzheimer's Disease Neuroimaging Initiative (2010) Brain beta-amyloid measures and magnetic resonance imaging atrophy both predict time-to-progression from mild cognitive impairment to Alzheimer's disease. *Brain: A Journal of Neurology* 133: 3336–3348.

James, B.D., Bennett, D.A., Boyle, P.A., Leurgans, S. & Schneider, J.A. (2012) Dementia from Alzheimer disease and mixed pathologies in the oldest old. *JAMA* 307: 1798–1800.

Jenkinson, M., Bannister, P., Brady, M. & Smith, S. (2002) Improved optimization for the robust and accurate linear registration and motion correction of brain images. *NeuroImage* 17: 825–841.

Jenkinson, M. & Smith, S. (2001) A global optimisation method for robust affine registration of brain images. *Medical image analysis* 5: 143–156.

Jones, D.K. (2004) The effect of gradient sampling schemes on measures derived from diffusion tensor MRI: a Monte Carlo study. *Magnetic Resonance in Medicine* 51: 807–815.

de Jong, D., Kremer, B.P.H., Olde Rikkert, M.G.M. & Verbeek, M.M. (2007) Current state and future directions of neurochemical biomarkers for Alzheimer's disease. *Clinical Chemistry and Laboratory Medicine* 45: 1421–1434.

Josephs, K.A., Whitwell, J.L., Ahmed, Z., Shiung, M.M., Weigand, S.D., Knopman, D.S., Boeve, B.F., Parisi, J.E., Petersen, R.C., Dickson, D.W. & Jack, C.R. (2008) Beta-amyloid burden is not associated with rates of brain atrophy. *Annals of neurology* 63: 204–212.

Kaitz, S.S. & Robertson, R.T. (1981) Thalamic connections with limbic cortex. II. Corticothalamic projections. *The Journal of Comparative Neurology* 195: 527–545.

Kandel, B.M., Avants, B.B., Gee, J.C., McMillan, C.T., Erus, G., Doshi, J., Davatzikos, C. & Wolk, D.A. (2016) White matter hyperintensities are more highly associated with preclinical Alzheimer's disease than imaging and cognitive markers of neurodegeneration. *Alzheimer's & Dementia (Amsterdam, Netherlands)* 4: 18–27.

Kaneko, T., Kaneko, K., Matsushita, M., Kadoya, M., Ihara, N., Ryokawa, A., Ogihara, T., Inuzuka, S. & Ueda, H. (2012) New visual rating system for medial temporal lobe atrophy: a simple diagnostic tool for routine examinations. *Psychogeriatrics: The Official Journal of the Japanese Psychogeriatric Society* 12: 88–92.

Kanno, S., Abe, N., Saito, M., Takagi, M., Nishio, Y., Hayashi, A., Uchiyama, M., Hanaki, R., Kikuchi, H., Hiraoka, K., Yamasaki, H., Iizuka, O., Takeda, A., Itoyama, Y., Takahashi, S. & Mori, E. (2011) White matter involvement in idiopathic normal pressure hydrocephalus: a voxel-based diffusion tensor imaging study. *Journal of neurology* 258: 1949–1957.

Kanno, S., Saito, M., Kashinoura, T., Nishio, Y., Iizuka, O., Kikuchi, H., Takagi, M., Iwasaki, M., Takahashi, S. & Mori, E. (2017) A change in brain white matter after shunt surgery in idiopathic normal pressure hydrocephalus: a tract-based spatial statistics study. *Fluids and barriers of the CNS* 14: 1.

Kantarci, K., Avula, R., Senjem, M.L., Samikoglu, A.R., Zhang, B., Weigand, S.D., Przybelski, S.A., Edmonson, H.A., Vemuri, P., Knopman, D.S., Ferman, T.J., Boeve, B.F., Petersen, R.C. & Jack, C.R. (2010) Dementia with Lewy bodies and Alzheimer disease: neurodegenerative patterns characterized by DTI. *Neurology* 74: 1814–1821.

Karas, G., Scheltens, P., Rombouts, S., van Schijndel, R., Klein, M., Jones, B., van der Flier, W., Vrenken, H. & Barkhof, F. (2007) Precuneus atrophy in early-onset Alzheimer's disease: a morphometric structural MRI study. *Neuroradiology* 49: 967–976.

Karas, G.B., Burton, E.J., Rombouts, S. a. R.B., van Schijndel, R.A., O'Brien, J.T., Scheltens, P. h, McKeith, I.G., Williams, D., Ballard, C. & Barkhof, F. (2003) A comprehensive study of gray matter loss in patients with Alzheimer's disease using optimized voxel-based morphometry. *NeuroImage* 18: 895–907.

Kavcic, V., Ni, H., Zhu, T., Zhong, J. & Duffy, C.J. (2008) White matter integrity linked to functional impairments in aging and early Alzheimer's disease. *Alzheimer's & Dementia: The Journal of the Alzheimer's Association* 4: 381–389.

Khan, A.R., Wang, L. & Beg, M.F. (2008) FreeSurfer-initiated fully-automated subcortical brain segmentation in MRI using Large Deformation Diffeomorphic Metric Mapping. *NeuroImage* 41: 735–746.

Kiefer, M. & Unterberg, A. (2012) The differential diagnosis and treatment of normal-pressure hydrocephalus. *Deutsches Arzteblatt International* 109: 15–25; quiz 26.

Kim, G.H., Kim, J.-E., Choi, K.-G., Lim, S.M., Lee, J.-M., Na, D.L. & Jeong, J.H. (2014) T1-weighted axial visual rating scale for an assessment of medial temporal atrophy in Alzheimer's disease. *Journal of Alzheimer's disease: JAD* 41: 169–178.

Kim, J.H., Budde, M.D., Liang, H.-F., Klein, R.S., Russell, J.H., Cross, A.H. & Song, S.-K. (2006) Detecting axon damage in spinal cord from a mouse model of multiple sclerosis. *Neurobiology of disease* 21: 626–632.

Kim, M.J., Seo, S.W., Lee, K.M., Kim, S.T., Lee, J.I., Nam, D.H. & Na, D.L. (2011a) Differential diagnosis of idiopathic normal pressure hydrocephalus from other dementias using diffusion tensor imaging. *AJNR. American journal of neuroradiology* 32: 1496–1503.

Kim, S., Youn, Y.C., Hsiung, G.-Y.R., Ha, S.-Y., Park, K.-Y., Shin, H.-W., Kim, D.-K., Kim, S.-S. & Kee, B.S. (2011b) Voxel-based morphometric study of brain volume changes in patients with Alzheimer's disease assessed according to the Clinical Dementia Rating score. *Journal of Clinical Neuroscience: Official Journal of the Neurosurgical Society of Australasia* 18: 916–921.

Kincses, Z.T., Hořínek, D., Szabó, N., Tóth, E., Csete, G., Stěpán-Buksakowska, I., Hort, J. & Vécsei, L. (2013) The pattern of diffusion parameter changes in Alzheimer's disease, identified by means of linked independent component analysis. *Journal of Alzheimer's disease: JAD* 36: 119–128.

Kincses, Z.T., Toldi, J. & Vécsei, L. (2010) Kynurenines, neurodegeneration and Alzheimer's disease. *Journal of Cellular and Molecular Medicine* 14: 2045–2054.

Kinkingnéhun, S., Sarazin, M., Lehéricy, S., Guichart-Gomez, E., Hergueta, T. & Dubois, B. (2008) VBM anticipates the rate of progression of Alzheimer disease: a 3-year longitudinal study. *Neurology* 70: 2201–2211.

Kipps, C.M., Davies, R.R., Mitchell, J., Kril, J.J., Halliday, G.M. & Hodges, J.R. (2007) Clinical significance of lobar atrophy in frontotemporal dementia: application of an MRI visual rating scale. *Dementia and Geriatric Cognitive Disorders* 23: 334–342.

Kiuchi, K., Morikawa, M., Taoka, T., Nagashima, T., Yamauchi, T., Makinodan, M., Norimoto, K., Hashimoto, K., Kosaka, J., Inoue, Y., Inoue, M., Kichikawa, K. & Kishimoto, T. (2009) Abnormalities of the uncinate fasciculus and posterior cingulate fasciculus in mild cognitive impairment and early Alzheimer's disease: a diffusion tensor tractography study. *Brain Research* 1287: 184–191.

Klassen, B.T. & Ahlskog, J.E. (2011) Normal pressure hydrocephalus: how often does the diagnosis hold water? *Neurology* 77: 1119–1125.

Klöppel, S., Stonnington, C.M., Chu, C., Draganski, B., Scahill, R.I., Rohrer, J.D., Fox, N.C., Jack, C.R., Ashburner, J. & Frackowiak, R.S.J. (2008) Automatic classification of MR scans in Alzheimer's disease. *Brain: A Journal of Neurology* 131: 681–689.

Klunk, W.E., Engler, H., Nordberg, A., Wang, Y., Blomqvist, G., Holt, D.P., Bergström, M., Savitcheva, I., Huang, G., Estrada, S., Ausén, B., Debnath, M.L., Barletta, J., Price, J.C., Sandell, J., Lopresti, B.J., Wall, A., Koivisto, P., Antoni, G., Mathis, C.A. & Långström, B. (2004) Imaging brain amyloid in Alzheimer's disease with Pittsburgh Compound-B. *Annals of Neurology* 55: 306–319.

Knopman, D.S., Parisi, J.E., Salviati, A., Floriach-Robert, M., Boeve, B.F., Ivnik, R.J., Smith, G.E., Dickson, D.W., Johnson, K.A., Petersen, L.E., McDonald, W.C., Braak, H. & Petersen, R.C. (2003) Neuropathology of cognitively normal elderly. *Journal of Neuropathology and Experimental Neurology* 62: 1087–1095.

Koedam, E.L.G.E., Lehmann, M., van der Flier, W.M., Scheltens, P., Pijnenburg, Y.A.L., Fox, N., Barkhof, F. & Wattjes, M.P. (2011) Visual assessment of posterior atrophy development of a MRI rating scale. *European Radiology* 21: 2618–2625.

Korf, E.S.C., Wahlund, L.-O., Visser, P.J. & Scheltens, P. (2004) Medial temporal lobe atrophy on MRI predicts dementia in patients with mild cognitive impairment. *Neurology* 63: 94–100.

Kreher, B.W., Mader, I. & Kiselev, V.G. (2008) Gibbs tracking: a novel approach for the reconstruction of neuronal pathways. *Magnetic Resonance in Medicine* 60: 953–963.

Kuhl, D.E., Metter, E.J., Riege, W.H. & Phelps, M.E. (1982) Effects of human aging on patterns of local cerebral glucose utilization determined by the [18F]fluorodeoxyglucose method. *Journal of Cerebral Blood Flow and Metabolism: Official Journal of the International Society of Cerebral Blood Flow and Metabolism* 2: 163–171.

Kynast, J., Lampe, L., Luck, T., Frisch, S., Arelin, K., Hoffmann, K.-T., Loeffler, M., Riedel-Heller, S.G., Villringer, A. & Schroeter, M.L. (2018) White matter hyperintensities associated with small vessel disease impair social cognition beside attention and memory. *Journal of Cerebral Blood Flow and Metabolism: Official Journal of the International Society of Cerebral Blood Flow and Metabolism* 38: 996–1009.

Lau, J.C., Lerch, J.P., Sled, J.G., Henkelman, R.M., Evans, A.C. & Bedell, B.J. (2008) Longitudinal neuroanatomical changes determined by deformation-based morphometry in a mouse model of Alzheimer's disease. *NeuroImage* 42: 19–27.

Lazar, M. (2010) MAPPING BRAIN ANATOMICAL CONNECTIVITY USING WHITE MATTER TRACTOGRAPHY. *NMR in biomedicine* 23: 821–835.

Lazar, M., Jensen, J.H., Xuan, L. & Helpern, J.A. (2008) Estimation of the orientation distribution function from diffusional kurtosis imaging. *Magnetic Resonance in Medicine* 60: 774–781.

Le Bihan, D. (1995) Molecular diffusion, tissue microdynamics and microstructure. *NMR in biomedicine* 8: 375–386.

Le Bihan, D., Mangin, J.F., Poupon, C., Clark, C.A., Pappata, S., Molko, N. & Chabriat, H. (2001) Diffusion tensor imaging: concepts and applications. *Journal of magnetic resonance imaging: JMRI* 13: 534–546.

Lee, D.Y., Fletcher, E., Martinez, O., Zozulya, N., Kim, J., Tran, J., Buonocore, M., Carmichael, O. & DeCarli, C. (2010) Vascular and degenerative processes differentially affect regional interhemispheric connections in normal aging, mild cognitive impairment, and Alzheimer disease. *Stroke* 41: 1791–1797.

Lee, J.S., Kim, C., Shin, J.-H., Cho, H., Shin, D., Kim, N., Kim, H.J., Kim, Y., Lockhart, S.N., Na, D.L., Seo, S.W. & Seong, J.-K. (2018) Machine Learning-based Individual Assessment of Cortical Atrophy Pattern in Alzheimer's Disease Spectrum: Development of the Classifier and Longitudinal Evaluation. *Scientific Reports* 8:.

Lehmann, H.C., Zhang, J., Mori, S. & Sheikh, K.A. (2010) Diffusion tensor imaging to assess axonal regeneration in peripheral nerves. *Experimental Neurology* 223: 238–244.

Lehmann, M., Koedam, E.L.G.E., Barnes, J., Bartlett, J.W., Ryan, N.S., Pijnenburg, Y.A.L., Barkhof, F., Wattjes, M.P., Scheltens, P. & Fox, N.C. (2012) Posterior cerebral atrophy in the

absence of medial temporal lobe atrophy in pathologically-confirmed Alzheimer's disease. *Neurobiology of Aging* 33: 627.e1-627.e12.

Leinonen, V., Koivisto, A.M., Alafuzoff, I., Pyykkö, O.T., Rummukainen, J., von Und Zu Fraunberg, M., Jääskeläinen, J.E., Soininen, H., Rinne, J. & Savolainen, S. (2012) Cortical brain biopsy in long-term prognostication of 468 patients with possible normal pressure hydrocephalus. *Neuro-Degenerative Diseases* 10: 166–169.

Lemkaddem, A., Daducci, A., Kunz, N., Lazeyras, F., Seeck, M., Thiran, J.-P. & Vulliémoz, S. (2014) Connectivity and tissue microstructural alterations in right and left temporal lobe epilepsy revealed by diffusion spectrum imaging. *NeuroImage. Clinical* 5: 349–358.

Lenfeldt, N., Larsson, A., Nyberg, L., Birgander, R., Eklund, A. & Malm, J. (2011) Diffusion tensor imaging reveals supplementary lesions to frontal white matter in idiopathic normal pressure hydrocephalus. *Neurosurgery* 68: 1586–1593; discussion 1593.

de Leon, M.J., Golomb, J., Convit, A., DeSanti, S., McRae, T.D. & George, A.E. (1993) Measurement of medial temporal lobe atrophy in diagnosis of Alzheimer's disease. *Lancet (London, England)* 341: 125–126.

Li, H., Xue, Z., Dulay, M.F., Verma, A., Karmonik, C., Grossman, R.G. & Wong, S.T. (2014) Fractional anisotropy asymmetry and the side of seizure origin for partial onset-temporal lobe epilepsy. *Computerized Medical Imaging and Graphics: The Official Journal of the Computerized Medical Imaging Society* 38: 481–489.

Li, W., Hao, N., Liu, W., An, D., Yan, B., Li, J., Liu, L., Luo, R., Zhang, H., Lei, D. & Zhou, D. (2019) The experience of the multidisciplinary team in epilepsy management from a resource-limited country. *Epilepsia Open* 4: 85–91.

Lim, S.M., Katsifis, A., Villemagne, V.L., Best, R., Jones, G., Saling, M., Bradshaw, J., Merory, J., Woodward, M., Hopwood, M. & Rowe, C.C. (2009) The 18F-FDG PET cingulate island sign and comparison to 123I-beta-CIT SPECT for diagnosis of dementia with Lewy bodies. *Journal of Nuclear Medicine: Official Publication, Society of Nuclear Medicine* 50: 1638–1645.

Liu, R.S.N., Lemieux, L., Bell, G.S., Sisodiya, S.M., Bartlett, P.A., Shorvon, S.D., Sander, J.W.A.S. & Duncan, J.S. (2005) Cerebral damage in epilepsy: a population-based longitudinal quantitative MRI study. *Epilepsia* 46: 1482–1494.

Liu, Y., Spulber, G., Lehtimäki, K.K., Könönen, M., Hallikainen, I., Gröhn, H., Kivipelto, M., Hallikainen, M., Vanninen, R. & Soininen, H. (2011) Diffusion tensor imaging and tract-based spatial statistics in Alzheimer's disease and mild cognitive impairment. *Neurobiology of aging* 32: 1558–1571.

Liu, Z., Xu, Y., An, J., Wang, J., Yin, X., Huang, R., Lv, X., Chen, L., Wang, W. & Qiu, S. (2014) Altered Brain White Matter Integrity in Temporal Lobe Epilepsy: A TBSS Study. *Journal of Neuroimaging: Official Journal of the American Society of Neuroimaging*.

Lockhart, A., Lamb, J.R., Osredkar, T., Sue, L.I., Joyce, J.N., Ye, L., Libri, V., Leppert, D. & Beach, T.G. (2007) PIB is a non-specific imaging marker of amyloid-beta (Abeta) peptide-related cerebral amyloidosis. *Brain: A Journal of Neurology* 130: 2607–2615.

Lojewski, X., Hermann, A., Wegner, F., Araúzo-Bravo, M.J., Hallmeyer-Elgner, S., Kirsch, M., Schwarz, J., Schöler, H.R. & Storch, A. (2014) Human adult white matter progenitor cells are multipotent neuroprogenitors similar to adult hippocampal progenitors. *Stem Cells Translational Medicine* 3: 458–469.

Lu, J., Li, W., He, H., Feng, F., Jin, Z. & Wu, L. (2013) Altered hemispheric symmetry found in left-sided mesial temporal lobe epilepsy with hippocampal sclerosis (MTLE/HS) but not found in right-sided MTLE/HS. *Magnetic Resonance Imaging* 31: 53–59.

MacDonald, D., Kabani, N., Avis, D. & Evans, A.C. (2000) Automated 3-D extraction of inner and outer surfaces of cerebral cortex from MRI. *NeuroImage* 12: 340–356.

Malm, J., Graff-Radford, N.R., Ishikawa, M., Kristensen, B., Leinonen, V., Mori, E., Owler, B.K., Tullberg, M., Williams, M.A. & Relkin, N.R. (2013) Influence of comorbidities in idiopathic normal pressure hydrocephalus - research and clinical care. A report of the ISHCSF task force on comorbidities in INPH. *Fluids and barriers of the CNS* 10: 22.

McKeith, I., O'Brien, J., Walker, Z., Tatsch, K., Booij, J., Darcourt, J., Padovani, A., Giubbini, R., Bonuccelli, U., Volterrani, D., Holmes, C., Kemp, P., Tabet, N., Meyer, I., Reininger, C. & DLB Study Group (2007) Sensitivity and specificity of dopamine transporter imaging with 123I-FP-CIT SPECT in dementia with Lewy bodies: a phase III, multicentre study. *The Lancet. Neurology* 6: 305–313.

McKeith, I.G., Boeve, B.F., Dickson, D.W., Halliday, G., Taylor, J.-P., Weintraub, D., Aarsland, D., Galvin, J., Attems, J., Ballard, C.G., Bayston, A., Beach, T.G., Blanc, F., Bohnen, N., Bonanni, L., Bras, J., Brundin, P., Burn, D., Chen-Plotkin, A., Duda, J.E., El-Agnaf, O., Feldman, H., Ferman, T.J., Ffytche, D., Fujishiro, H., Galasko, D., Goldman, J.G., Gomperts, S.N., Graff-Radford, N.R., Honig, L.S., Iranzo, A., Kantarci, K., Kaufer, D., Kukull, W., Lee, V.M.Y., Leverenz, J.B., Lewis, S., Lippa, C., Lunde, A., Masellis, M., Masliah, E., McLean, P., Mollenhauer, B., Montine, T.J., Moreno, E., Mori, E., Murray, M., O'Brien, J.T., Orimo, S., Postuma, R.B., Ramaswamy, S., Ross, O.A., Salmon, D.P., Singleton, A., Taylor, A., Thomas, A., Tiraboschi, P., Toledo, J.B., Trojanowski, J.Q., Tsuang, D., Walker, Z., Yamada, M. & Kosaka, K. (2017) Diagnosis and management of dementia with Lewy bodies: Fourth consensus report of the DLB Consortium. *Neurology* 89: 88–100.

McKhann, G., Drachman, D., Folstein, M., Katzman, R., Price, D. & Stadlan, E.M. (1984) Clinical diagnosis of Alzheimer's disease: report of the NINCDS-ADRDA Work Group under the auspices of Department of Health and Human Services Task Force on Alzheimer's Disease. *Neurology* 34: 939–944.

McKhann, G.M. (2011) Changing concepts of Alzheimer disease. *JAMA* 305: 2458–2459.

McKhann, G.M., Knopman, D.S., Chertkow, H., Hyman, B.T., Jack, C.R., Kawas, C.H., Klunk, W.E., Koroshetz, W.J., Manly, J.J., Mayeux, R., Mohs, R.C., Morris, J.C., Rossor, M.N., Scheltens, P., Carrillo, M.C., Thies, B., Weintraub, S. & Phelps, C.H. (2011) The diagnosis of dementia due to Alzheimer's disease: recommendations from the National Institute on Aging-Alzheimer's Association workgroups on diagnostic guidelines for Alzheimer's disease. *Alzheimer's & Dementia: The Journal of the Alzheimer's Association* 7: 263–269.

Medina, D., DeToledo-Morrell, L., Urresta, F., Gabrieli, J.D.E., Moseley, M., Fleischman, D., Bennett, D.A., Leurgans, S., Turner, D.A. & Stebbins, G.T. (2006) White matter changes in mild cognitive impairment and AD: A diffusion tensor imaging study. *Neurobiology of Aging* 27: 663–672.

Medina, D.A. & Gaviria, M. (2008) Diffusion tensor imaging investigations in Alzheimer's disease: the resurgence of white matter compromise in the cortical dysfunction of the aging brain. *Neuropsychiatric Disease and Treatment* 4: 737–742.

Metzler-Baddeley, C., Jones, D.K., Steventon, J., Westacott, L., Aggleton, J.P. & O'Sullivan, M.J. (2012) Cingulum microstructure predicts cognitive control in older age and mild cognitive impairment. *The Journal of Neuroscience: The Official Journal of the Society for Neuroscience* 32: 17612–17619.

Mielke, M.M., Kozauer, N.A., Chan, K.C.G., George, M., Toroney, J., Zerrate, M., Bandeen-Roche, K., Wang, M.-C., Vanzijl, P., Pekar, J.J., Mori, S., Lyketsos, C.G. & Albert, M. (2009) Regionally-specific diffusion tensor imaging in mild cognitive impairment and Alzheimer's disease. *NeuroImage* 46: 47–55.

Miller, M.I., Trouvé, A. & Younes, L. (2006) Geodesic Shooting for Computational Anatomy. *Journal of Mathematical Imaging and Vision* 24: 209–228.

Miller, M.I., Trouve, A. & Younes, L. (2002) On the metrics and euler-lagrange equations of computational anatomy. *Annual Review of Biomedical Engineering* 4: 375–405.

Miller, M.I., Younes, L., Ratnanather, J.T., Brown, T., Reigel, T., Trinh, H., Tang, X., Barker, P., Mori, S. & Albert, M. (2012) Amygdala Atrophy in MCI/Alzheimer's Disease in the BIOCARD cohort based on Diffeomorphic Morphometry. *Medical image computing and computer-assisted intervention : MICCAI ... International Conference on Medical Image Computing and Computer-Assisted Intervention* 2012: 155–166.

Miller, M.I., Younes, L. & Trouvé, A. (2014) Diffeomorphometry and geodesic positioning systems for human anatomy. *Technology* 2: 36.

Mirra, S.S., Heyman, A., McKeel, D., Sumi, S.M., Crain, B.J., Brownlee, L.M., Vogel, F.S., Hughes, J.P., van Belle, G. & Berg, L. (1991) The Consortium to Establish a Registry for Alzheimer's Disease (CERAD). Part II. Standardization of the neuropathologic assessment of Alzheimer's disease. *Neurology* 41: 479–486.

Möller, C., Hafkemeijer, A., Pijnenburg, Y.A.L., Rombouts, S.A.R.B., van der Grond, J., Dopper, E., van Swieten, J., Versteeg, A., Steenwijk, M.D., Barkhof, F., Scheltens, P., Vrenken, H. & van der Flier, W.M. (2016) Different patterns of cortical gray matter loss over time in behavioral variant frontotemporal dementia and Alzheimer's disease. *Neurobiology of Aging* 38: 21–31.

Moradi, E., Pepe, A., Gaser, C., Huttunen, H., Tohka, J. & Alzheimer's Disease Neuroimaging Initiative (2015) Machine learning framework for early MRI-based Alzheimer's conversion prediction in MCI subjects. *NeuroImage* 104: 398–412.

Mosconi, L. (2005) Brain glucose metabolism in the early and specific diagnosis of Alzheimer's disease. *European Journal of Nuclear Medicine and Molecular Imaging* 32: 486–510.

Mosconi, L., Tsui, W.H., Herholz, K., Pupi, A., Drzezga, A., Lucignani, G., Reiman, E.M., Holthoff, V., Kalbe, E., Sorbi, S., Diehl-Schmid, J., Perneczky, R., Clerici, F., Caselli, R., Beuthien-Baumann, B., Kurz, A., Minoshima, S. & de Leon, M.J. (2008) Multicenter standardized 18F-FDG PET diagnosis of mild cognitive impairment, Alzheimer's disease, and other dementias. *Journal of Nuclear Medicine: Official Publication, Society of Nuclear Medicine* 49: 390–398.

Moseley, M.E., Cohen, Y., Kucharczyk, J., Mintorovitch, J., Asgari, H.S., Wendland, M.F., Tsuruda, J. & Norman, D. (1990) Diffusion-weighted MR imaging of anisotropic water diffusion in cat central nervous system. *Radiology* 176: 439–445.

Mueller, S.G., Laxer, K.D., Cashdollar, N., Buckley, S., Paul, C. & Weiner, M.W. (2006) Voxel-based optimized morphometry (VBM) of gray and white matter in temporal lobe epilepsy (TLE) with and without mesial temporal sclerosis. *Epilepsia* 47: 900–907.

Mukherjee, P., Berman, J.I., Chung, S.W., Hess, C.P. & Henry, R.G. (2008) Diffusion Tensor MR Imaging and Fiber Tractography: Theoretic Underpinnings. *American Journal of Neuroradiology* 29: 632–641.

Nakata, Y., Sato, N., Nemoto, K., Abe, O., Shikakura, S., Arima, K., Furuta, N., Uno, M., Hirai, S., Masutani, Y., Ohtomo, K., Barkovich, A.J. & Aoki, S. (2009) Diffusion abnormality in the posterior cingulum and hippocampal volume: correlation with disease progression in Alzheimer's disease. *Magnetic Resonance Imaging* 27: 347–354.

National Institute on Aging (2018).

Nedelska, Z., Ferman, T.J., Boeve, B.F., Przybelski, S.A., Lesnick, T.L., Murray, M.E., Gunter, J.L., Senjem, M.L., Vemuri, P., Smith, G.E., Geda, Y.E., Graff-Radford, J., Knopman, D.S., Petersen, R.C., Parisi, J.E., Dickson, D.W., Jack, C.R., Jr & Kantarci, K. (2015) Pattern of Brain Atrophy Rates in Autopsy-Confirmed Dementia with Lewy Bodies. *Neurobiology of aging* 36: 452.

Nelson, P.T., Abner, E.L., Schmitt, F.A., Kryscio, R.J., Jicha, G.A., Santacruz, K., Smith, C.D., Patel, E. & Markesbery, W.R. (2009) Brains with medial temporal lobe neurofibrillary

tangles but no neuritic amyloid plaques are a diagnostic dilemma but may have pathogenetic aspects distinct from Alzheimer disease. *Journal of Neuropathology and Experimental Neurology* 68: 774–784.

Nelson, P.T., Head, E., Schmitt, F.A., Davis, P.R., Neltner, J.H., Jicha, G.A., Abner, E.L., Smith, C.D., Van Eldik, L.J., Kryscio, R.J. & Scheff, S.W. (2011) Alzheimer's disease is not "brain aging": neuropathological, genetic, and epidemiological human studies. *Acta Neuropathologica* 121: 571–587.

Neumann, M. & Mackenzie, I.R.A. (2019) Review: Neuropathology of non-tau frontotemporal lobar degeneration. *Neuropathology and Applied Neurobiology* 45: 19–40.

Nguyen, D., Vargas, M.I., Khaw, N., Seeck, M., Delavelle, J., Lovblad, K.O. & Haller, S. (2011) Diffusion tensor imaging analysis with tract-based spatial statistics of the white matter abnormalities after epilepsy surgery. *Epilepsy Research* 94: 189–197.

Ni, H., Kavcic, V., Zhu, T., Ekholm, S. & Zhong, J. (2006) Effects of number of diffusion gradient directions on derived diffusion tensor imaging indices in human brain. *AJNR. American journal of neuroradiology* 27: 1776–1781.

Nichols, T.E. & Holmes, A.P. (2002) Nonparametric permutation tests for functional neuroimaging: a primer with examples. *Human brain mapping* 15: 1–25.

Noè, F., Cattalini, A., Vila Verde, D., Alessi, C., Colciaghi, F., Figini, M., Zucca, I. & de Curtis, M. (2019) Epileptiform activity contralateral to unilateral hippocampal sclerosis does not cause the expression of brain damage markers. *Epilepsia*.

Nowrangi, M.A., Lyketsos, C.G., Leoutsakos, J.-M.S., Oishi, K., Albert, M., Mori, S. & Mielke, M.M. (2013) Longitudinal, region-specific course of diffusion tensor imaging measures in mild cognitive impairment and Alzheimer's disease. *Alzheimer's & Dementia: The Journal of the Alzheimer's Association* 9: 519–528.

Nowrangi, M.A. & Rosenberg, P.B. (2015) The Fornix in Mild Cognitive Impairment and Alzheimer's Disease. *Frontiers in Aging Neuroscience* 7:.

O'Brien, J.T., Firbank, M.J., Davison, C., Barnett, N., Bamford, C., Donaldson, C., Olsen, K., Herholz, K., Williams, D. & Lloyd, J. (2014) 18F-FDG PET and perfusion SPECT in the diagnosis of Alzheimer and Lewy body dementias. *Journal of Nuclear Medicine: Official Publication, Society of Nuclear Medicine* 55: 1959–1965.

O'Donnell, L.J. & Westin, C.-F. (2011) An introduction to diffusion tensor image analysis. *Neurosurgery clinics of North America* 22: 185–viii.

O'Donovan, J., Watson, R., Colloby, S.J., Firbank, M.J., Burton, E.J., Barber, R., Blamire, A.M. & O'Brien, J.T. (2013) Does posterior cortical atrophy on MRI discriminate between Alzheimer's disease, dementia with Lewy bodies, and normal aging? *International Psychogeriatrics* 25: 111–119.

O'Dwyer, L., Lamberton, F., Bokde, A.L.W., Ewers, M., Faluyi, Y.O., Tanner, C., Mazoyer, B., O'Neill, D., Bartley, M., Collins, D.R., Coughlan, T., Prvulovic, D. & Hampel, H. (2011) Multiple indices of diffusion identifies white matter damage in mild cognitive impairment and Alzheimer's disease. *PloS One* 6: e21745.

Oguz, K.K., Tezer, I., Sanverdi, E., Has, A.C., Bilginer, B., Dolgun, A. & Saygi, S. (2013) Effect of patient sex on white matter alterations in unilateral medial temporal lobe epilepsy with hippocampal sclerosis assessed by diffusion tensor imaging. *AJNR. American journal of neuroradiology* 34: 1010–1015.

Ossenkoppele, R., Tolboom, N., Foster-Dingley, J.C., Adriaanse, S.F., Boellaard, R., Yaqub, M., Windhorst, A.D., Barkhof, F., Lammertsma, A.A., Scheltens, P., van der Flier, W.M. & van Berckel, B.N.M. (2012) Longitudinal imaging of Alzheimer pathology using [11C]PIB, [18F]FDDNP and [18F]FDG PET. *European Journal of Nuclear Medicine and Molecular Imaging* 39: 990–1000.

Otte, W.M., van Eijsden, P., Sander, J.W., Duncan, J.S., Dijkhuizen, R.M. & Braun, K.P.J. (2012) A meta-analysis of white matter changes in temporal lobe epilepsy as studied with diffusion tensor imaging. *Epilepsia* 53: 659–667.

Pajevic, S. & Pierpaoli, C. (1999) Color schemes to represent the orientation of anisotropic tissues from diffusion tensor data: application to white matter fiber tract mapping in the human brain. *Magnetic Resonance in Medicine* 42: 526–540.

Parker, G.J.M., Haroon, H.A. & Wheeler-Kingshott, C.A.M. (2003) A framework for a streamline-based probabilistic index of connectivity (PICo) using a structural interpretation of MRI diffusion measurements. *Journal of magnetic resonance imaging: JMRI* 18: 242–254.

Pasquier, F., Leys, D., Weerts, J.G., Mounier-Vehier, F., Barkhof, F. & Scheltens, P. (1996) Inter- and intraobserver reproducibility of cerebral atrophy assessment on MRI scans with hemispheric infarcts. *European Neurology* 36: 268–272.

Patenaude, B., Smith, S.M., Kennedy, D.N. & Jenkinson, M. (2011) A Bayesian model of shape and appearance for subcortical brain segmentation. *NeuroImage* 56: 907–922.

Patterson, C. (2018) World Alzheimer Report 2018 - The state of the art of dementia research: New frontiers. *NEW FRONTIERS* 48.

Payton, N.M., Kalpouzos, G., Rizzuto, D., Fratiglioni, L., Kivipelto, M., Bäckman, L. & Laukka, E.J. (2018) Combining Cognitive, Genetic, and Structural Neuroimaging Markers to Identify Individuals with Increased Dementia Risk. *Journal of Alzheimer's disease: JAD* 64: 533–542.

Poels, M.M.F., Ikram, M.A., van der Lugt, A., Hofman, A., Krestin, G.P., Breteler, M.M.B. & Vernooij, M.W. (2011) Incidence of cerebral microbleeds in the general population: the Rotterdam Scan Study. *Stroke* 42: 656–661.

Postuma, R.B., Berg, D., Stern, M., Poewe, W., Olanow, C.W., Oertel, W., Obeso, J., Marek, K., Litvan, I., Lang, A.E., Halliday, G., Goetz, C.G., Gasser, T., Dubois, B., Chan, P., Bloem, B.R., Adler, C.H. & Deuschl, G. (2015) MDS clinical diagnostic criteria for Parkinson's disease. *Movement Disorders: Official Journal of the Movement Disorder Society* 30: 1591–1601.

Price, J.L. & Morris, J.C. (1999) Tangles and plaques in nondemented aging and "preclinical" Alzheimer's disease. *Annals of Neurology* 45: 358–368.

Provenzano, F.A., Muraskin, J., Tosto, G., Narkhede, A., Wasserman, B.T., Griffith, E.Y., Guzman, V.A., Meier, I.B., Zimmerman, M.E., Brickman, A.M. & Alzheimer's Disease Neuroimaging Initiative (2013) White matter hyperintensities and cerebral amyloidosis: necessary and sufficient for clinical expression of Alzheimer disease? *JAMA neurology* 70: 455–461.

Qiu, A., Younes, L., Miller, M.I. & Csernansky, J.G. (2008) Parallel transport in diffeomorphisms distinguishes the time-dependent pattern of hippocampal surface deformation due to healthy aging and the dementia of the Alzheimer's type. *NeuroImage* 40: 68–76.

Rascovsky, K., Hodges, J.R., Knopman, D., Mendez, M.F., Kramer, J.H., Neuhaus, J., van Swieten, J.C., Seelaar, H., Dopper, E.G.P., Onyike, C.U., Hillis, A.E., Josephs, K.A., Boeve, B.F., Kertesz, A., Seeley, W.W., Rankin, K.P., Johnson, J.K., Gorno-Tempini, M.-L., Rosen, H., Prioleau-Latham, C.E., Lee, A., Kipps, C.M., Lillo, P., Piguet, O., Rohrer, J.D., Rossor, M.N., Warren, J.D., Fox, N.C., Galasko, D., Salmon, D.P., Black, S.E., Mesulam, M., Weintraub, S., Dickerson, B.C., Diehl-Schmid, J., Pasquier, F., Deramecourt, V., Lebert, F., Pijnenburg, Y., Chow, T.W., Manes, F., Grafman, J., Cappa, S.F., Freedman, M., Grossman, M. & Miller, B.L. (2011) Sensitivity of revised diagnostic criteria for the behavioural variant of frontotemporal dementia. *Brain: A Journal of Neurology* 134: 2456–2477.

Reisberg, B., Franssen, E.H., Hasan, S.M., Monteiro, I., Boksay, I., Souren, L.E., Kenowsky, S., Auer, S.R., Elahi, S. & Kluger, A. (1999) Retrogenesis: clinical, physiologic, and pathologic

mechanisms in brain aging, Alzheimer's and other dementing processes. *European Archives of Psychiatry and Clinical Neuroscience* 249 Suppl 3: 28–36.

Reivich, M., Kuhl, D., Wolf, A., Greenberg, J., Phelps, M., Ido, T., Casella, V., Fowler, J., Hoffman, E., Alavi, A., Som, P. & Sokoloff, L. (1979) The [18F]fluorodeoxyglucose method for the measurement of local cerebral glucose utilization in man. *Circulation Research* 44: 127–137.

Rice, L. & Bisdas, S. (2017) The diagnostic value of FDG and amyloid PET in Alzheimer's disease-A systematic review. *European Journal of Radiology* 94: 16–24.

Richter, Z., Janszky, J., Sétáló, G., Horváth, R., Horváth, Z., Dóczi, T., Seress, L. & Ábrahám, H. (2016) Characterization of neurons in the cortical white matter in human temporal lobe epilepsy. *Neuroscience* 333: 140–150.

Riley, J.D., Franklin, D.L., Choi, V., Kim, R.C., Binder, D.K., Cramer, S.C. & Lin, J.J. (2010) Altered white matter integrity in temporal lobe epilepsy: association with cognitive and clinical profiles. *Epilepsia* 51: 536–545.

Roher, A.E., Weiss, N., Kokjohn, T.A., Kuo, Y.-M., Kalback, W., Anthony, J., Watson, D., Luehrs, D.C., Sue, L., Walker, D., Emmerling, M., Goux, W. & Beach, T. (2002) Increased A beta peptides and reduced cholesterol and myelin proteins characterize white matter degeneration in Alzheimer's disease. *Biochemistry* 41: 11080–11090.

Rohrer, J.D., Lashley, T., Schott, J.M., Warren, J.E., Mead, S., Isaacs, A.M., Beck, J., Hardy, J., de Silva, R., Warrington, E., Troakes, C., Al-Sarraj, S., King, A., Borroni, B., Clarkson, M.J., Ourselin, S., Holton, J.L., Fox, N.C., Revesz, T., Rossor, M.N. & Warren, J.D. (2011) Clinical and neuroanatomical signatures of tissue pathology in frontotemporal lobar degeneration. *Brain: A Journal of Neurology* 134: 2565–2581.

Rosas, H.D., Tuch, D.S., Hevelone, N.D., Zaleta, A.K., Vangel, M., Hersch, S.M. & Salat, D.H. (2006) Diffusion tensor imaging in presymptomatic and early Huntington's disease: Selective white matter pathology and its relationship to clinical measures. *Movement Disorders: Official Journal of the Movement Disorder Society* 21: 1317–1325.

Rose, S.E., McMahon, K.L., Janke, A.L., O'Dowd, B., de Zubicaray, G., Strudwick, M.W. & Chalk, J.B. (2006) Diffusion indices on magnetic resonance imaging and neuropsychological performance in amnestic mild cognitive impairment. *Journal of Neurology, Neurosurgery, and Psychiatry* 77: 1122–1128.

Rowe, C.C., Ellis, K.A., Rimajova, M., Bourgeat, P., Pike, K.E., Jones, G., Fripp, J., Tochon-Danguy, H., Morandeau, L., O'Keefe, G., Price, R., Raniga, P., Robins, P., Acosta, O., Lenzo, N., Szoeke, C., Salvado, O., Head, R., Martins, R., Masters, C.L., Ames, D. & Villemagne, V.L. (2010) Amyloid imaging results from the Australian Imaging, Biomarkers and Lifestyle (AIBL) study of aging. *Neurobiology of Aging* 31: 1275–1283.

Rueckert, D., Sonoda, L.I., Hayes, C., Hill, D.L., Leach, M.O. & Hawkes, D.J. (1999) Nonrigid registration using free-form deformations: application to breast MR images. *IEEE transactions on medical imaging* 18: 712–721.

Salat, D.H., Buckner, R.L., Snyder, A.Z., Greve, D.N., Desikan, R.S.R., Busa, E., Morris, J.C., Dale, A.M. & Fischl, B. (2004) Thinning of the cerebral cortex in aging. *Cerebral Cortex (New York, N.Y.: 1991)* 14: 721–730.

Salat, D.H., Tuch, D.S., van der Kouwe, A.J.W., Greve, D.N., Pappu, V., Lee, S.Y., Hevelone, N.D., Zaleta, A.K., Growdon, J.H., Corkin, S., Fischl, B. & Rosas, H.D. (2010) White matter pathology isolates the hippocampal formation in Alzheimer's disease. *Neurobiology of aging* 31: 244–256.

Sanches, P., Fujisao, E.K., Braga, A.M.S., Cristaldo, N.R., Dos Reis, R., Yamashita, S. & Betting, L.E. (2017) Voxel-based analysis of diffusion tensor imaging in patients with mesial temporal lobe epilepsy. *Epilepsy Research* 132: 100–108.

Sarazin, M., Chauviré, V., Gerardin, E., Colliot, O., Kinkingnéhun, S., de Souza, L.C., Hugonot-Diener, L., Garnero, L., Lehéricy, S., Chupin, M. & Dubois, B. (2010) The amnestic syndrome of hippocampal type in Alzheimer's disease: an MRI study. *Journal of Alzheimer's disease: JAD* 22: 285–294.

Savva, G.M., Wharton, S.B., Ince, P.G., Forster, G., Matthews, F.E., Brayne, C. & Medical Research Council Cognitive Function and Ageing Study (2009) Age, neuropathology, and dementia. *The New England Journal of Medicine* 360: 2302–2309.

Scanlon, C., Mueller, S.G., Cheong, I., Hartig, M., Weiner, M.W. & Laxer, K.D. (2013) Grey and white matter abnormalities in temporal lobe epilepsy with and without mesial temporal sclerosis. *Journal of Neurology* 260: 2320–2329.

Scheel, M., Diekhoff, T., Sprung, C. & Hoffmann, K.-T. (2012) Diffusion tensor imaging in hydrocephalus--findings before and after shunt surgery. *Acta neurochirurgica* 154: 1699–1706.

Scheltens, P., Leys, D., Barkhof, F., Huglo, D., Weinstein, H.C., Vermersch, P., Kuiper, M., Steinling, M., Wolters, E.C. & Valk, J. (1992) Atrophy of medial temporal lobes on MRI in "probable" Alzheimer's disease and normal ageing: diagnostic value and neuropsychological correlates. *Journal of Neurology, Neurosurgery, and Psychiatry* 55: 967–972.

Scheltens, P., Pasquier, F., Weerts, J.G., Barkhof, F. & Leys, D. (1997) Qualitative assessment of cerebral atrophy on MRI: inter- and intra-observer reproducibility in dementia and normal aging. *European Neurology* 37: 95–99.

Scher, A.I., Xu, Y., Korf, E.S.C., White, L.R., Scheltens, P., Toga, A.W., Thompson, P.M., Hartley, S.W., Witter, M.P., Valentino, D.J. & Launer, L.J. (2007) Hippocampal shape analysis in Alzheimer's disease: a population-based study. *NeuroImage* 36: 8–18.

Schmahmann, J.D. & Pandya, D.N. (2007) Cerebral white matter--historical evolution of facts and notions concerning the organization of the fiber pathways of the brain. *Journal of the History of the Neurosciences* 16: 237–267.

Schmierer, K., Wheeler-Kingshott, C.A.M., Tozer, D.J., Boulby, P.A., Parkes, H.G., Yousry, T.A., Scaravilli, F., Barker, G.J., Tofts, P.S. & Miller, D.H. (2008) Quantitative magnetic resonance of postmortem multiple sclerosis brain before and after fixation. *Magnetic Resonance in Medicine* 59: 268–277.

Schneider, J.A., Arvanitakis, Z., Leurgans, S.E. & Bennett, D.A. (2009) The neuropathology of probable Alzheimer disease and mild cognitive impairment. *Annals of Neurology* 66: 200–208.

Schoene-Bake, J.-C., Faber, J., Trautner, P., Kaaden, S., Tittgemeyer, M., Elger, C.E. & Weber, B. (2009) Widespread affections of large fiber tracts in postoperative temporal lobe epilepsy. *NeuroImage* 46: 569–576.

Sexton, C.E., Kalu, U.G., Filippini, N., Mackay, C.E. & Ebmeier, K.P. (2011) A meta-analysis of diffusion tensor imaging in mild cognitive impairment and Alzheimer's disease. *Neurobiology of aging* 32: 2322.e5–18.

Shen, T., Li, H. & Huang, X. (2011) Active volume models for medical image segmentation. *IEEE transactions on medical imaging* 30: 774–791.

Skrobot, O.A., Black, S.E., Chen, C., DeCarli, C., Erkinjuntti, T., Ford, G.A., Kalaria, R.N., O'Brien, J., Pantoni, L., Pasquier, F., Roman, G.C., Wallin, A., Sachdev, P., Skoog, I., VICCCS group, Ben-Shlomo, Y., Passmore, A.P., Love, S. & Kehoe, P.G. (2018) Progress toward standardized diagnosis of vascular cognitive impairment: Guidelines from the Vascular Impairment of Cognition Classification Consensus Study. *Alzheimer's & Dementia: The Journal of the Alzheimer's Association* 14: 280–292.

Sluimer, J.D., Bouwman, F.H., Vrenken, H., Blankenstein, M.A., Barkhof, F., van der Flier, W.M. & Scheltens, P. (2010) Whole-brain atrophy rate and CSF biomarker levels in MCI and AD: a longitudinal study. *Neurobiology of Aging* 31: 758–764.

Smith, S.M. (2002) Fast robust automated brain extraction. *Human Brain Mapping* 17: 143–155.

Smith, S.M., Jenkinson, M., Johansen-Berg, H., Rueckert, D., Nichols, T.E., Mackay, C.E., Watkins, K.E., Ciccarelli, O., Cader, M.Z., Matthews, P.M. & Behrens, T.E.J. (2006) Tract-based spatial statistics: voxelwise analysis of multi-subject diffusion data. *NeuroImage* 31: 1487–1505.

Smith, S.M., Jenkinson, M., Woolrich, M.W., Beckmann, C.F., Behrens, T.E.J., Johansen-Berg, H., Bannister, P.R., De Luca, M., Drobnjak, I., Flitney, D.E., Niazy, R.K., Saunders, J., Vickers, J., Zhang, Y., De Stefano, N., Brady, J.M. & Matthews, P.M. (2004) Advances in functional and structural MR image analysis and implementation as FSL. *NeuroImage* 23 Suppl 1: S208-219.

Smith, S.M. & Nichols, T.E. (2009) Threshold-free cluster enhancement: addressing problems of smoothing, threshold dependence and localisation in cluster inference. *NeuroImage* 44: 83–98.

Smith, S.M., Zhang, Y., Jenkinson, M., Chen, J., Matthews, P.M., Federico, A. & De Stefano, N. (2002) Accurate, robust, and automated longitudinal and cross-sectional brain change analysis. *NeuroImage* 17: 479–489.

Sone, D., Sato, N., Kimura, Y., Watanabe, Y., Okazaki, M. & Matsuda, H. (2018) Brain morphological and microstructural features in cryptogenic late-onset temporal lobe epilepsy: a structural and diffusion MRI study. *Neuroradiology* 60: 635–641.

Song, S.-K., Sun, S.-W., Ju, W.-K., Lin, S.-J., Cross, A.H. & Neufeld, A.H. (2003) Diffusion tensor imaging detects and differentiates axon and myelin degeneration in mouse optic nerve after retinal ischemia. *NeuroImage* 20: 1714–1722.

Song, S.-K., Sun, S.-W., Ramsbottom, M.J., Chang, C., Russell, J. & Cross, A.H. (2002) Dysmyelination revealed through MRI as increased radial (but unchanged axial) diffusion of water. *NeuroImage* 17: 1429–1436.

Song, S.-K., Yoshino, J., Le, T.Q., Lin, S.-J., Sun, S.-W., Cross, A.H. & Armstrong, R.C. (2005) Demyelination increases radial diffusivity in corpus callosum of mouse brain. *NeuroImage* 26: 132–140.

Sörensen, A., Blazhenets, G., Rücker, G., Schiller, F., Meyer, P.T., Frings, L. & Alzheimer's Disease Neuroimaging Initiative (2019) Prognosis of conversion of mild cognitive impairment to Alzheimer's dementia by voxel-wise Cox regression based on FDG PET data. *NeuroImage. Clinical* 21: 101637.

Stejskal, E.O. (1965) Use of Spin Echoes in a Pulsed Magnetic-Field Gradient to Study Anisotropic, Restricted Diffusion and Flow. *The Journal of Chemical Physics* 43: 3597.

Stěpán-Buksakowska, I., Keller, J., Laczó, J., Rulseh, A., Hort, J., Lisý, J., Charvát, F., Roček, M. & Hořínek, D. (2012) Diffusion tensor imaging in Alzheimer disease and mild cognitive impairment. *Neurologia I Neurochirurgia Polska* 46: 462–471.

Stokin, G.B., Lillo, C., Falzone, T.L., Brusch, R.G., Rockenstein, E., Mount, S.L., Raman, R., Davies, P., Masliah, E., Williams, D.S. & Goldstein, L.S.B. (2005) Axonopathy and transport deficits early in the pathogenesis of Alzheimer's disease. *Science (New York, N.Y.)* 307: 1282–1288.

van Straaten, E.C.W., Scheltens, P., Knol, D.L., van Buchem, M.A., van Dijk, E.J., Hofman, P.A.M., Karas, G., Kjartansson, O., de Leeuw, F.-E., Prins, N.D., Schmidt, R., Visser, M.C., Weinstein, H.C. & Barkhof, F. (2003) Operational definitions for the NINDS-AIREN criteria for vascular dementia: an interobserver study. *Stroke* 34: 1907–1912.

Stricker, N.H., Schweinsburg, B.C., Delano-Wood, L., Wierenga, C.E., Bangen, K.J., Haaland, K.Y., Frank, L.R., Salmon, D.P. & Bondi, M.W. (2009) Decreased white matter integrity in late-myelinating fiber pathways in Alzheimer's disease supports retrogenesis. *NeuroImage* 45: 10–16.

Sun, S.-W., Liang, H.-F., Cross, A.H. & Song, S.-K. (2008) Evolving Wallerian degeneration after transient retinal ischemia in mice characterized by diffusion tensor imaging. *NeuroImage* 40: 1–10.

Sun, S.-W., Liang, H.-F., Schmidt, R.E., Cross, A.H. & Song, S.-K. (2007) Selective vulnerability of cerebral white matter in a murine model of multiple sclerosis detected using diffusion tensor imaging. *Neurobiology of Disease* 28: 30–38.

Szabó, N., Kincses, Z.T., Párdutz, A., Tajti, J., Szok, D., Tuka, B., Király, A., Babos, M., Vörös, E., Bomboi, G., Orzi, F. & Vécsei, L. (2012) White matter microstructural alterations in migraine: a diffusion-weighted MRI study. *Pain* 153: 651–656.

Tanaka, N., Yamaguchi, S., Ishikawa, H., Ishii, H. & Meguro, K. (2009) Prevalence of possible idiopathic normal-pressure hydrocephalus in Japan: the Osaki-Tajiri project. *Neuroepidemiology* 32: 171–175.

Taoka, T., Iwasaki, S., Sakamoto, M., Nakagawa, H., Fukusumi, A., Myochin, K., Hirohashi, S., Hoshida, T. & Kichikawa, K. (2006) Diffusion anisotropy and diffusivity of white matter tracts within the temporal stem in Alzheimer disease: evaluation of the "tract of interest" by diffusion tensor tractography. *AJNR. American journal of neuroradiology* 27: 1040–1045.

Teipel, S.J., Stahl, R., Dietrich, O., Schoenberg, S.O., Perneczky, R., Bokde, A.L.W., Reiser, M.F., Möller, H.-J. & Hampel, H. (2007) Multivariate network analysis of fiber tract integrity in Alzheimer's disease. *NeuroImage* 34: 985–995.

Teipel, S.J., Wegrzyn, M., Meindl, T., Frisoni, G., Bokde, A.L.W., Fellgiebel, A., Filippi, M., Hampel, H., Klöppel, S., Hauenstein, K. & Ewers, M. (2012) Anatomical MRI and DTI in the diagnosis of Alzheimer's disease: a European multicenter study. *Journal of Alzheimer's disease: JAD* 31 Suppl 3: S33-47.

Tournier, J.-D., Calamante, F. & Connelly, A. (2007) Robust determination of the fibre orientation distribution in diffusion MRI: non-negativity constrained super-resolved spherical deconvolution. *NeuroImage* 35: 1459–1472.

Tournier, J.-D., Mori, S. & Leemans, A. (2011) Diffusion Tensor Imaging and Beyond. *Magnetic Resonance in Medicine* 65: 1532–1556.

Tournier, S.M.-D. ed. (2014) Copyright. In: *Introduction to Diffusion Tensor Imaging (Second Edition)*. p. iv. Academic Press, San Diego.

Tsuda, K., Tsuji, T., Ishida, T., Takahashi, S., Yamada, S., Ohoshi, Y., Terada, M., Shinosaki, K. & Ukai, S. (2018) Widespread abnormalities in white matter integrity and their relationship with duration of illness in temporal lobe epilepsy. *Epilepsia Open* 3: 247–254.

Tuch, D.S. (2004) Q-ball imaging. *Magnetic Resonance in Medicine* 52: 1358–1372.

Tullberg, M., Hultin, L., Ekholm, S., Månsson, J.-E., Fredman, P. & Wikkelsø, C. (2002) White matter changes in normal pressure hydrocephalus and Binswanger disease: specificity, predictive value and correlations to axonal degeneration and demyelination. *Acta neurologica Scandinavica* 105: 417–426.

Tuokkola, T., Koikkalainen, J., Parkkola, R., Karrasch, M., Lötjönen, J. & Rinne, J.O. (2018) Longitudinal changes in the brain in mild cognitive impairment: a magnetic resonance imaging study using the visual rating method and tensor-based morphometry. *Acta Radiologica (Stockholm, Sweden: 1987)* 59: 973–979.

Tustison, N.J., Cook, P.A., Klein, A., Song, G., Das, S.R., Duda, J.T., Kandel, B.M., van Strien, N., Stone, J.R., Gee, J.C. & Avants, B.B. (2014) Large-scale evaluation of ANTs and FreeSurfer cortical thickness measurements. *NeuroImage* 99: 166–179.

Urs, R., Potter, E., Barker, W., Appel, J., Loewenstein, D.A., Zhao, W. & Duara, R. (2009) Visual rating system for assessing magnetic resonance images: a tool in the diagnosis of mild cognitive impairment and Alzheimer disease. *Journal of Computer Assisted Tomography* 33: 73–78.

Vemuri, P., Gunter, J.L., Senjem, M.L., Whitwell, J.L., Kantarci, K., Knopman, D.S., Boeve, B.F., Petersen, R.C. & Jack, C.R. (2008) Alzheimer's disease diagnosis in individual subjects using structural MR images: validation studies. *NeuroImage* 39: 1186–1197.

Verrees, M. & Selman, W.R. (2004) Management of normal pressure hydrocephalus. *American Family Physician* 70: 1071–1078.

Voets, N.L., Bernhardt, B.C., Kim, H., Yoon, U. & Bernasconi, N. (2011) Increased temporolimbic cortical folding complexity in temporal lobe epilepsy. *Neurology* 76: 138–144.

Wahlund, L.O., Barkhof, F., Fazekas, F., Bronge, L., Augustin, M., Sjögren, M., Wallin, A., Ader, H., Leys, D., Pantoni, L., Pasquier, F., Erkinjuntti, T., Scheltens, P. & European Task Force on Age-Related White Matter Changes (2001) A new rating scale for age-related white matter changes applicable to MRI and CT. *Stroke* 32: 1318–1322.

Wang, P.N., Lirng, J.F., Lin, K.N., Chang, F.C. & Liu, H.C. (2006) Prediction of Alzheimer's disease in mild cognitive impairment: a prospective study in Taiwan. *Neurobiology of Aging* 27: 1797–1806.

Weaver, K.E., Richards, T.L., Liang, O., Laurino, M.Y., Samii, A. & Aylward, E.H. (2009) Longitudinal diffusion tensor imaging in Huntington's Disease. *Experimental Neurology* 216: 525–529.

Westman, E., Cavallin, L., Muehlboeck, J.-S., Zhang, Y., Mecocci, P., Vellas, B., Tsolaki, M., Kłoszewska, I., Soininen, H., Spenger, C., Lovestone, S., Simmons, A., Wahlund, L.-O. & AddNeuroMed consortium (2011) Sensitivity and specificity of medial temporal lobe visual ratings and multivariate regional MRI classification in Alzheimer's disease. *PloS One* 6: e22506.

Whitwell, J.L. & Josephs, K.A. (2012) Neuroimaging in frontotemporal lobar degeneration--predicting molecular pathology. *Nature Reviews. Neurology* 8: 131–142.

Whitwell, J.L., Weigand, S.D., Boeve, B.F., Senjem, M.L., Gunter, J.L., DeJesus-Hernandez, M., Rutherford, N.J., Baker, M., Knopman, D.S., Wszolek, Z.K., Parisi, J.E., Dickson, D.W., Petersen, R.C., Rademakers, R., Jack, C.R. & Josephs, K.A. (2012) Neuroimaging signatures of frontotemporal dementia genetics: C9ORF72, tau, progranulin and sporadics. *Brain: A Journal of Neurology* 135: 794–806.

Whitwell, J.L., Xu, J., Mandrekar, J., Boeve, B.F., Knopman, D.S., Parisi, J.E., Senjem, M.L., Dickson, D.W., Petersen, R.C., Rademakers, R., Jack, C.R. & Josephs, K.A. (2013) Frontal asymmetry in behavioral variant frontotemporal dementia: clinicoimaging and pathogenetic correlates. *Neurobiology of Aging* 34: 636–639.

Wilson, R.S., Segawa, E., Boyle, P.A., Anagnos, S.E., Hizel, L.P. & Bennett, D.A. (2012) The natural history of cognitive decline in Alzheimer's disease. *Psychology and Aging* 27: 1008–1017.

Wipf, D. & Nagarajan, S. A new view of automatic relevance determination. In: *Advances in Neural Information Processing Systems 20, Platt JC, Koller D, Singer Y, Roweis S, eds. MIT Press, Cambridge*. .

Xie, J., Alcantara, D., Amenta, N., Fletcher, E., Martinez, O., Persianinova, M., DeCarli, C. & Carmichael, O. (2009) Spatially localized hippocampal shape analysis in late-life cognitive decline. *Hippocampus* 19: 526–532.

Xie, S., Xiao, J.X., Gong, G.L., Zang, Y.F., Wang, Y.H., Wu, H.K. & Jiang, X.X. (2006) Voxel-based detection of white matter abnormalities in mild Alzheimer disease. *Neurology* 66: 1845–1849.

Xuereb, J.H., Perry, R.H., Candy, J.M., Perry, E.K., Marshall, E. & Bonham, J.R. (1991) Nerve cell loss in the thalamus in Alzheimer's disease and Parkinson's disease. *Brain: A Journal of Neurology* 114 (Pt 3): 1363–1379.

Yamada, S., Ishikawa, M. & Yamamoto, K. (2015) Optimal Diagnostic Indices for Idiopathic Normal Pressure Hydrocephalus Based on the 3D Quantitative Volumetric Analysis for the Cerebral Ventricle and Subarachnoid Space. *AJNR. American journal of neuroradiology* 36: 2262–2269.

Yoo, H.S., Chung, S.J., Lee, Y.H., Lee, H.S., Ye, B.S., Sohn, Y.H. & Lee, P.H. (2019) Levodopa-induced dyskinesia is closely linked to progression of frontal dysfunction in PD. *Neurology*.

Yuan, W., McAllister, J.P., Lindquist, D.M., Gill, N., Holland, S.K., Henkel, D., Rajagopal, A. & Mangano, F.T. (2012) Diffusion tensor imaging of white matter injury in a rat model of infantile hydrocephalus. *Child's Nervous System: ChNS: Official Journal of the International Society for Pediatric Neurosurgery* 28: 47–54.

Yuan, Z., Pan, C., Xiao, T., Liu, M., Zhang, W., Jiao, B., Yan, X., Tang, B. & Shen, L. (2019) Multiple Visual Rating Scales Based on Structural MRI and a Novel Prediction Model Combining Visual Rating Scales and Age Stratification in the Diagnosis of Alzheimer's Disease in the Chinese Population. *Frontiers in Neurology* 10: 93.

Zarei, M., Patenaude, B., Damoiseaux, J., Morgese, C., Smith, S., Matthews, P.M., Barkhof, F., Rombouts, S.A.R.B., Sanz-Arigita, E. & Jenkinson, M. (2010) Combining shape and connectivity analysis: an MRI study of thalamic degeneration in Alzheimer's disease. *NeuroImage* 49: 1–8.

Zeng, C., Lee, J.T., Chen, H., Chen, S., Hsu, C.Y. & Xu, J. (2005) Amyloid-beta peptide enhances tumor necrosis factor-alpha-induced iNOS through neutral sphingomyelinase/ceramide pathway in oligodendrocytes. *Journal of Neurochemistry* 94: 703–712.

Zhang, Y., Brady, M. & Smith, S. (2001) Segmentation of brain MR images through a hidden Markov random field model and the expectation-maximization algorithm. *IEEE transactions on medical imaging* 20: 45–57.

Zhang, Y., Schuff, N., Du, A.-T., Rosen, H.J., Kramer, J.H., Gorno-Tempini, M.L., Miller, B.L. & Weiner, M.W. (2009) White matter damage in frontotemporal dementia and Alzheimer's disease measured by diffusion MRI. *Brain: A Journal of Neurology* 132: 2579–2592.

Zhang, Y., Schuff, N., Jahng, G.-H., Bayne, W., Mori, S., Schad, L., Mueller, S., Du, A.-T., Kramer, J.H., Yaffe, K., Chui, H., Jagust, W.J., Miller, B.L. & Weiner, M.W. (2007) Diffusion tensor imaging of cingulum fibers in mild cognitive impairment and Alzheimer disease. *Neurology* 68: 13–19.